DISSERTATION

HIGH PERFORMANCE MULTI-CARRIER TECHNOLOGIES WITH EXPANDED APPLICABILITY TO CDMA SYSTEMS (DS-CDMA AND MC-CDMA)

Submitted by

Zhiqiang Wu

Department of Electrical and Computer Engineering

In partial fulfillment of the requirements

For the Degree of Doctor of Philosophy

Colorado State University

Fort Collins, Colorado

Spring 2002

UMI Number: 3053461

ProQuest Information and Learning Company
300 North Zeeb Road
P.O. Box 1346
Ann Arbor, MI 48106-1346

COLORADO STATE UNIVERSITY

December 7, 2001

WE HEREBY RECOMMEND THAT THE DISSERTATION PREPARED UNDER OUR SUPERVISION BY ZHIQIANG WU ENTITLED "HIGH PERFORMANCE MULTI-CARRIER TECHNOLOGIES WITH EXPANDED APPLICABILITY TO CDMA SYSTEMS (DS-CDMA AND MC-CDMA)" BE ACCEPTED AS FULFILLING IN PART REQUIREMENTS FOR THE DEGREE OF DOCTOR OF PHILOSOPHY.

Committee on Graduate Work

Michael Kirby

Advisor

Department Head

ABSTRACT OF DISSERTATION

HIGH PERFORMANCE MULTI-CARRIER TECHNOLOGIES WITH EXPANDED APPLICABILITY TO CDMA SYSTEMS (DS-CDMA AND MC-CDMA)

Code division multiple access (CDMA) has been an important component in wireless communication systems since the early 1980's. Now the frontrunner in the 3G cellular standard, CDMA techniques have come a long way since their inception. However, these systems are not without their limitations – both in terms of performance and network capacity.

In this work, we significantly enhance the performance of existing CDMA systems via the introduction of novel multi-carrier architectures. Specifically, we demonstrate a doubling in the network capacity of existing DS-CDMA and MC-CDMA systems without loss in performance, or we provide significant performance gains over existing networks at their current system load. The novel CDMA techniques introduced in this thesis will help significantly enhance the impact of CDMA in the years to come.

Zhiqiang Wu
Electrical and Computer Engineering Department
Colorado State University
Fort Collins, CO 80523
Spring 2002

To my dearest sister Zhijin Wu

TABLE OF CONTENTS

Part I

Introduction

Chapter 1 Introduction

The rapid development of low-cost, high-speed signal processing coupled with advances in communication engineering are bridging the gap between wireless systems and fundamental information theory limits. However, there still exists a need for even more efficient use of the channel bandwidth and even better system performance in wireless communication systems.

One important area in the ongoing development wireless systems is multiple access techniques. Multiple access techniques, i.e., the sharing of the communication channel between multiple users, dates back to 1920's. Frequency-Division Multiple Access (FDMA) was proposed first [1][2]: here, each user is assigned a unique transmit carrier, and band-pass filtering (or heterodyning) at the receiver enables separation of users. Time-Division Multiple Access (TDMA) was the next multiple access scheme to emerge [1][2]: here, time is partitioned into slots and each user is assigned a unique slot(s). Receivers detect the desired user's signal by simply "switching" to the received signal at the appropriate time epoch. In FDMA and TDMA, the various users operating in non-overlapping channels.

1.1 DS-CDMA

Recently, CDMA [3-23] has emerged an important multiple access technology in mobile radio communications. CDMA provides higher network capacity when compared to conventional multiple access techniques (namely FDMA and TDMA), and it is able to effectively combat hostile frequency selective fading channels.

In Code-Division Multiple Access (CDMA) systems, the information bearing signal for user k is multiplied by a signal called the codeword or spreading code. The spreading code is a pseudo-noise code sequence. All users in a CDMA system transmit at the same frequency and time, but each user has its own spreading code which is orthogonal to all the other users' spreading codes. At the receiver, a correlation operation allows the receiver to detect the desired user's signal.

The features of CDMA system including the following [3][4][6]:

- Users of a CDMA system share the same frequency band and time interval.
- Users of a CDMA system can be asynchronous, that is, their transmit times need not be aligned, and yet "quasi-orthogonality" can be maintained by adequate design of spreading signals.

- CDMA systems have a soft capacity limit. That is, increasing the number of users in a CDMA system only raises the noise floor observed at the receiver, thus, there is no absolute limit on the number of users supported by CDMA.

- In CDMA systems, sharing of channel resources in inherently dynamic: reliability depends on the number of active users, rather than on the total number of potential users.

- Multipath fading, (observed because the spreading code spreads the transmitter output over a large bandwidth), is used to improve performance at the receiver. This is achieved by application of a RAKE receiver.

CDMA systems, however, are not without their drawbacks. They suffer from performance degradation when spreading codes of different users are not perfectly orthogonal (e.g., due to multipath fading). Multi-user detection (MUD) techniques may be used to mitigate the non-orthogonal properties of the spreading codes [19][24] but these come at a large cost in terms of receiver complexity.

Another problem characteristic of CDMA is the near-far problem [3][4][6][21][23]. This arises whenever an undesired user has a high power relative to the desired user. Because this problem is so severe, tight power control is maintained in most CDMA systems to assure that each mobile provides the same received signal power to the base station receiver [21][23].

1.2 MC-CDMA

The mulitcarrier multiple access scheme known as MC-CDMA [25-38] has received a great deal of attention in the field of wireless communications, and has emerged a strong alternative to DS-CDMA for next generation wireless communication systems.

MC-CDMA was first introduced in 1993 as a combining CDMA and OFDM (orthogonal frequency division multiplex) techniques. In MC-CDMA systems, each user sends its data on N orthogonal carriers. That is, all users send information over the same N carriers simultaneously. To allow users to be separable from one another, each user is allocated a unique spreading sequence. These spreading sequences are carefully selected to ensure orthogonality (or pseudo-orthogonality) between users. At the MC-CDMA receiver, the received signal is decomposed into its N carriers, despread, and finally optimally recombined in the frequency domain. In this way, the receiver exploits the received signal energy scattered in the frequency domain.

MC-CDMA systems offer frequency diversity benefits instead of the path diversity benefits achieved in DS-CDMA systems. It has been shown that MC-CDMA outperforms DS-CDMA in multipath fading channels [31]. There are two reasons for this:

(1) MC-CDMA systems are capable of better exploiting the energy spread introduced by the multipath fading channels. Considering a DS-CDMA RAKE receiver, this receiver typically attempts to detect and separate the 3 or 4 highest-energy paths introduced in the channel. However, the energy is spread out over far more paths than these 3 or 4, and hence the energy spread onto the other paths is completely lost at the DS-CDMA RAKE receiver. On the other hand, carefully designed MC-CDMA receivers make full use of the received signal energy in the frequency domain.

(2) More importantly, when the MC-CDMA receiver separates carriers, one observes little to no inter-carrier interference. That is, the SIR (signal to interference ratio) on each carrier branch is very large. In DS-CDMA, where a time domain processing is applied, one has no control over where the paths arrive. As a result, it is not possible to effectively separate paths. Here, the SIR on each branch of the RAKE receiver is low (relative to that in MC-CDMA carrier branches). Specifically, consider the DS-CDMA RAKE receiver, which attempts to separate paths, and assume for a moment that there are four dominant paths the RAKE receiver is attempting to separate. When writing the output equation for each branch of the RAKE receiver, one finds that there exists a large number of interfering terms. Most significant of all is the term representing interference from all N users present on the three other paths. This path-interference term demonstrates a large power, and causes the branch terms output from the RAKE receiver to demonstrate a low SIR (i.e., large interference). By contrast, consider MC-CDMA. Here, rather than attempting to

separate paths in the time domain to exploit path diversity, there is an attempt to separate narrow-band carriers in the frequency domain to achieve frequency diversity. At the transmitter side, these carriers were selected with a frequency spacing that ensured orthogonality, and it is easily shown that carriers still remain almost perfectly separable at the receiver side. Hence, each carrier branch experiences a high SIR (low interference), and as such the MC-CDMA receiver can significantly outperform its DS-CDMA counterpart.

1.3 Statement of Work

In this dissertation, (1) we bring the benefits of multi-carrier systems (e.g., MC-CDMA) to DS-CDMA to improve DS-CDMA performance and network capacity and (2) we improve the performance of current MC-CDMA systems.

Regarding DS-CDMA systems:

- By introducing novel Carrier Interferometry chip shapes into DS-CDMA, we create an innovative multi-carrier implementation of DS-CDMA [39-41]. The resulting CI/DS-CDMA systems exploits frequency diversity instead of path diversity at the receiver, and as a result, significantly outperform traditional DS-CDMA systems in terms of bit error rate in multipath fading channels.

- By introducing pseudo-orthogonal Carrier Interferometry chip shapes into DS-CDMA, we create CI/DS-CDMA systems which double network capacity in traditional DS-CDMA systems without extra bandwidth or performance degradation [39][42].

- By introducing Carrier Interferometry chip shapes into DS-CDMA, we create CI/DS-CDMA systems capable of operating over non-adjacent frequency bands [43]. In this way, a DS-CDMA system is derived that is capable of supporting next generation ultra wideband communication.

- By introducing novel orthogonal complex Carrier Interferometry *spreading codes* into traditional DS-CDMA systems, we improve performance of traditional DS-CDMA systems in terms of bit error rate in multipath fading channels [44].

- By introducing pseudo-orthogonal complex Carrier Interferometry spreading codes into traditional DS-CDMA systems, we again double the network capacity of traditional DS-CDMA systems without extra bandwidth or performance degradation [45].

- By applying our CI/DS-CDMA to IEEE 802.11 wireless LAN, we show how the above benefits can be applied to a modern day system [46][47]. Specifically, the resulting system supports four times the throughput of the traditional IEEE 802.11 system while simultaneously achieving a 2dB performance gain at a probability of error of 10^{-3}.

With regarding MC-CDMA systems:

- We derive the maximum likelihood combining (MLC) scheme for MC-CDMA receiver, a theoretically optimal combining method [48][49].
- We create MC-CDMA systems capable of operating over non-adjacent frequency bands, a requirement for next generation ultra wideband communication [50].
- By combining FDMA and MC-CDMA, we create a novel multiple access technique capable of outperforming its predecessors [51].
- By developing a MUD (multi user detector) for the proposed MC-CDMA and FDMA merger, we further improve the performance of the new hybrid multiple access technique [52].

Wireless communication has come a long way in the past two decades. Over that time period, two powerful techniques emerged as front runners in the wireless world: first came DS-CDMA in the late 1980's and early 1990's; this was followed by the emergence of multicarrier technologies (e.g., MC-CDMA) in the mid 1990's. This thesis, understanding the important roles these technologies will play in the years to come, introduced powerful innovations sure to make both DS-CDMA and MC-CDMA system far better in terms of performance, network capacity, and overall implementation.

Part II

DS-CDMA

Chapter 2 Introduction to DS-CDMA

DS-CDMA (direct sequence code division multiple access) has emerged as a dominant player in the world of wireless telecommunications [3-23]. Among DS-CDMA's successes is its adoption as the standard of choice in 3G wireless (see, e.g., [53][54]). However, DS-CDMA is not without its drawbacks, including limits to the probability of error performance and network capacity.

With regard to performance, DS-CDMA systems use RAKE receivers [3][4] in an attempt to exploit path diversity and improve probability of error performance. However, it is difficult for the DS-CDMA RAKE receiver to fully benefit from the path diversity and make efficient use of the received signal energy scattered in the time domain because (1) the multi-path effect that induces path diversity also causes a loss of user orthogonality (this leads to large inter-path interference and hence lowered SIR (signal to interference ratio)), and (2) only a limited number of taps are available to the RAKE receiver.

In this chapter, we briefly review the DS-CDMA concept, its transmitter design, receiver design, and its performance.

2.1 Introduction

DS-CDMA systems come with a wide range of far-reaching benefits: these include enhanced privacy, inherent resistance to fading, and spectral efficiency in a cellular system. The block diagram representation of today's DS-CDMA transmitter is shown in Figure 2.1. As is evident from the figure, the DS-CDMA transmitter for user k spreads the original data stream via a spreading code applied in the time domain ($c_k(t)$). Each user is allocated a unique spreading code (typically orthogonal in the downlink and pseudo-orthogonal in the uplink). The ability to suppress multi-user interference is determined by the cross-correlation characteristics of the spreading codes.

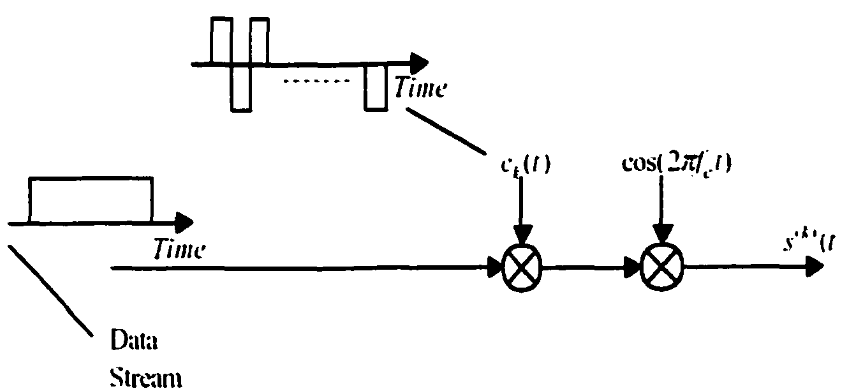

Figure 2.1 Conceptual Transmitter for DS-CDMA

After transmission over a frequency selective fading channel (typical of wideband DS-CDMA), the received signal is the superposition of several multipath signals each arriving with different delays (in the time domain). Here, the cross-correlation of different users' signals on different paths is no longer the cross-correlation of the time-aligned spreading codes.

In today's DS-CDMA receiver (Figure 2.2), a tapped delay line RAKE receiver [3][4] improves performance in the presence of multipath propagation. That is, assuming L separable multi-paths, the RAKE receiver attempts to provide L^{th}-order diversity via path separation (of the L paths) and a weighted coherent recombining (typically MRC (maximum ratio combining)). However, the multipath effect causes a loss of orthogonality between different user's signals (even in the synchronous case) thereby degrading the SIR (signal to interference ratio) on each branch of the RAKE (due to large inter-path interference). As a result, it is difficult for the DS-CDMA receivers employing path diversity to make full use of the received signal energy scattered in the time domain.

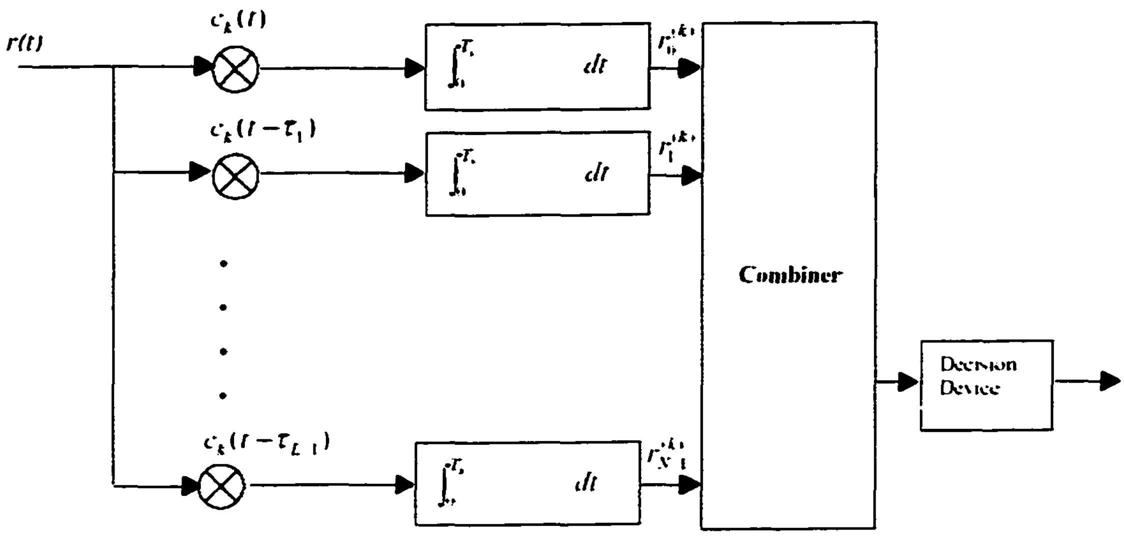

Figure 2.2 RAKE Receiver for DS-CDMA

2.2 DS-CDMA Transmit and Receive Signal

As seen in Figure 2.1, user *k*'s data bit is spread (in the time domain) by a multiplication with the spreading code $c_k(t)$. This code $c_k(t)$ is composed of N chips per bit, each modulated by either +1 or −1. Mathematically, this corresponds to

$$c_k(t) = \sum_{i=0}^{N-1} \beta_i^{(k)} P_{T_c}(t - iT_c) \tag{2.1}$$

where $\beta_i^{(k)} \in \{-1,+1\}$ is the i^{th} element of user k's spreading code $\{\beta_0^{(k)}, \beta_1^{(k)}, \cdots, \beta_{N-1}^{(k)}\}$, and $P_{T_c}(t)$ is the chip shaping filter. In current DS-CDMA systems, the most commonly used spreading codes are the Hadamard-Walsh codes (as this maintains the orthogonality between different users' time aligned signals); the chip shaping is either the usual sinc function or raised cosine function. Including code creation in the DS-CDMA transmitter side, we can redraw Figure 2.1 in a more detailed manner, as shown in Figure 2.3:

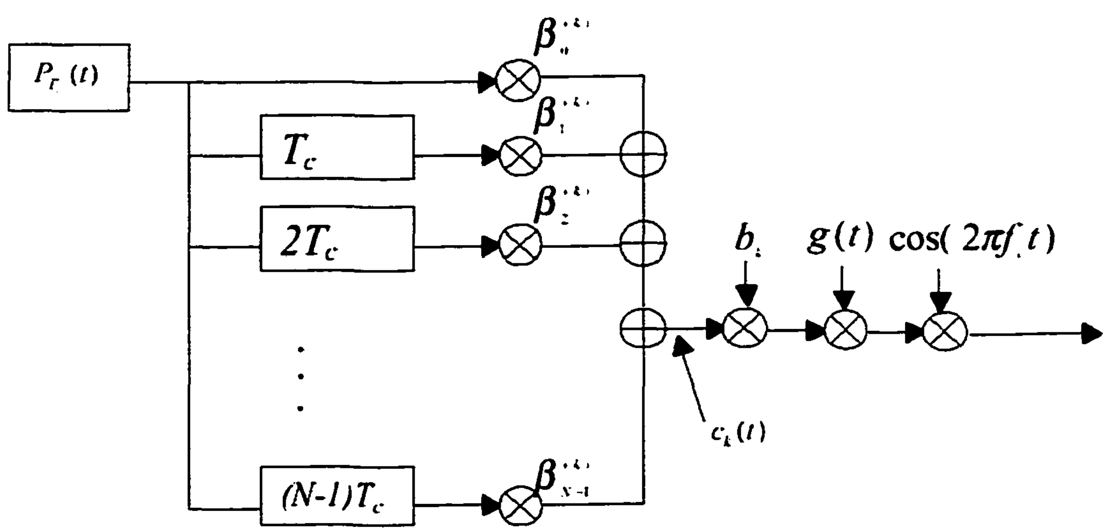

Figure 2.3 Transmitter for DS-CDMA

Thus, in DS-CDMA, the k^{th} user's transmitted signal (for one bit) corresponds to (at baseband):

$$s^{(k)}(t) = Ab_k c_k(t) \tag{2.2}$$

$$s^{(k)}(t) = Ab_k \sum_{i=0}^{N-1} \beta_i^{(k)} P_{T_c}(t - iT_c) \tag{2.3}$$

where A is constant ensuring a bit energy of unity. (Also, BPSK has been assumed for ease in presentation, i.e., $b_k \in \{-1,+1\}$). The total transmit signal considering all K users' signals (and assuming downlink or synchronous uplink communications) is:

$$s(t) = A\sum_{k=0}^{K-1} b_k \sum_{i=0}^{N-1} \beta_i^{(k)} P_{T_c}(t - iT_c) \tag{2.4}$$

Transmitted over a multipath fading channel at carrier frequency f_c, the signal arriving at the receiver side corresponds to

$$r(t) = A\sum_{l=0}^{L-1} \alpha_l s(t-\tau_l)\cos(2\pi f_c t + \theta_l) + \eta(t) \tag{2.5}$$

where L is the total number of paths; α_l is the fading parameter of the l^{th} path; τ_l is the time delay of the l^{th} path; θ_l is the phase offset of the l^{th} path; and $\eta(t)$ is the additive white Gaussian noise.

In current DS-CDMA systems, tapped delay line RAKE receivers (Figure 2.2) are commonly employed to achieve path diversity gains. In a frequency-selective multipath channel with L separable paths, the RAKE receiver attempts to provide up to L^{th}-order diversity. Specifically, in RAKE receivers, each "finger" extracts one of the multi-paths, and the fingers' outputs are then combined to exploit path diversity and overcome multi-path effects.

That is, for the RAKE receiver of Figure 2.2 and the *r(t)* of equation (2.5), the m^{th} finger's output for user k corresponds to

$$r_m^{(k)} = \sum_{l=0}^{m-1} \alpha_l \cos(\theta_l - \theta_m)[\sum_n b_n R_{n,k}(T_s - (\tau_m - \tau_l)) + \sum_n b_n^{(+1)} R_{k,n}(\tau_m - \tau_l)] + \alpha_m b_k + \alpha_m \sum_{n \neq k} b_n R_{n,k}(0)$$
$$+ \sum_{l=m+1}^{L-1} \alpha_l \cos(\theta_l - \theta_m)[\sum_n b_n^{(-1)} R_{n,k}(\tau_l - \tau_m) + \sum_n b_n R_{k,n}(T_s - (\tau_l - \tau_m))] + \eta_m$$

(2.6)

where $b_k^{(-1)}$ is user k's previous data bit, $b_k^{(+1)}$ is user k's next data bit, η_m is additive Gaussian noise, and $R_{k,n}(T)$ represents the partial cross-correlation of user k and n at time delay $T=qT_c$:

$$R_{k,n}(T) = \int_0^T s^{(k)}(t-T) s^{(n)}(t) dt \tag{2.7}$$

Also in equation (2.6), we have assumed path indexed path such that $\tau_0 < \tau_1 < \tau_2 < \cdots < \tau_{L-1}$.

Specifically, when there is no time delay and when orthogonal spreading codes (e.g., Hadamard-Walsh codes) are employed

$$R_{k,n}(0) = 0 \qquad k \neq n \tag{2.8}$$

Assuming orthogonal codes, we rewrite equation (2.6) as

$$r_m^{(k)} = \alpha_m b_k + \sum_{l=0}^{m-1} \alpha_l \cos(\theta_l - \theta_m)[\sum_n b_n R_{n,k}(T_s - (\tau_m - \tau_l)) + \sum_n b_n^{(+1)} R_{k,n}(\tau_m - \tau_l)\ ]$$
$$+ \sum_{l=m+1}^{L-1} \alpha_l \cos(\theta_l - \theta_m)[\sum_n b_n^{(-1)} R_{n,k}(\tau_l - \tau_m) + \sum_n b_n R_{k,n}(T_s - (\tau_l - \tau_m))] + \eta_m$$

(2.9)

In RAKE receivers, the decision variables $\{r_m^{(n)}, m = 0,1,\cdots, L-1\}$ are combined, i.e., the decision variables are combined across paths to exploit the path diversity gain. The final decision statistic for user k corresponds to

$$R^{(k)} = \sum_{m=0}^{L-1} W_m r_m^{(k)} \tag{2.10}$$

Maximum Ratio Combining (MRC) is usually applied, i.e,

$$W_m = \alpha_m \tag{2.11}$$

and a hard decision device follows:

$$\hat{b}_k = \begin{cases} +1 & \text{if } R^{(k)} > 0 \\ -1 & \text{else} \end{cases} \tag{2.12}$$

As seen in equation (2.9), the received DS-CDMA signal on each branch of the RAKE receiver suffers from large inter-path interference. (This inter-path interference is detailed by the second and third terms of equation (2.9).) As a result, each diversity component $\{r_m^{(k)}, m = 0,1,\cdots, L-1\}$ demonstrates a significantly reduced SIR, which limits the performance of the RAKE receiver. Figure 2.4 shows a typical DS-CDMA BER performance versus signal to noise ratio (SNR) curve in the hilly terrain (HT) channel and Figure 2.5 shows the results in typical urban (TU) channel. The HT and TU channel models will be discussed in section 3.4. The processing gain is N=32 and the system is fully loaded: the high error floor due to the multipath interference is clearly evident.

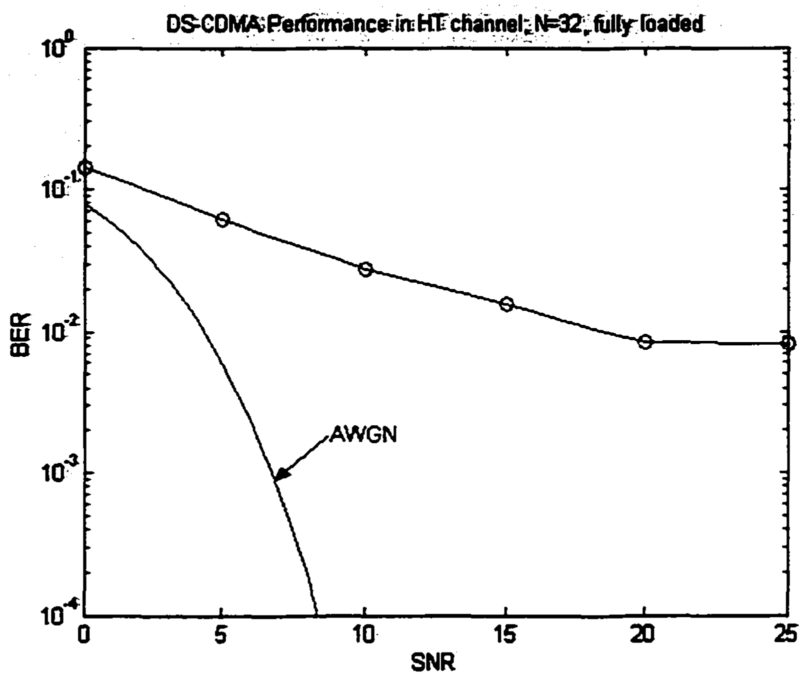

Figure 2.4 BER Performance of DS-CDMA in HT Channel

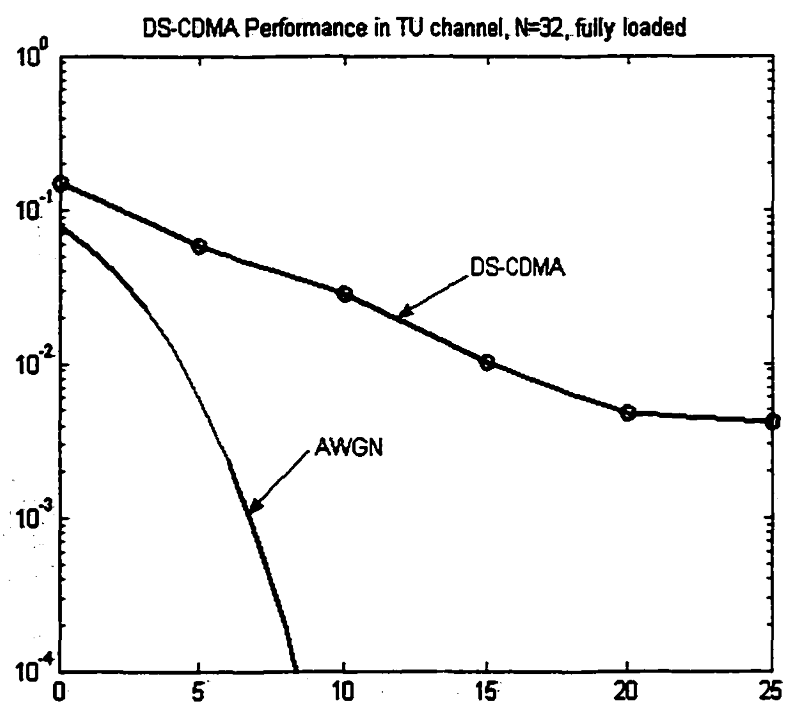

Figure 2.5 BER Performance of DS-CDMA in TU Channel

2.3 Conclusions

In this chapter, we have briefly reviewed DS-CDMA, explaining the transmitter structure, receiver structure, and characterizing the performance limit to performance, namely error floor, are evident in DS-CDMA performance curves. In the chapters follow, we provide innovative ways to improve upon DS-CDMA systems.

Chapter 3 DS-CDMA with CI Chip Shaping

One system that has emerged recently, capable of outperforming DS-CDMA, is MC-CDMA (multi-carrier code division multiple access) [25-38]. As will be detailed in Chapter 8, MC-CDMA employs receivers which offer frequency diversity benefits instead of path diversity benefits to enhance performance in a multipath channel. Here, carefully designed MC-CDMA receivers make efficient use of the received signal energy in the frequency domain, demonstrating significant performance improvements over DS-CDMA with RAKE receivers (e.g., [31]).

In this chapter, we demonstrate the power of multi-carrier chip shaping in DS-CDMA: by replacing the usual sinc and raised cosine chip shapes with the CI (carrier interferometry) chip shapes, we bring the performance benefits of MC-CDMA to DS-CDMA, bridging the gap between DS-CDMA and MC-CDMA performances. Specifically, by employing CI chip shaping in DS-CDMA, we introduce a exploitable frequency diversity at the DS-CDMA receiver and enable DS-CDMA receivers to make full use of the received signal energy [39-42][55].

3.1 Novel Multi-Carrier Chip Shapes and Novel Transmitters for DS-CDMA

We propose a novel chip shape for DS-CDMA: the chip shape corresponds to the superpositioning of N carriers equally spaced in frequency by $\Delta f = 1/T_s$ (where N corresponds to the processing gain in DS-CDMA and T_s is the symbol duration). This chip shape (implemented using an IFFT), represented in complex baseband notation, corresponds to [39-42]

$$h'(t) = \sum_{n=-\frac{N}{2}}^{\frac{N}{2}-1} A e^{j2\pi(n+\frac{1}{2})\Delta f t} \tag{3.1}$$

where A refers to the constant that ensures a chip energy of $1/N$ over one period (symbol duration T_s). Figure 3.1 shows the creation of the new chip shape.

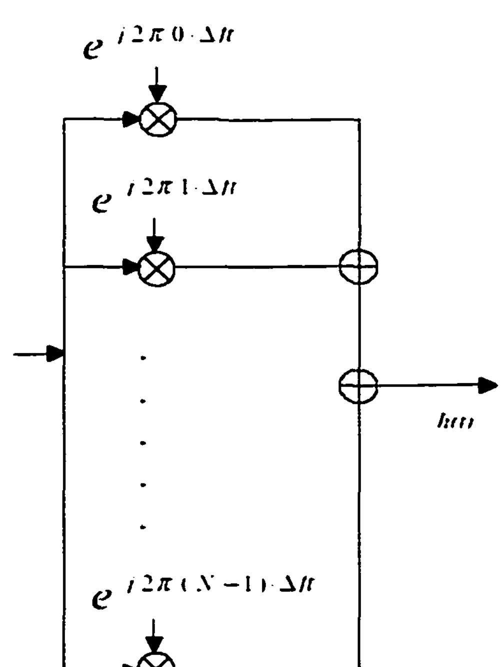

Figure 3.1 *Creation of CI Chip Shape*

When the CI signal is modulated to carrier frequency F_c, the transmit signal is of the form

$$h_{passband}(t) = \mathrm{Re}\{h'(t)e^{j2\pi F_c t}\} = \mathrm{Re}\left\{\sum_{n=-\frac{N}{2}}^{\frac{N}{2}-1} Ae^{j2\pi(F_c+(n+\frac{1}{2})\Delta f)t}\right\} \tag{3.2}$$

However, for notational convenience and because of ease in presenting time/frequency analogies, we choose to represent our CI signal in the complex form

$$h(t) = \sum_{n=0}^{N-1} Ae^{j2\pi n\Delta f t} \tag{3.3}$$

and, hence, for the same passband representation

$$h_{passband}(t) = \mathrm{Re}\{h'(t)e^{j2\pi F_c t}\} = \mathrm{Re}\left\{h(t)e^{j2\pi[F_c-\frac{(N-1)}{2}\Delta f]t}\right\} \tag{3.4}$$

$$h_{passband}(t) = \mathrm{Re}\{h(t)e^{j2\pi f_c t}\} \tag{3.5}$$

where

$$f_c = F_c - \frac{(N-1)}{2}\Delta f \tag{3.6}$$

Figure 3.2(a) plots the envelope of the chip shape *h(t)* over symbol duration T_s, and Figure 3.2(b) plots *h(t)* in the frequency domain. As evident from Figure 3.2(b), the CI chip shape is simply an N-point frequency sampling of the sinc chip shape. As a direct consequence, it is important to note that these proposed chips (*h(t)*'s) satisfy the usual orthogonality condition:

$$\int_0^{T_s} h(t-pT_c)h(t-qT_c)dt = 0 \quad (p \neq q) \tag{3.7}$$

Moreover, considering Figure 3.2(a), the chip shape demonstrates an interferometry pattern in the time domain: hence, the chip shape is referred to as the carrier interferometry (CI) chip shape.

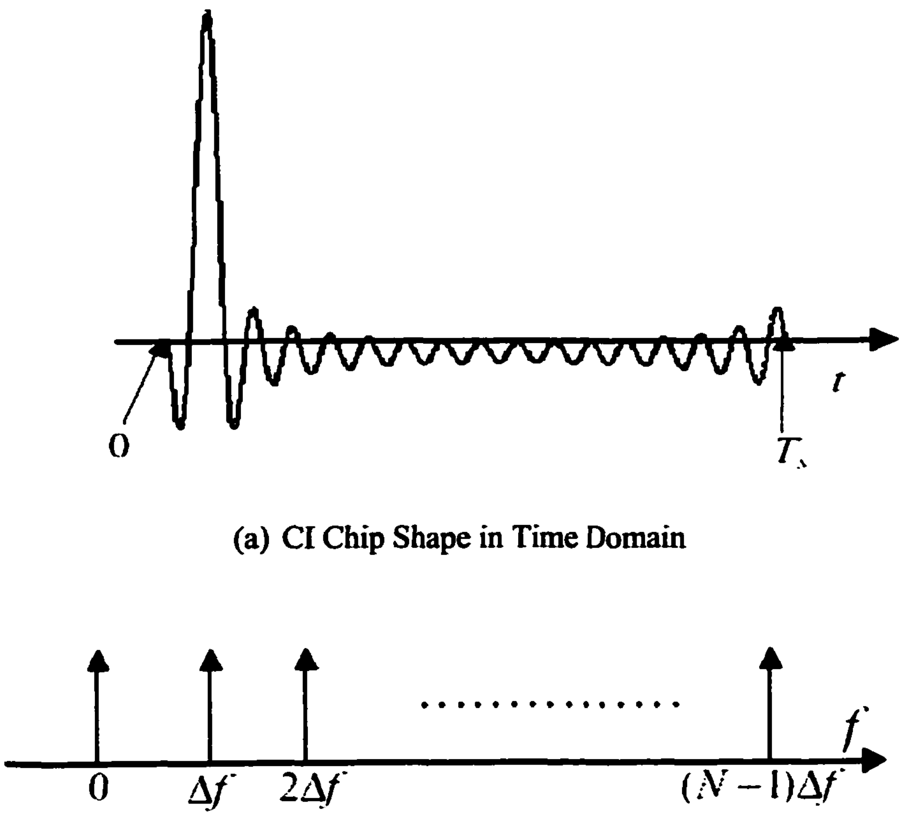

(a) CI Chip Shape in Time Domain

(b) CI Chip Shape in Frequency Domain

Figure 3.2 CI Chip Shape

To generate the DS-CDMA code for user k, $c_k(t)$, the i^{th} value of the spreading sequence, $\beta_i^{(k)}$ (typically +1 or −1), modulates the CI chip shape filter $h(t-iT_c)$ [39-42]:

$$c_k(t) = \sum_{i=0}^{N-1} \beta_i^{(k)} h(t-iT_c) \tag{3.8}$$

where $h(t)$ is as shown in equation (3.1). Correspondingly, user k's output signal at the transmitter side is

$$s^{(k)}(t) = \mathrm{Re}[b_k g(t) \cdot c_k(t) \cdot e^{j2\pi f_c t}] \tag{3.9}$$

$$s^{(k)}(t) = b_k \sum_{i=0}^{N-1} \beta_i^{(k)} h(t - iT_c) \cdot g(t) \cdot e^{j2\pi f_c t} \tag{3.10}$$

$$s^{(k)}(t) = b_k \sum_{i=0}^{N-1} \beta_i^{(k)} \sum_{n=0}^{N-1} A\cos(2\pi f_c t + 2\pi n\Delta f(t - iT_c)) \cdot g(t) \tag{3.11}$$

where b_k is the data bit of the k^{th} user ($b_k \in \{+1,-1\}$), and $g(t)$ is a unit amplitude rectangular waveform of duration T_s, and A is a constant that ensures the symbol energy of user k is unity.

Noting that $T_c = \frac{1}{N} T_s = \frac{1}{N\Delta f}$, we can rewrite equation (3.11) as:

$$s^{(k)}(t) = b_k \sum_{i=0}^{N-1} \beta_i^{(k)} \sum_{n=0}^{N-1} A\cos(2\pi f_c t + 2\pi n\Delta f t - 2\pi n i\Delta f \cdot \frac{1}{N\Delta f}) \cdot g(t) \tag{3.12}$$

$$s^{(k)}(t) = b_k \sum_{i=0}^{N-1} \beta_i^{(k)} \sum_{n=0}^{N-1} A\cos(2\pi f_c t + 2\pi n\Delta f t - 2\pi n i / N) \cdot g(t) \tag{3.13}$$

Using equation (3.13), it is evident that the chip $h(t-iT_c)$ corresponds to the linear combining of the N carriers as seen in equation (3.1), where now the n^{th} carrier is phase offset by $n \cdot i2\pi / N = n \cdot \theta_i$, where $\theta_i = i2\pi / N$.

The total transmit signal for K users in a downlink (or synchronous uplink) is simply:

$$S(t)=\sum_{k=0}^{K-1}s^{(k)}(t) \tag{3.14}$$

$$S(t)=\sum_{k=0}^{K-1}b_k\sum_{i=0}^{N-1}\beta_i^{(k)}\sum_{n=0}^{N-1}A\cos(2\pi f_c t+2\pi n\Delta ft-ni2\pi/N)\cdot g(t) \tag{3.15}$$

Figure 3.3 presents the block diagram for the DS-CDMA transmitter employing CI chip shapes.

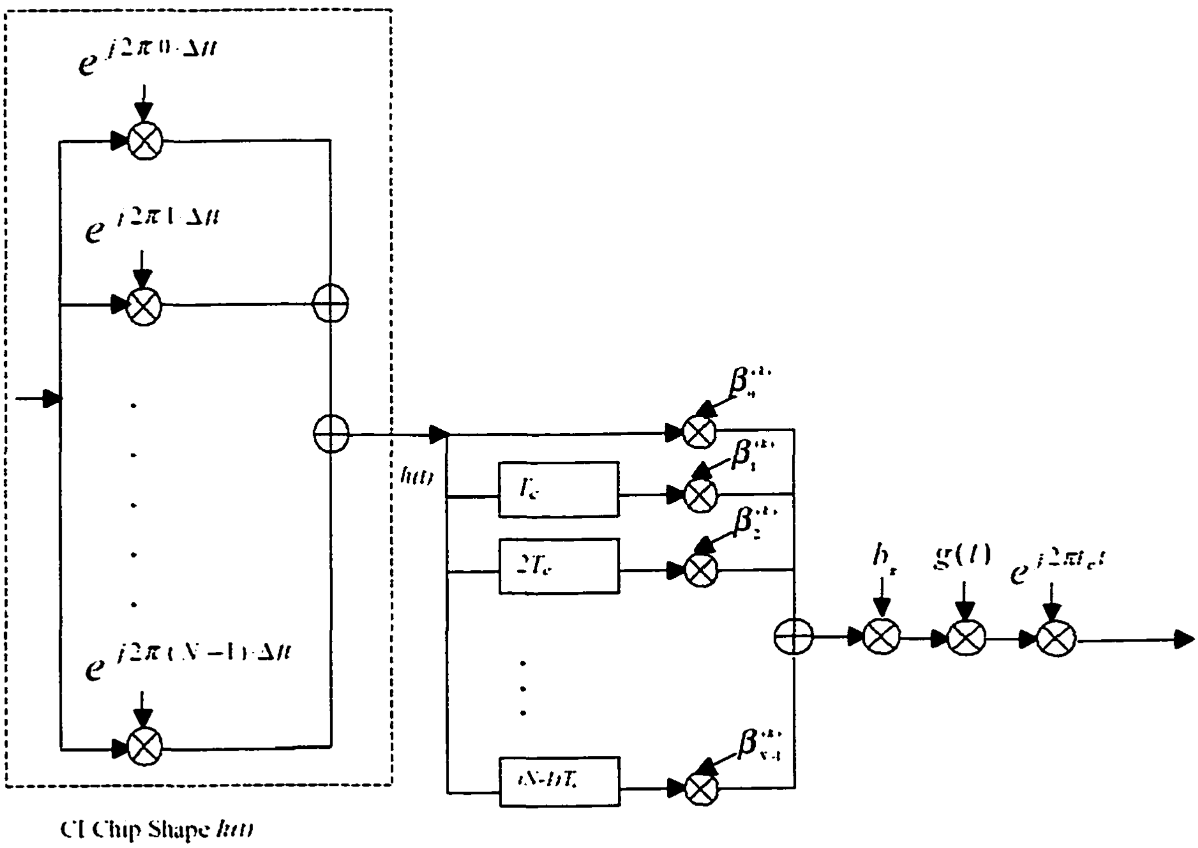

Figure 3.3 Transmitter for CI/DS-CDMA

It is apparent from Figure 3.3 that the transmitter for CI/DS-CDMA is identical to that of traditional DS-CDMA (Figure 2.3) with the one exception: the CI chip shaping filter $h(t)$ replaced the usual chip shaping filter $P_{T_c}(t)$.

As evidenced in Figure 3.2(b), our chip shaping strategy creates DS-CDMA signals which are made up of N separable frequency components. That is, the CI chip shape will allow DS-CDMA receivers to separate the incoming wideband signal into frequency components (enabling frequency diversity at the receiver).

3.2 Novel Receiver Design for CI/DS-CDMA

The receiver for the novel CI/DS-CDMA system is shown in Figure 3.4. This receiver is detailed next.

Assuming a Rayleigh frequency-selective slow fading channel (typical of wideband DS-CDMA), frequency selectivity exists over the entire bandwidth, but not over the individual carriers that make up the CI chip shape. Hence, each frequency component making up the CI chip shape experiences a unique flat fade. That is, the received signal (assuming the transmit signal in equation (3.15)) is characterized by:

$$r(t) = \sum_{k=0}^{K-1} b_k \sum_{i=0}^{N-1} \beta_i^{(k)} \sum_{n=0}^{N-1} A\alpha_n \cos(2\pi f_c t + 2\pi n\Delta f t - ni2\pi / N + \phi_n) g(t) + \eta(t) \tag{3.16}$$

where α_n is the gain and ϕ_n the phase offset in the n^{th} carrier of the CI chip shape (due to the channel fade), and $\eta(t)$ represents additive white Gaussian noise. To simplify the analysis, exact phase synchronization is assumed.

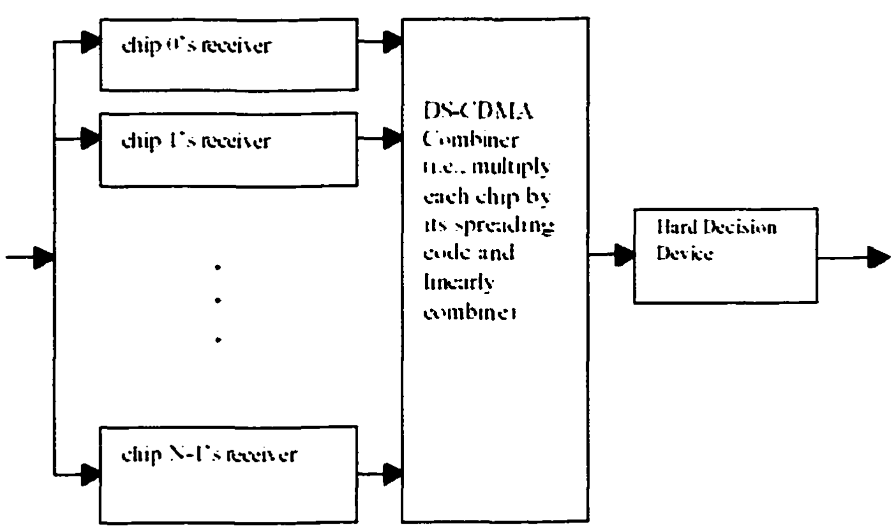

(a) Receiver Structure

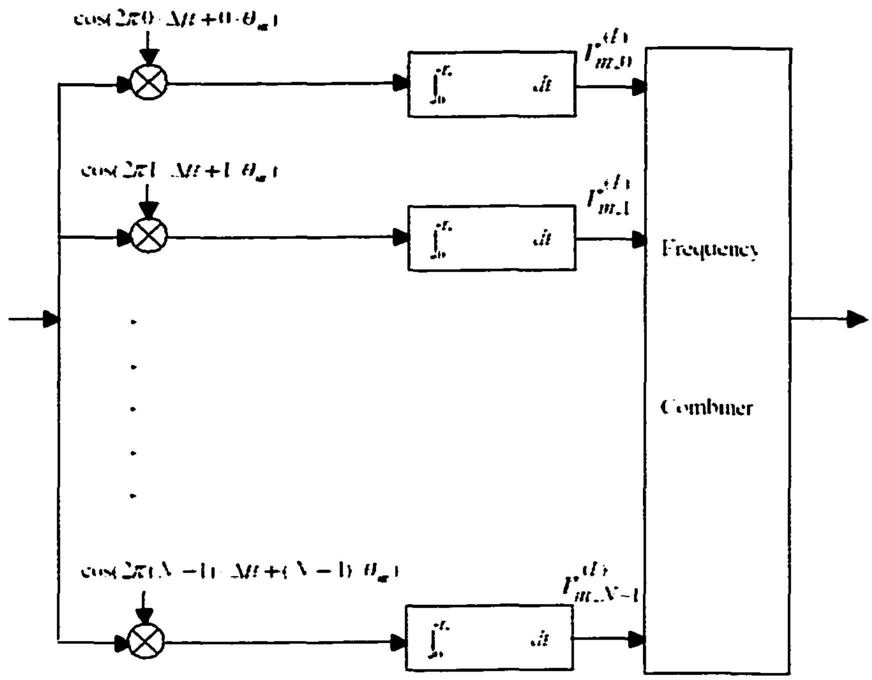

(b) Chip *m*'s Receiver

Figure 3.4 Receiver for CI/DS-CDMA

The CI/DS-CDMA receiver shown in Figure 3.4 consists of three main components: (1) the incoming DS-CDMA signal is separated into its N chip components, and each chip is decomposed into its carriers and recombined to exploit frequency diversity and minimize inter-chip interference and noise; (2) the newly recreated CI chips are despread and linearly combined to eliminate the presence of other users (typical of DS-CDMA receivers); and (3) a hard decision device creates the final bit decisions. The processing of the m^{th} chip for user l is detailed in Figure 3.4(b). Here, the m^{th} chip is separated into its N carrier components by a bank of mixers and integrators. Each carrier contributes one decision variable $r_{m,n}^{(l)}$ corresponding to

$$r_{m,n}^{(l)} = \sum_{k=0}^{K-1} b_k \sum_{i=0}^{N-1} \beta_i^{(k)} \alpha_n \cos(nm2\pi / N - ni2\pi / N) + \eta_{m,n} \tag{3.17}$$

We can rewrite this equation as

$$\begin{aligned} r_{m,n}^{(l)} &= b_l \beta_m^{(l)} \alpha_n + b_l \alpha_n \sum_{\substack{i=0 \\ i \neq m}}^{N-1} \beta_i^{(l)} \cos(nm2\pi / N - ni2\pi / N) \\ &+ \sum_{\substack{k=0 \\ k \neq l}}^{K-1} b_k \beta_m^{(k)} \alpha_n + \sum_{\substack{k=0 \\ k \neq l}}^{K-1} b_k \alpha_n \sum_{\substack{i=0 \\ i \neq m}}^{N-1} \beta_i^{(k)} \cos(nm2\pi / N - ni2\pi / N) + \eta_{m,n} \end{aligned} \tag{3.18}$$

The first term represents the desired contribution from user l, chip m and carrier n. The second term represents the presence (in the n^{th} carrier) of the remaining $N-1$ chips of the same user (user l). The third term represents the presence of other users' interference due to their m^{th} chip. The fourth term represents the presence (in the n^{th} carrier) of the other users' remaining $N-1$ chips. The fifth term is a zero mean Gaussian random variable with variance $\sigma_n^2=N_0/2$. It is important to note that the $\eta_{m,n}$ terms are correlated across chips (but not across carriers). The covariance matrix of the vector noise $(\eta_{0,n}, \eta_{1,n}, \eta_{2,n}, \ldots \eta_{N-1,n})$ corresponding to a fixed n (carrier number) and a different m (chip number) is:

$$C_n = \frac{N_0}{2} \begin{pmatrix} 1 & \cos(n \cdot 2\pi / N) & \cos(2 \cdot n \cdot 2\pi / N) \cdots\cdots \cos((N-1) \cdot n \cdot 2\pi / N) \\ \cos(n \cdot 2\pi / N) & 1 & \cos(n \cdot 2\pi / N) \ \cdots\cdots \cos((N-2) \cdot n \cdot 2\pi / N) \\ & & \cdot \\ & & \cdot \\ & & \cdot \\ \cos((N-1) \cdot n \cdot 2\pi / N) & & \cdots\cdots \qquad 1 \end{pmatrix} \tag{3.19}$$

A suitable frequency combining strategy is employed in Figure 3.4(b) to combine the $r_{m,n}^{(l)}$'s across carriers. The intention here is to: (1) offer frequency diversity gains when recreating the chip, and (2) remove the second and fourth interference term in equation (3.13) (removing the inter-chip interference) while minimizing noise.

Orthogonality Restoring Combining (ORC) refers to the combining where each $r_{m,n}^{(l)}$ is scaled by α_n then summed, i.e.,

$$R_m^{(l)} = \sum_{n=0}^{N-1} r_{m,n}^{(l)} / \alpha_n \tag{3.20}$$

This enables a perfect elimination of the second term and fourth term (due to the chip orthogonality condition of equation (3.2)), while providing optimal frequency diversity combining. However, it can result in substantial noise enhancement, and as a result is only suitable in low noise conditions (high SNR).

When SNR is low, Equal Gain Combining (EGC) is a good choice for the combining strategy as it minimizes noise. Here, the N carrier terms for the m^{th} chip are combined to create:

$$R_m^{(l)} = \sum_{n=0}^{N-1} r_{m,n}^{(l)} \tag{3.21}$$

Finally, Minimum Mean Square Error Combining (MMSEC) is a powerful alternative which attempts to jointly minimize the second term and the fourth term and achieve maximum frequency diversity, while minimizing the effect of the noise term. Extending traditional MC-CDMA MMSE combining to our CI/DS-CDMA system leads to the decision variable for the m^{th} chip:

$$R_m^{(l)} = \sum_{n=0}^{N-1} r_{m,n} \cdot (\alpha_n / (K\alpha_n^{\ 2} + \frac{N_0}{2})) \tag{3.22}$$

After frequency combining across chips' carriers, we return to Figure 3.4(a) where a final decision variable for user l is generated by combining across chips in the usual DS-CDMA fashion, eliminating multi-user interference (the third term of equation (3.18)):

$$D^{(l)} = \sum_{m=0}^{N-1} R_m^{(l)} \beta_m^{(l)} \tag{3.23}$$

That is, the m^{th} chip decision variable $R_m^{(l)}$ is multiplied by m^{th} spreading code and the resulting product terms are combined together. The orthogonal cross-correlation between spreading codes of different users enables this combining to minimize multi-user interference in a conventional DS-CDMA manner.

3.3 Advanced Receiver Design for CI/DS-CDMA

In this section, we propose novel combiners for the CI/DS-CDMA receiver structure of Figure 3.4, where each combiner is determined under a different optimization criteria.

3.3.1 Minimized Mean Square Error Combining for CI/DS-CDMA

In the previous section, the MMSE combining of equation (3.22) was a direct extension of traditional MC-CDMA MMSE combining. However, this is not optimized for our CI/DS-CDMA system. Employing the true Minimized Mean Square Error Criteria, we can derive the MMSE combining weights for CI/DS-CDMA as follows [56]:

Recall the decision variable for the m^{th} chip and n^{th} carrier corresponds to:

$$\begin{aligned} r_{m,n}^{(l)} &= b_l \beta_m^{(l)} \alpha_n + b_l \alpha_n \sum_{\substack{i=0 \\ i \neq m}}^{N-1} \beta_i^{(l)} \cos(nm2\pi / N - ni2\pi / N) \\ &+ \sum_{\substack{k=0 \\ k \neq l}}^{K-1} b_k \beta_m^{(k)} \alpha_n + \sum_{\substack{k=0 \\ k \neq l}}^{K-1} b_k \alpha_n \sum_{\substack{i=0 \\ i \neq m}}^{N-1} \beta_i^{(k)} \cos(nm2\pi / N - ni2\pi / N) + \eta_{m,n} \end{aligned} \tag{3.24}$$

Now, the minimized mean square error criteria, mandates the frequency combining based on the equation

$$R_m = \sum_{n=0}^{N-1} r_{m,n}^{(l)} \cdot A_n^{\bullet} \tag{3.25}$$

where

$$A_n^{\bullet} = \arg\min(E[A_n r_{m,n}^{(l)} - \beta_m^{(l)} b_l]^2) \tag{3.26}$$

is the n^{th} frequency combining weight. We solve for $A_n^{\bullet}$ using partial derivatives, i.e.:

$$\left. \frac{\partial E[r_{m,n}^{(l)} A_n - \beta_m^{(l)} b_l]^2}{\partial A_n} \right|_{A_n^{\bullet}} = 0 \tag{3.27}$$

$$E[(r_{m,n}^{(l)}A_n^* - \beta_m^{(l)}b_l)r_{m,n}] = 0 \tag{3.28}$$

$$E[r_{m,n}^{(l)}A_n^* r_{m,n}] = E[\beta_m^{(l)}b_l r_{j,n}] \tag{3.29}$$

We can now solve equation (3.29) to get the optimal MMSE combining weights for CI/DS-CDMA.

Case I: A_n^* assuming no knowledge of spreading codes

The simplest case is when one assumes that user l doesn't have any information about spreading codes (other users and his own). The only information assumed known at the receiver is the total number of users and estimation of one's own the channel fading parameters. In this case, solving equation (3.24) leads to:

$$A_n^* = \frac{\alpha_n}{K\alpha_n^2 \sum_{i=0}^{N-1} \cos(nm\frac{2\pi}{N} - ni\frac{2\pi}{N}) + \frac{N_0}{2}} \tag{3.30}$$

i.e.,

$$A_n^* = \frac{\alpha_n}{KP_n\alpha_n^2 + \frac{N_0}{2}} \tag{3.31}$$

where

$$P_n = \sum_{i=0}^{N-1} \cos^2(n(m-i)\frac{2\pi}{N}) = \begin{cases} \frac{N}{2} & n = 1,2,\ldots,N-1, n \neq \frac{N}{2} \\ N & n = 0, \frac{N}{2} \end{cases} \tag{3.32}$$

Case II: A_n^* assuming knowledge of your own spreading code

Here, we assume that the CI/DS-CDMA receiver for user l knows its own spreading code. (This is a very reasonable assumption.) Then, from equation (3.29):

$$A_n^* = \frac{\alpha_n(1 + \sum_{\substack{i=0 \\ i \neq m}}^{N-1} \beta_i^{(l)} \beta_m^{(l)} \cos(nm\frac{2\pi}{N} - ni\frac{2\pi}{N}))}{K\alpha_n^2 \sum_{i=0}^{N-1} \cos(nm\frac{2\pi}{N} - ni\frac{2\pi}{N}) + \frac{N_0}{2}} \tag{3.33}$$

$$A_n^* = \frac{\alpha_n(1 + \sum_{\substack{i=0 \\ i \neq m}}^{N-1} \beta_i^{(l)} \beta_m^{(l)} \cos(nm\frac{2\pi}{N} - ni\frac{2\pi}{N}))}{KP_n\alpha_n^2 + \frac{N_0}{2}} \tag{3.34}$$

where

$$P_n = \sum_{i=0}^{N-1} \cos^2(n(m-i)\frac{2\pi}{N}) = \begin{cases} \frac{N}{2} & n = 1,2,\ldots,N-1 \\ N & n = 0, \frac{N}{2} \end{cases} \tag{3.35}$$

3.3.2 Matrix MMSE Combining for CI/DS-CDMA

Minimized Mean Square Error Combining derived in previous section is based on the assumption that the multi-chip interference on each carrier is independent (with respect to the interference on other carriers). This is a common assumption, leading to a combiner (a MMSEC) that is very simple to implement (in large part because it doesn't consider the correlation among carriers). Introducing this correlation, we create a more accurate minimized mean square error combining as follows. We begin with the generalized matrix MMSE criteria:

$$R_m = \bar{A}^* \bar{r}_m{}^T \tag{3.36}$$

where

$$\bar{r}_m = (r_{m,0}, r_{m,1}, \ldots, r_{m,N-1}) \tag{3.37}$$

$$\bar{A}^* = (A_0^*, A_1^*, \ldots, A_{N-1}^*) \tag{3.38}$$

Here, $\bar{A}^*$ is the vector of frequency combining weights and corresponding to

$$\bar{A}^* = \arg\min E[(\bar{r}_m \bar{A}^T - \beta_m^{(l)} b_l)^2] \tag{3.39}$$

$$\left. \frac{\partial E[(\bar{r}\bar{A}^T - \beta_m^{(l)} b_l)^2]}{\partial \bar{A}} \right|_{\bar{A}^*} = 0 \tag{3.40}$$

Case I: $\bar{A}_n^*$ assuming no knowledge of spreading codes

Here, we assume the detector for each chip doesn't utilize any information regarding spreading codes. Hence, from equation (3.40),

$$\bar{A}^* = \mathbf{R}^{-1}\bar{\alpha} \tag{3.41}$$

where $\boldsymbol{R}$ is the covariance matrix of $\bar{r}_m$:

$$\mathbf{R} = E[(\bar{r} - E[\bar{r}])^T(\bar{r} - E[\bar{r}])] \tag{3.42}$$

Case II: $\bar{A}_n^*$ assuming knowledge of the intended user's spreading code

If we know the spreading code of the user under consideration, we find (using equation (3.40))

$$\bar{A} = \mathbf{R}^{-1}\bar{\alpha} \otimes \bar{B} \tag{3.43}$$

where $\bar{\alpha} \otimes \bar{B} = (\alpha_0 \cdot B_0, \alpha_1 \cdot B_1, \ldots, \alpha_{N-1} \cdot B_{N-1})$ and

$$B_n = 1 + \sum_{\substack{i=0 \\ i \neq m}}^{N-1} \beta_i^{(l)} \beta_m^{(l)} \cos(nm\frac{2\pi}{N} - ni\frac{2\pi}{N}) \tag{3.44}$$

3.3.3 Maximum Likelihood Combining

Simulation results for CI/DS-CDMA employing different combining schemes (se section 3.5) shows MMSE combining offering much better performance than other combining schemes. However, while Minimized mean square error criteria is very good for signal estimation, in a minimized probability of error sense it is not necessarily optimal (or even very good).

Here, we derive the Maximum Likelihood (ML) receiver for the CI/DS-CDMA system, a receiver that is truly optimal from a probability of error standpoint. By comparing this result to the MMSEC result, we will be able to determine the merits of MMSE combining introduced earlier.

Case I: assuming no knowledge of spreading codes

We begin by assuming the CI/DS-CDMA receiver has no information regarding spreading codes. The maximum posterior (MAP) probability criteria is simply the well-known equation [1]:

$$P(b_l = 1 | \bar{r}) >< P(b_l = -1 | \bar{r}) \tag{3.45}$$

where $><$ means if the term on the right is greater than the one on the left, decide the bit -1; and if the term on the right is less than the one on the left, decide $+1$. Now, assume

$$P(b_l = 1) = P(b_l = -1) = 0.5 \tag{3.46}$$

(which turns the MAP receiver into the ML (maximum likelihood) receiver). This leads to the restating of equation (3.45) as

$$P(\bar{r} \mid b_l = 1) >< P(\bar{r} \mid b_l = -1) \tag{3.47}$$

$$\log_e P(\bar{r} \mid b_l = 1) >< \log_e P(\bar{r} \mid b_l = -1) \tag{3.48}$$

Now, since the receiver has no information regarding spreading codes, the decision variables $r_{m,n}^{(l)}$ are assumed independent from one another, i.e.:

$$P(\bar{r} | b_l) = \prod_{m,n} P(r_{m,n}^{(l)} | b_l) \tag{3.49}$$

$$\log_e P(\bar{r} | b_l) = \sum_{m,n} \log_e P(r_{m,n}^{(l)} | b_l) \tag{3.50}$$

where

$$P(r_{m,n}^{(l)}|b_l) = P(r_{m,n}^{(l)}\beta_m^{(l)} = \alpha_n b_l + \alpha_n b_l \sum_{i\neq m} \beta_i^{(l)}\beta_m^{(l)} \cos(nm\frac{2\pi}{N} - ni\frac{2\pi}{N})$$

$$+\alpha_n \sum_{k\neq l} b_k \beta_m^{(k)}\beta_m^{(l)} + \alpha_n \sum_{k\neq l}\sum_{i\neq m} b_k \beta_i^{(k)}\beta_m^{(l)} \cos(nm\frac{2\pi}{N} - ni\frac{2\pi}{N}) + \eta_{m,n})$$

(3.51)

$$P(r_{m,n}^{(l)} \mid b_l) = P(r_{m,n}^{(l)} = \alpha_n b_l + \eta'_{m,n}) \tag{3.52}$$

where $\eta'_{m,n}$ encompasses the last four terms on the right hand side of equation (3.51), i.e., $\eta'_{m,n}$ is a Gaussian random variable with 0 mean and variance

$$\sigma_{m,n}^2 = E\left[\left(\begin{array}{l}\alpha_n b_l \sum_{i\neq m} \beta_i^{(l)}\beta_m^{(l)} \cos(nm\frac{2\pi}{N} - ni\frac{2\pi}{N}) \\ +\alpha_n \sum_{k\neq l} b_k \beta_m^{(k)}\beta_m^{(l)} + \alpha_n \sum_{k\neq l}\sum_{i\neq m} b_k \beta_i^{(k)}\beta_m^{(l)} \cos(nm\frac{2\pi}{N} - ni\frac{2\pi}{N}) + \eta_{m,n}\end{array}\right)^2\right] \tag{3.53}$$

$$\sigma_{m,n}^2 = E\left[\left(\alpha_n \sum_k \sum_i b_k \beta_i^{(k)}\beta_m^{(l)} \cos(nm\frac{2\pi}{N} - ni\frac{2\pi}{N}) + \eta_{m,n} - \alpha_n b_l\right)^2\right] \tag{3.54}$$

$$\sigma_{m,n}^2 = \alpha_n^2 K \sum_{i=0}^{N-1} \cos^2(n(m-i)\frac{2\pi}{N}) - \alpha_n^2 + \frac{N_0}{2} \tag{3.55}$$

$$\sigma_{m,n}^2 = \alpha_n^2 (KP_n - 1) + \frac{N_0}{2} \tag{3.56}$$

where

$$P_n = \sum_{i=0}^{N-1} \cos^2(n(m-i)\frac{2\pi}{N}) = \begin{cases} \frac{N}{2} & n = 1,2,\ldots,N-1 \\ N & n = 0, \frac{N}{2} \end{cases} \tag{3.57}$$

Hence, using (3.50)

$$\log P(\bar{r}|b_l = 1) >< \log P(\bar{r}|b_l = -1) \tag{3.58}$$

$$\sum_{m,n} \log \frac{1}{\sqrt{2\pi\sigma_{m,n}^2}} - \sum_{m,n}[\frac{(\alpha_n - r_{m,n}^{(l)}\beta_m^{(l)})^2}{2\sigma_{m,n}^2}] >< \sum_{m,n} \log \frac{1}{\sqrt{2\pi\sigma_{m,n}^2}} - \sum_{m,n}[\frac{(-\alpha_n - r_{m,n}^{(l)}\beta_m^{(l)})^2}{2\sigma_{m,n}^2}] \tag{3.59}$$

$$\sum_{m,n} \frac{\alpha_n r_{m,n} \beta_m^{(l)}}{\sigma_{m,n}^2} >< 0 \tag{3.60}$$

$$\sum_m \{\beta_m^{(l)}[\sum_n \frac{r_{m,n}\alpha_n}{\sigma_{m,n}^2}]\} >< 0 \tag{3.61}$$

$$\sum_m \{\beta_m^{(l)}[\sum_n \frac{r_{m,n}\alpha_n}{\alpha_n^2(KP_n - 1) + \frac{N_0}{2}}]\} >< 0 \tag{3.62}$$

Equation (3.62) indicates that optimal ML combining corresponds to the flowing receiver description. The inner sum indicates that you combine $r_{m,n}^{(l)}$'s across carriers first to create $R_m^{(l)}$'s, where each $r_{m,n}^{(l)}$ is weighted by $\frac{\alpha_n}{\sigma_{m,n}^2}$; the outer sum indicates that next you combine $R_m^{(l)}$'s across chips in a usual DS-CDMA manner. The ><sign indicates that you conclude with a hard decision on $R_m^{(l)}$.

The optimal ML combining in equation (3.62) can be rewritten as

$$D^{(l)} = \sum_{m=0}^{N-1} R_m^{(l)} \beta_m^{(l)} \tag{3.63}$$

where

$$R_m = \sum_{n=0}^{N-1} r_{m,n}^{(l)} \cdot A_n^{ML} \tag{3.64}$$

and

$$A_n^{ML} = \frac{\alpha_n}{K(P_n - 1)\alpha_n^2 + \frac{N_0}{2}} \tag{3.65}$$

Hence, we find that: (1) the ML criteria justifies separating the receiver design into two stages: frequency combining first across carriers (Figure 3.4 (b)) then time combining across chips (Figure 3.4(a)); and (2) MMSE combing (equation (3.31)) is very close to MLC (equation (3.65)). This explains why MMSE combining provides better BER performance than other combining schemes.

Case II: assuming knowledge of the intended user's spreading code

Similarly, if we know the spreading code of the user under consideration, equation (3.51) can be rewritten as

$$P(r_{m,n}^{(l)}|b_l) = P(r_{m,n}^{(l)}\beta_m^{(l)} = \alpha_n b_l + \alpha_n b_l \sum_{i \neq m} \beta_i^{(l)} \beta_m^{(l)} \cos(nm\frac{2\pi}{N} - ni\frac{2\pi}{N}) + \eta''_{m,n}) \tag{3.66}$$

$$P(r_{m,n}^{(l)}|b_l) = P(r_{m,n}^{(l)}\beta_m^{(l)} = \alpha_n b_l (1 + \sum_{i \neq m} \beta_i^{(l)} \beta_m^{(l)} \cos(nm\frac{2\pi}{N} - ni\frac{2\pi}{N})) + \eta''_{m,n}) \tag{3.67}$$

where $\eta''_{m,n}$ encompasses the last four terms on the right hand side of equation (3.51), i.e., $\eta''_{m,n}$ is a Gaussian random variable with 0 mean and variance

$$\sigma_{m,n}^2 = \alpha_n^2 (K-1) P_n + \frac{N_0}{2} \tag{3.68}$$

The ML combining corresponds to

$$\sum_m \{\beta_m^{(l)} [\sum_n \frac{r_{m,n}\alpha_n (1 + \sum_{i \neq m} \beta_i^{(l)} \beta_m^{(l)} \cos(nm\frac{2\pi}{N} - ni\frac{2\pi}{N})}{\alpha_n^2 (K-1) P_n + \frac{N_0}{2}}]\} >< 0 \tag{3.69}$$

Compare equation (3.69) with MMSEC in equation (3.34), we also find that MLC is very close to MMSEC.

3.4 Channel Model for Simulation

The multipath fading channel model used to assess the performance of the CI/DS-CDMA system is the Hilly Terrain (HT) channel and Typical Urban (TU) channel taken from the COST-207 GSM standard [57]. These two channel models are defined as a transversal filter with time varying coefficients whose average power is determined by the multipath power delay profile (PDP) given in Table 3.1 and Table 3.2.

Tap No.	$\tau(\mu s)$	Average power (dB)
1	0.0	0.0
2	0.2	-2.0
3	0.4	-4.0
4	0.6	-7.0
5	15.0	-6.0
6	17.2	-12.0

Table 3.1 Multipath Power Delay Profiles for the HT channel

Tap No.	$\tau(\mu s)$	Average power (dB)
1	0.0	-3.0
2	0.2	0
3	0.5	-2.0
4	1.6	-6.0

5	2.3	-8.0
6	5.0	-10.0

Table 3.2 Multipath Power Delay Profiles for the TU channel

We assume bandwidth consistent with the GSM standard. That is, we choose chip duration T_c=3.69 μs and hence bandwidth $BW = 270.8kHz$. For such a DS-CDMA system, the HT channel is a two path Rayleigh fading channel (path 1-4 in the HT power delay profile converge to one path, and path 5 and 6 converge to the second path). The average power of the second path is 8.5 dB lower than the first. And the TU channel is a two path Rayleigh fading channel (path 1-5 in the TU power delay profile converge to one path, and path 6 converges to the second path). The average power of the second path is 14 dB lower than the first.

In a DS-CDMA system with CI chip shapes, the chip shapes consist of multiple carrier transmissions (frequency separated at the receiver). In this case, the channel must be characterized in the frequency domain by $(\Delta f)_c$, the coherence bandwidth (defined here as the bandwidth over which the frequency correlation function is above 0.5). This can be computed from a multipath power delay profile by using the approximate relationship [2]

$$(\Delta f)_c \cong \frac{1}{5\sigma_\tau} \tag{3.70}$$

where σ_τ is the rms delay spread and is computed according to

$$\sigma_\tau = \sqrt{\overline{\tau^2} - \left(\overline{\tau}\right)^2} \tag{3.71}$$

$$\overline{\tau^2} = \frac{\sum_{l=0}^{L-1} \alpha_l^{\,2} \tau_l^{\,2}}{\sum_l \alpha_l^{\,2}} \tag{3.72}$$

$$\bar{\tau} = \frac{\sum_{l=0}^{L-1} \alpha_l^{\,2} \tau_l}{\sum_l \alpha_l^{\,2}} \tag{3.73}$$

Here, α_l^2 is the power of the multipath component arriving at delay τ_l. This leads to the following coherence bandwidth result: for the HT channel model of Table 3.1, $(\Delta f)_c$ = 39.72 KHz and for the TU channel model of Table 3.2, $(\Delta f)_c$= 178.01 KHz. These $(\Delta f)_c$ values satisfy

$$\Delta f << (\Delta f)_c < BW \tag{3.74}$$

where $BW = 1/T_c$ is the total bandwidth of the system. Equation (4.54) indicates that the HT channel and TU channel are frequency selective over the entire bandwidth of transmission, but not over each carrier [1][58]. Specifically, with N carriers residing over the entire bandwidth, BW, each carrier undergoes a flat fade, with the correlation between the i^{th} subcarrier fade and the j^{th} subcarrier fade characterized by [1][58]

$$\rho_{i,j} = \frac{1}{1 + ((f_i - f_j)/(\Delta f)_c)^2} \tag{3.75}$$

where $(f_i\text{-}f_j)$ indicates the frequency separation between the i^{th} and the j^{th} subcarriers. Generation of fades with correlation has been discussed in [59].

3.5 Simulation Results: Performance Improvement

CI/DS-CDMA is simulated using the HT channel model of section 4.4. (Please note that simulations over other channel models [60-68] have been conducted, and results are consistent with the HT results presented here.) Results for a conventional DS-CDMA system with a RAKE receiver are generated to form a benchmark for comparison.

We assume a synchronous downlink channel (or, equivalently, an uplink channel where synchronousity is maintained). To make a fair comparison, we assume the processing gains are 32 for all systems and each uses Hadamard-Walsh codes in all simulations. All simulations are performed with a fully loaded system.

Figure 3.5 presents bit error probability (BER) versus SNR performance curves for the HT channel. The line marked with circles represents the CI/DS-CDMA system with MMSE combining at the receiver, and the line marked with stars represents the benchmark DS-CDMA system. From the figure, traditional DS-CDMA's BER floor, due to inter-path interference in the RAKE receiver branches, severely limits its performance. The proposed CI/DS-CDMA system with MMSEC combining suppresses this floor. By employing frequency diversity, CI/DS-CDMA achieves performance gains on the order of 14 dB at BER=$8 \cdot 10^{-3}$.

Figure 3.6 compares the BER results of traditional DS-CDMA with a CI/DS-CDMA system using EGC combining. From the figure we observe CI/DS-CDMA, even with the low complexity EGC combining, achieves much better performances than DS-CDMA.

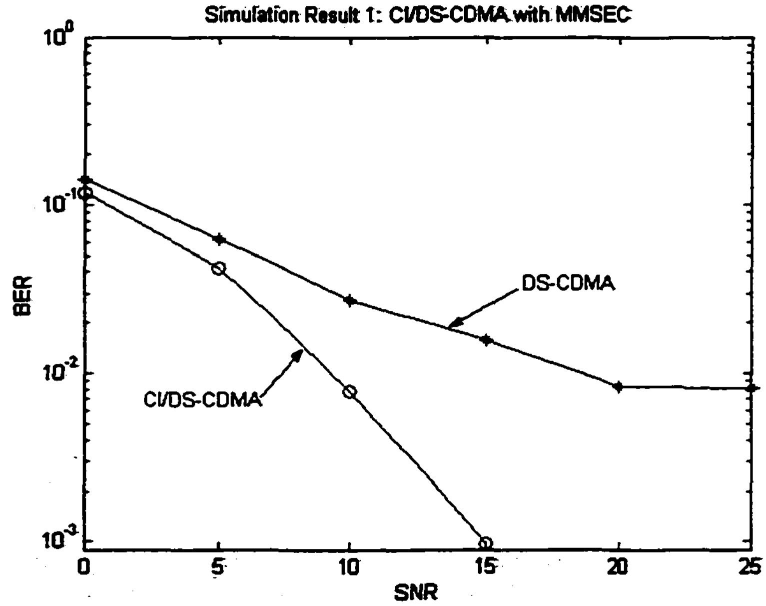

Figure 3.5 Simulation Result 1: CI/DS-CDMA with MMSEC vs DS-CDMA

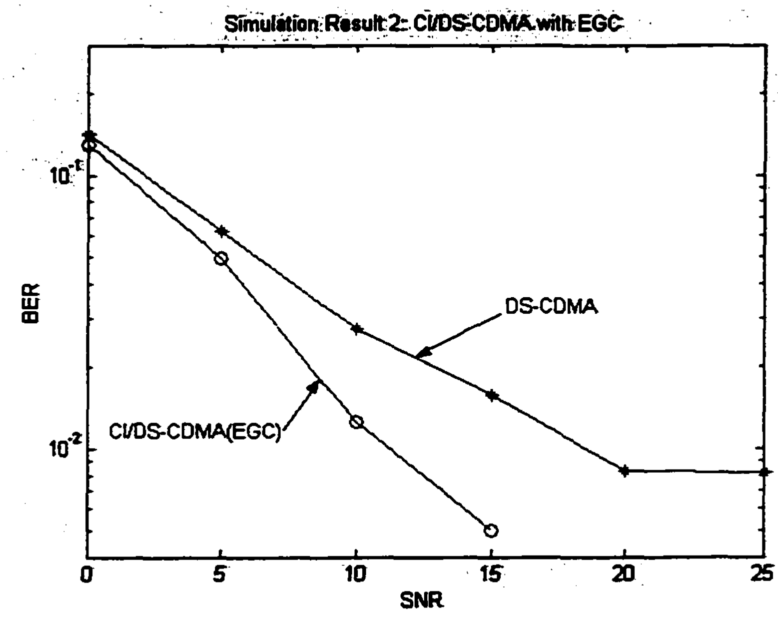

Figure 3.6 Simulation Result 2: CI/DS-CDMA with EGC vs DS-CDMA

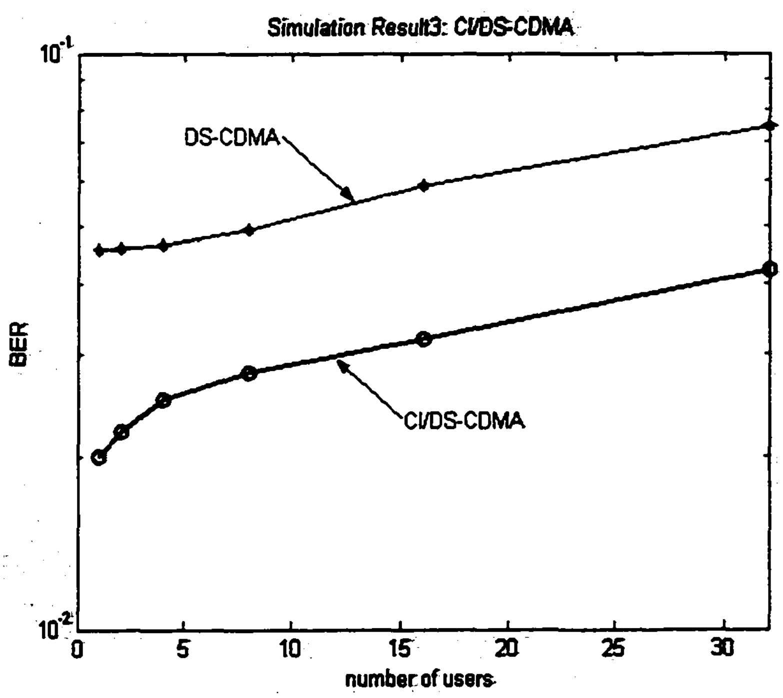

Figure 3.7 Simulation Result 3: CI/DS-CDMA vs DS-CDMA (SNR=5dB)

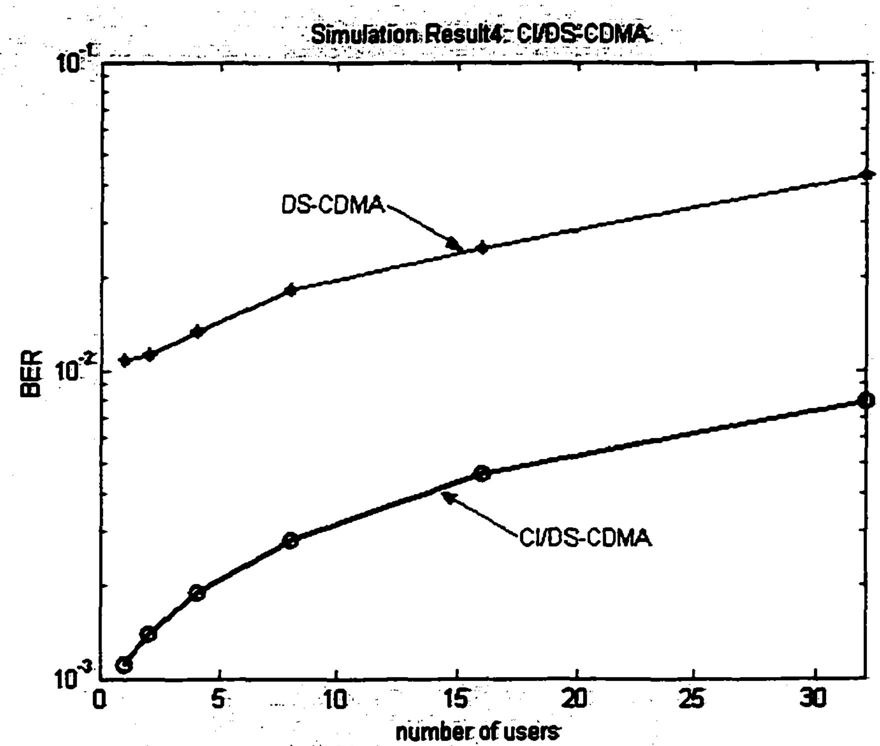

Figure 3.8 Simulation Result 4: CI/DS-CDMA vs DS-CDMA (SNR=10dB)

Figure 3.7 presents the BER performance versus network capacity (in terms of number of users) for CI/DS-CDMA and DS-CDMA system in HT channel at SNR=5dB. Figure 3.8 presents the same results for SNR=10dB. From these figures, it is apparent that CI/DS-CDMA outperforms DS-CDMA system significantly.

Figure 3.9 compares different combining schemes for CI/DS-CDMA system in HT channel. It is evidenced from this figure that MMSEC outperforms other combining schemes.

Figure 3.10 to Figure 3.13 show the simulation results for TU channel. Similar result is observed in TU channel.

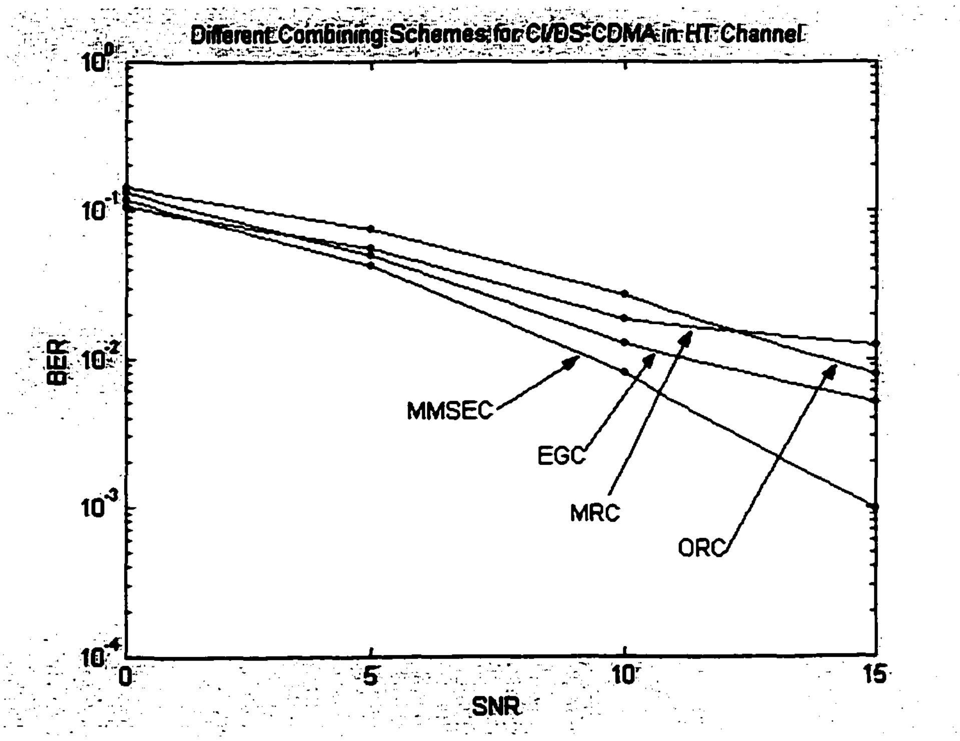

Figure 3.9 Different Combining Schemes for CI/DS-CDMA in HT Channel, Fully Loaded

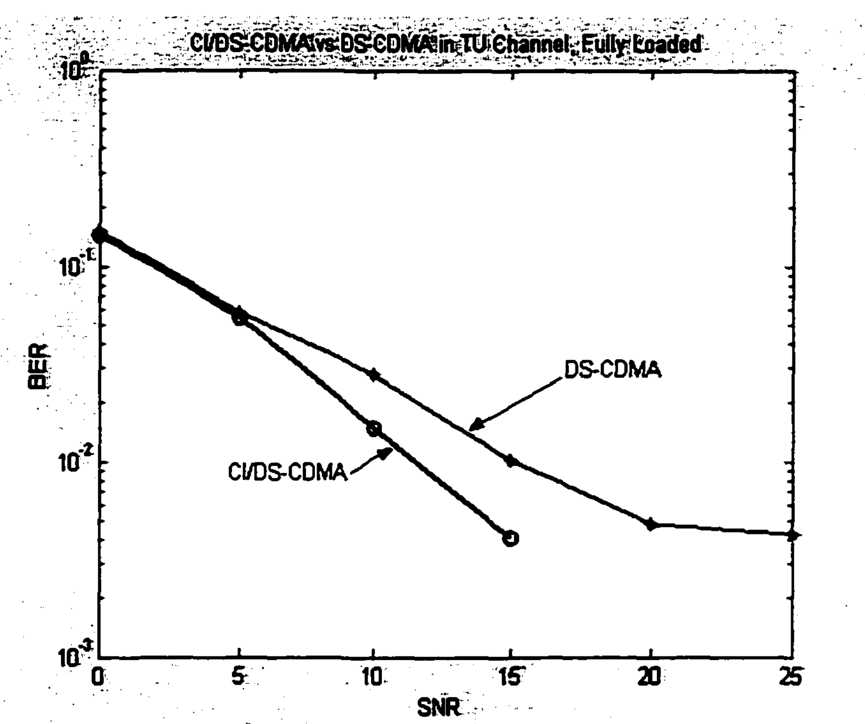

Figure 3.10 CI/DS-CDMA in TU Channel, Fully Loaded, MMSEC

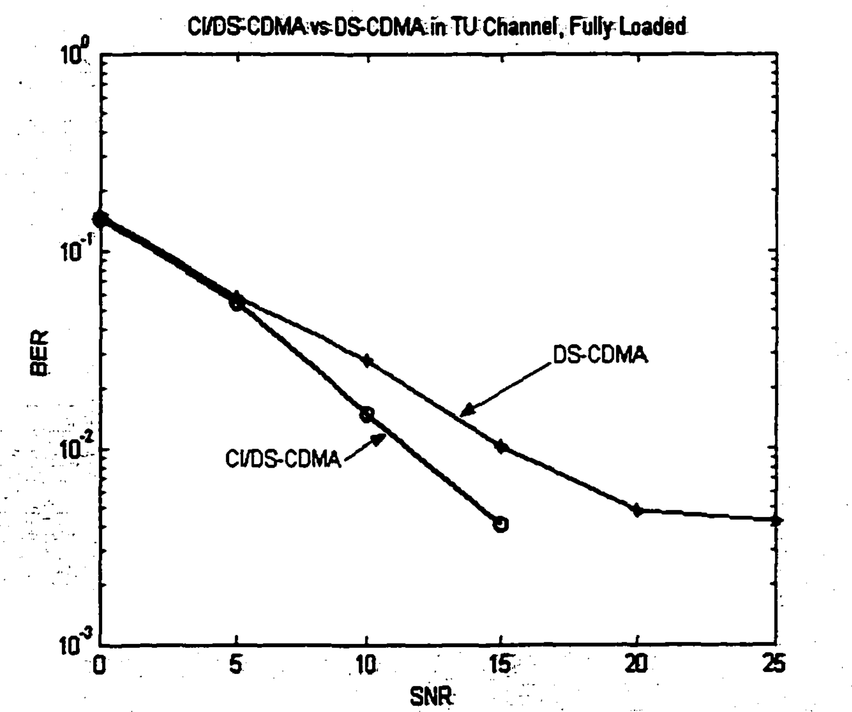

Figure 3.11 CI/DS-CDMA in TU Channel, Fully Loaded, EGC

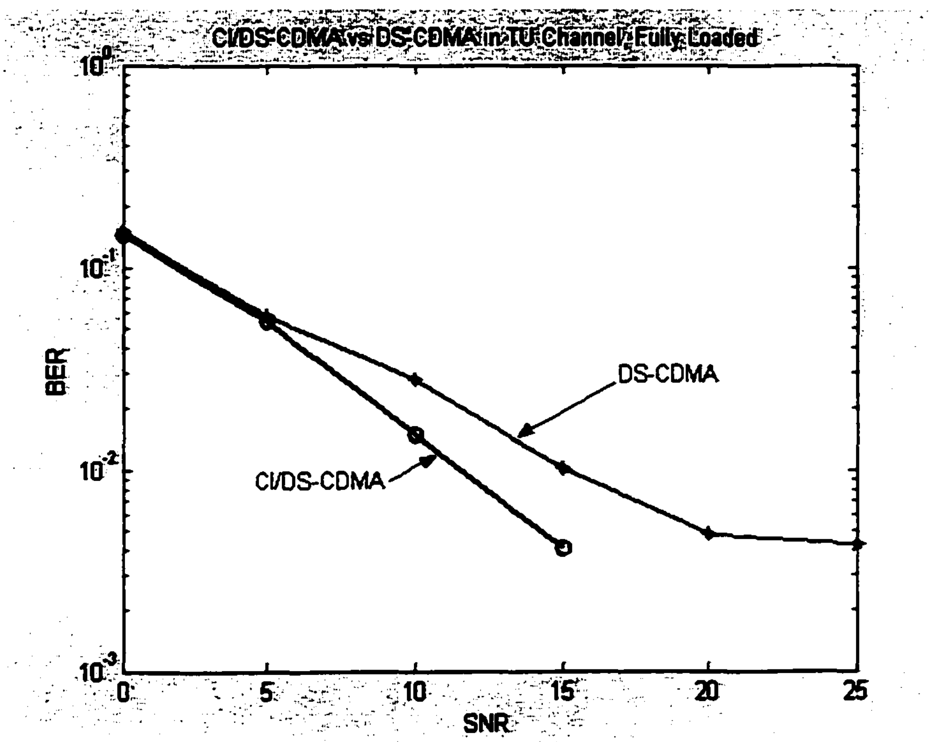

Figure 3.12 CI/DS-CDMA in TU Channel (SNR=10dB)

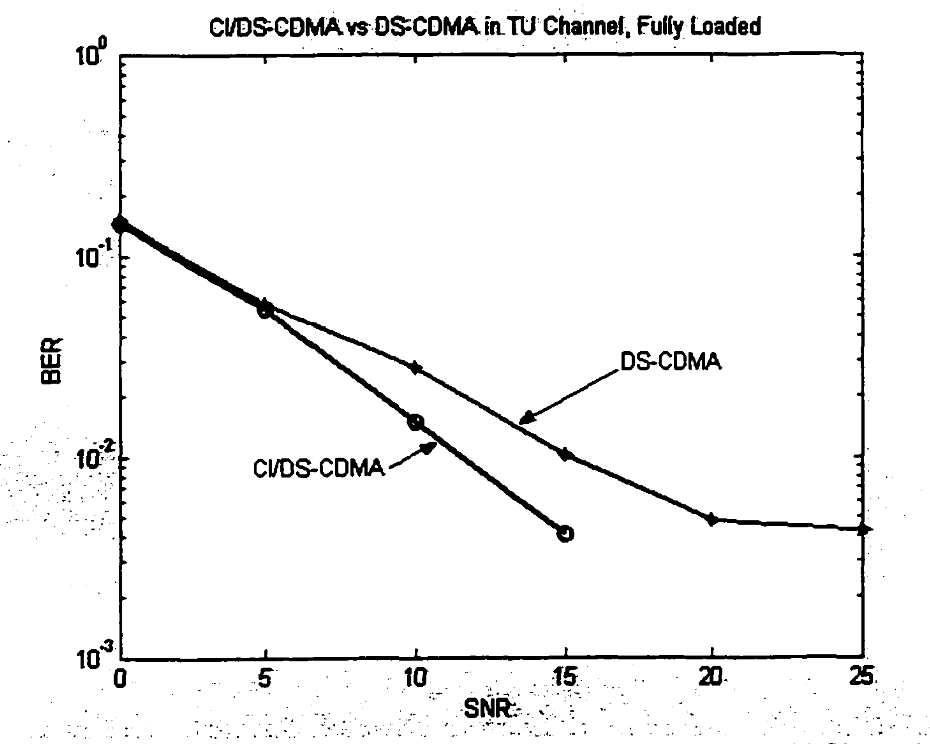

Figure 3.13 Different Combining Schemes for CI/DS-CDMA in TU Channel, Fully Loaded

3.6 High-Capacity DS-CDMA via CI Chip Shaping

In previous sections we have already shown how novel CI chip shaping technology can bring significant performance gain into current DS-CDMA systems. We now continue to demonstrate the power of CI chip shaping in DS-CDMA to increase the network capacity of DS-CDMA systems [39][42][69]. Here, we introduce the concept of pseudo-orthogonal chip shaping. Specifically, a second set of N CI chips (where N is the processing gain) were sent out with the original DS-CDMA N chips set (the two sets of chips were sent within the same symbol duration to support more users). Each set of these N chip sets is an orthogonal set; that is, every chip within one chip set is orthogonal to all other chips in the same set. However, the two chips sets are pseudo-orthogonal to each other, i.e., a chip in orthogonal chip set 1 is pseudo-orthogonal to a chip in orthogonal chip set 2. The positioning of the new (second) N chips set was based on minimum mean square cross correlation criteria.

3.6.1 Transmitter

In CI/DS-CDMA, a chip shape is created by superpositioning N carriers equally spaced in frequency by $\Delta f=1/T_s$ (where N corresponds to the processing gain in traditional DS-CDMA, and T_s is the symbol duration). That is, the CI chip shape corresponds to

$$h(t)=\sum_{n=0}^{N-1} A\cos(2\pi n\Delta f t) \qquad 0\le t<T_s \tag{3.76}$$

It is important to note that these chips, referred to as CI chips, satisfy the usual orthogonality condition $\int_0^{T_s} h(t-pT_c)h(t-qT_c)dt=0\ \ (p\neq q)$. That is, the N chip set $\{h(t),h(t-T_c),\cdots,h(t-(N-1)T_c)\}$ is an orthogonal set.

Now, consider a second set of N CI chip shapes, namely $\{h(t-\tau),h(t-T_c-\tau),\cdots,h(t-(N-1)T_c-\tau)\}$. These N chips are time delayed by $\tau\in[0,T_c)$ with respect to the original N chips set $\{h(t),h(t-T_c),\cdots,h(t-(N-1)T_c)\}$. Since the chips in the first set are orthogonal to one another, it is obvious that the chips in the second set are also orthogonal to each other, i.e.,

$$\int_0^{T_s} h(t-pT_c-\tau)h(t-qT_c-\tau)dt=0\ \ (p\neq q) \tag{3.77}$$

To double network capacity in DS-CDMA, we propose that the second set of N orthogonal CI chip shapes be sent out simultaneously with the original N-chip set. With two sets of CI chip shapes, we can support two groups of N users each.

However, even though the N CI chip shapes that make up each set are orthogonal to one another, the CI chips in the first set and the CI chip shapes in the second set are *not* orthogonal to one another. There exists a cross correlation between the chip shapes from different sets.

We now determine the value τ in the second CI chips set such that there exists a minimum average cross-correlation between the sets. Let $R_{1,2}(j,k)$ denote the cross correlation between the j^{th} chip in chip set 1 $(\tau=0)$ and the k^{th} chip in chip set 2 (constructed with $\tau=\tau$). Also, let

$$R_{1,2} = [\frac{1}{N^2}\sum_{j=0}^{N-1}\sum_{k=0}^{N-1}(R_{1,2}(j,k))^2]^{\frac{1}{2}} \tag{3.78}$$

represent the root mean square cross correlation that exists between chip shapes in set *1* and set *2*. We seek to find the two sets of chip shapes (i.e., the τ value) that minimizes $R_{1,2}$. Now, it is easily shown that

$$\begin{aligned} R_{1,2}(j,k) &= \frac{1}{2\Delta f}\sum_{i=0}^{N-1}\cos[\ i(\theta_j - (\theta_k + 2\pi\Delta f\tau))] \\ &= \frac{1}{2\Delta f}\sum_{i=0}^{N-1}\cos[\ i(\frac{2\pi}{N}j - \frac{2\pi}{N}k - 2\pi\Delta f\tau)] \end{aligned} \tag{3.79}$$

It is also easily shown that

$$\sum_{j=0}^{N-1}(R_{1,2}(j,k))^2 = \sum_{j=0}^{N-1}(R_{1,2'}(j,k'))^2 \tag{3.80}$$

That is, the total cross-correlation between the k^{th} chip in orthogonal chip set 2 and all chips in set 1 is identical to the cross-correlation between the $(k')^{th}$ chip in chip set 2 and all chips in set 1. Using equation (3.80), we rewrite equation (3.78) as

$$R_{1,2} = [\frac{1}{N}\sum_{j=0}^{N-1}(R_{1,2}(j,0))^2]^{\frac{1}{2}} \tag{3.81}$$

and, using equation (3.79), this becomes

$$R_{1,2} = [\frac{1}{N}\sum_{j=0}^{N-1}[\frac{1}{2\Delta f}\sum_{i=0}^{N-1}\cos[\, i(\frac{2\pi}{N}j - 2\pi\Delta f\tau)]]^2]^{\frac{1}{2}} \tag{3.82}$$

We now determine the selection of $2\pi\Delta f\tau$, which we refer to as θ, minimizing the root mean square correlation between the two chip sets. To do this, we seek the θ value that solves

$$\frac{\partial R_{1,2}}{\partial \theta} = 0 \tag{3.83}$$

Now,

$$\frac{\partial R_{1,2}}{\partial \theta} = \frac{1}{2}[\frac{1}{N}\sum_{j=0}^{N-1}(R_{1,2}(j,0))^2]^{-\frac{1}{2}}\frac{1}{N}\frac{\partial[\sum_{j=0}^{N-1}(R_{1,2}(j,0))^2]}{\partial \theta} \tag{3.84}$$

$$\frac{\partial R_{1,2}}{\partial \theta} = \frac{1}{2}[\frac{1}{N}\sum_{j=0}^{N-1}(R_{1,2}(j,0))^2]^{-\frac{1}{2}}\frac{1}{N}\cdot I \tag{3.85}$$

where

$$I = \frac{\partial[\sum_{j=0}^{N-1}(R_{1,2}(j,0))^2]}{\partial \theta} \tag{3.86}$$

$$I=\frac{\partial[\sum_{j=0}^{N-1}(\sum_{i=0}^{N-1}\cos[i(\frac{2\pi}{N}j-\theta)])^2]}{\partial\theta} \tag{3.87}$$

Now,

$$I=\sum_{j=0}^{N-1}2\left[\sum_{i=0}^{N-1}\cos[i(\frac{2\pi}{N}j-\theta)]\right]\cdot\left[\sum_{k=0}^{N-1}k\sin[k(\frac{2\pi}{N}j-\theta)]\right] \tag{3.88}$$

$$I=\sum_{j=0}^{N-1}\sum_{i=0}^{N-1}\sum_{k=0}^{N-1}2k\cos[i(\frac{2\pi}{N}j-\theta)]\sin[k(\frac{2\pi}{N}j-\theta)] \tag{3.89}$$

$$I=\sum_{j=0}^{N-1}\sum_{i=0}^{N-1}\sum_{k=0}^{N-1}k\left\{\sin[(k+i)(\frac{2\pi}{N}j-\theta)]+\sin[(k-i)(\frac{2\pi}{N}j-\theta)]\right\} \tag{3.90}$$

$$I=\mathrm{Im}(\sum_{j=0}^{N-1}\sum_{i=0}^{N-1}\sum_{k=0}^{N-1}k\{e^{j(k+i)(\frac{2\pi}{N}j-\theta)}+e^{j(k-i)(\frac{2\pi}{N}j-\theta)}\}) \tag{3.91}$$

$$I=\mathrm{Im}(\sum_{i=0}^{N-1}\sum_{k=0}^{N-1}ke^{-j(k+i)\theta}\sum_{j=0}^{N-1}e^{j\frac{2\pi}{N}j(k+i)}+\sum_{i=0}^{N-1}\sum_{k=0}^{N-1}ke^{-j(k-i)\theta}\sum_{j=0}^{N-1}e^{j\frac{2\pi}{N}j(k-i)}) \tag{3.92}$$

$$I=\mathrm{Im}(\sum_{i=0}^{N-1}\sum_{k=0}^{N-1}ke^{-j(k+i)\theta}\delta(k+i-N)N+\sum_{i=0}^{N-1}\sum_{k=0}^{N-1}ke^{-j(k-i)\theta}\delta(k-i)N) \tag{3.93}$$

$$I=\mathrm{Im}(\sum_{i=0}^{N-1}(N-i)e^{-jN\theta}+\sum_{i=0}^{N-1}i)N \tag{3.94}$$

From (3.94), when $\theta=\frac{k\pi}{N}, k=0,1,2,\ldots$, we have $I=0$ and, therefore, from equation (3.85), $\frac{\partial R_{1,2}}{\partial\theta}=0$.

Seeking to determine which $\theta = \frac{k\pi}{N}, k = 0,1,2,...$ are maxima and which are minima, we calculate the second order partial derivative at $\theta = \frac{k\pi}{N}$ and determine:

$$\begin{aligned} \frac{\partial R^2}{\partial^2 \theta} > 0 \quad & when \quad \theta = \frac{(2k+1)\pi}{N} \\ \frac{\partial R^2}{\partial^2 \theta} < 0 \quad & when \quad \theta = \frac{2k\pi}{N} \end{aligned} \tag{3.95}$$

Hence, $\theta = \frac{2k\pi}{N}$ corresponds to maxima and $\theta = \frac{(2k+1)\pi}{N}$ provides minima. Selecting $k=0$, we choose $\theta = \frac{\pi}{N}$ as our minima. Figure 3.14 plots the root mean square cross correlation, $R_{1,2}$ as a function of θ, verifying our selection of $\theta = \frac{\pi}{N}$ as a minima.

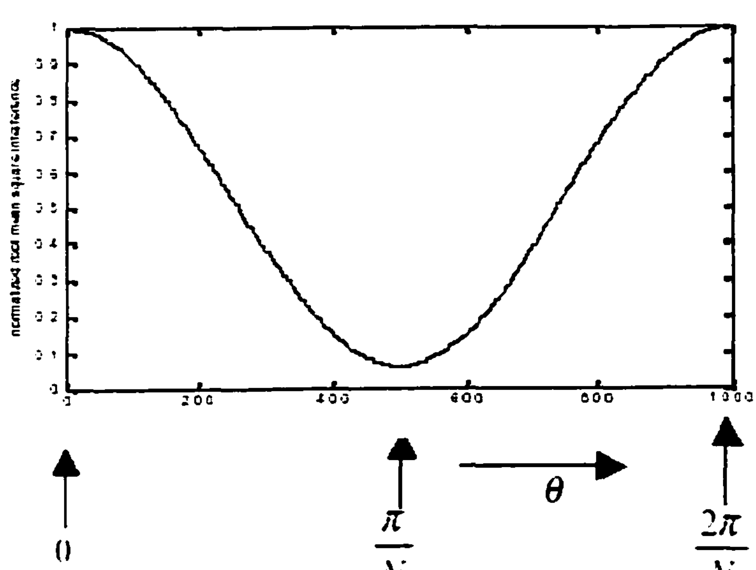

Figure 3.14: Root Mean Square Cross Correlation versus θ

Hence, if we have one set of N orthogonal CI chip shapes, and we want to increase system capacity to $2N$ users, we can introduce a second set of N orthogonal CI chip shapes. To best do that, in a minimum inter-chip interference sense, introduce a second set of CI chip shapes with phase offset by $\theta = \frac{\pi}{N}$ with respect to the first set of CI chip shapes. Remembering that $\theta = 2\pi\Delta f\tau$, the selection of $\theta = \frac{\pi}{N}$ leads to

$$\tau = \theta / 2\pi\Delta f = T_c / 2 \tag{3.96}$$

That is, the second set of CI chip shapes with minimum cross correlation to the original set of CI chip shapes is just the time delayed version of the original set with delay corresponding to a half chip duration delay.

With these two sets of N CI chip shapes each, two groups of N users can be supported simultaneously in the DS-CDMA system. The first group of N users spreads its data bits over the first set of N CI chips and the second group uses the second set. The total transmit signal in a CI/DS-CDMA system supporting all $2N$ users corresponds to

$$S(t) = \sum_{k=0}^{N-1} b_k c_k^1(t) + \sum_{k=N}^{2N-1} b_k c_k^2(t) \tag{3.97}$$

$$S(t) = \sum_{k=0}^{N-1} b_k \left[\sum_{i=0}^{N-1} \beta_i^{(k)} h(t - iT_c) \right] + \sum_{k=N}^{2N-1} b_k \left[\sum_{i=0}^{N-1} \beta_i^{(k)} h(t - iT_c - T_c/2) \right] \tag{3.98}$$

$$S(t)=\sum_{k=0}^{N-1} b_k \sum_{i=0}^{N-1} \beta_i^{(k)} \sum_{n=0}^{N-1} A\cdot\cos(2\pi f_c t+2\pi n\Delta f t-2\pi n i/N)g(t)$$
$$+\sum_{k=N}^{2N-1} b_k \sum_{i=0}^{N-1} \beta_i^{(k)} \sum_{n=0}^{N-1} A\cdot\cos(2\pi f_c t+2\pi n\Delta f t-2\pi n i/N-n\pi/N)g(t) \tag{3.99}$$

3.6.2 Receiver

The receiver for the novel CI/DS-CDMA system with two sets of chips is consistent with the receiver structure in section 3.2. This receiver is detailed next.

Assuming a Rayleigh frequency-selective slow fading channel (typical of wideband DS-CDMA), frequency selectivity exists over the entire bandwidth, but not over the individual carriers that make up the CI chip shape. Hence, each frequency component making up the CI chip shape experiences a unique flat fade. That is, the received signal (assuming the transmit signal in equation (3.99)) is characterized by:

$$r(t)=\sum_{k=0}^{N-1} b_k \sum_{i=0}^{N-1} \beta_i^{(k)} \sum_{n=0}^{N-1} A\alpha_n \cos(2\pi f_c t+2\pi n\Delta f t-ni2\pi/N+\phi_n)g(t)$$
$$+\sum_{k=N}^{2N-1} b_k \sum_{i=0}^{N-1} \beta_i^{(k)} \sum_{n=0}^{N-1} \alpha_n A\cos(2\pi f_c t+2\pi n\Delta f t-ni2\pi/N-n\pi/N+\phi_n)+\eta(t)$$

(3.100)

where α_n is the gain and ϕ_n the phase offset in the n^{th} carrier of the CI chip shape (due to the channel fade), and $\eta(t)$ represents additive white Gaussian noise. To simplify the analysis, exact phase synchronization is assumed.

Consistent with Figure 3.4, the CI/DS-CDMA receiver with two sets of chips consists of three main components: (1) the incoming CI/DS-CDMA is separated into its N chip components, and each chip is decomposed into its carriers and recombined to exploit frequency diversity and minimize inter-chip interference and noise; (2) the newly recreated CI chips are despread and linearly combined to eliminate the presence of other users, in the usual DS-CDMA fashion; and (3) a hard decision device creates the final decision. Here, when the m^{th} chip is separated into its N carrier components, the n^{th} carrier contributes one decision variable $r_{m,n}^{(l)}$ corresponding to

$$\begin{aligned} r_{m,n}^{(l)} &= \sum_{k=0}^{N-1} b_k \sum_{i=0}^{N-1} \beta_i^{(k)} \alpha_n \cos(nm2\pi/N - ni2\pi/N) \\ &+ \sum_{k=N}^{2N-1} b_k \sum_{i=0}^{N-1} \beta_i^{(k)} \alpha_n \cos(nm2\pi/N - ni2\pi/N - n\pi/N) + \eta_{m,n} \end{aligned} \tag{3.101}$$

Minimum Mean Square Error Combining (MMSEC) is employed as a frequency combiner which attempts to jointly minimize the inter chip interference and noise *and* achieve maximum frequency diversity:

$$R_m^{(l)} = \sum_{n=0}^{N-1} r_{m,n}^{(l)} \cdot \frac{\alpha_n}{KP_n\alpha_n^2 + N_0/2} \tag{3.102}$$

where

$$P_n = \begin{cases} \dfrac{N}{2} & n = 1,2,\ldots N-1 \\ N & n = 0 \end{cases} \tag{3.103}$$

After the frequency combining, we create a final decision variable for user l by combining across chips in the usual DS-CDMA fashion (see Figure 3.4).

3.7 Simulation Results for High-Capacity CI/DS-CDMA

To demonstrate the proposed CI/DS-CDMA system's ability to double network capacity, we again employ the Hilly Terrain channel from the COST-207 GSM standard described in section 3.4, and we assumed bandwidth consistent with GSM, i.e., BW=270.8 KHz and hence chip duration T_c=3.69 μs [57].

We assume a total of N=32 orthogonal chips located in symbol duration T_s. In traditional DS-CDMA, capacities can be increased by use of pseudo-orthogonal codes. Thus, benchmark results are generated using the following systems: (1) a traditional DS-CDMA system with a RAKE receiver using N=32 Hadamard-Walsh codes and (2) traditional DS-CDMA using pseudo-orthogonal codes where the first 33 users use one set of Gold codes and the next 32 users use a second set of Gold codes (for a total capacity of 65 users). We assume a synchronous downlink channel.

In Figure 3.15, the curve marked with asterisks represents the performance of traditional DS-CDMA with Gold codes, while the curves marked with circles represents the performance of DS-CDMA with Hadamard-Walsh codes. The curves marked with dots represents the performance of the proposed CI/DS-CDMA system with two chip sets of size N=32 chips each. For $K \leq 32$ users, the performance benefits of CI/DS-CDMA over traditional DS-CDMA confirms that energy harnessed from a frequency domain combining (creating frequency diversity benefits) provides greater benefit than the time domain combining based on the RAKE receiver structure. The ability to locate the second set of CI chip shapes results in the ability to support an extra 32 users, doubling network capacity without any increase in bandwidth or loss in throughput. Even when doubling the network capacity of the system, the CI/DS-CDMA with two N=32 chip sets still *outperforms* conventional DS-CDMA systems with Hadamard-Walsh codes and RAKE reception. It is apparent from Figure 3.15 that CI/DS-CDMA supporting 64 users provides the same BER performance as a traditional DS-CDMA system with only 16 users.

In traditional DS-CDMA, network capacities can be increased by use of pseudo-orthogonal codes. Referring to Figure 3.15, it is evident that the use of pseudo-orthogonal CI chips offers a performance far better than that achieved by use of pseudo-orthogonal codes (for comparable network capacity). The CI/DS-CDMA system supporting 64 users has the same BER performance of a DS-CDMA system using Gold codes and supporting only 6 users.

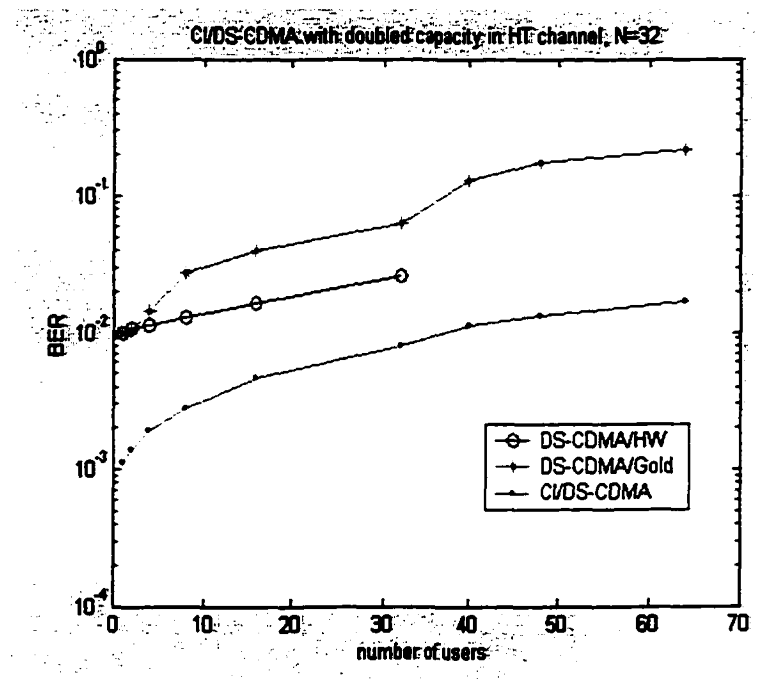

Figure 3.15 BER Performance of CI/DS-CDMA with two sets of CI chip shapes

3.8 Conclusions

In this chapter, the novel CI chip shaping method is investigated and is shown to support the DS-CDMA architecture with improved performance and increased network capacity. This multi-carrier scheme does not require a RAKE receiver. Instead, using suitable combining strategies at the receiver, the system exploits frequency diversity benefits that are inherent in the proposed multi-carrier chip shaping. Simulation results show dramatically improved BER performance when the new architecture is applied (when compared to a traditional DS-CDMA system). By introducing pseudo-orthogonal chips into the system, we demonstrate increases in the network capacity of the system by 100% while outperforming traditional DS-CDMA.

Chapter 4 DS-CDMA with CI Spreading Codes

In today's DS-CDMA systems, Hadamard-Walsh (HW) codes are employed as spreading codes in the downlink to maintain the orthogonality between users. However, after transmission through multipath fading channels, interference arises between different paths, leading to MPI (multi-path interference) in the DS-CDMA RAKE receiver. This, in turn, degrades the DS-CDMA system's probability of error performance. In this chapter, we propose a set of novel complex spreading codes called Carrier Interferometry (CI) codes, and we demonstrate how these novel *orthogonal* spreading codes achieve crosscorrelations independent of the phase offsets between different paths (after transmission over a multipath fading channel) [44][45]. This improved crosscorrelation property (relative to HW codes) leads to higher SIR in the DS-CDMA RAKE receiver, and, as a direct result, better performances in terms of probability-of-error.

As the name suggests, CI spreading codes are related to CI chip shape (Chapter 3). Specifically, the delay applied to create each multi-carrier CI chip shape can be represented as a group of phase offset. This group of phase offset in turn corresponds to a complex spreading code – the CI spreading codes. While we choose not to present CI spreading codes from this standpoint in this chapter, it is important to note that CI chip shape and CI spreading codes are closely related.

4.1 Introduction

In the DS-CDMA downlink, the transmitter typically employs orthogonal spreading codes, namely Hadamard-Walsh codes (layered with an m-sequence) to maintain orthogonality between users. At the receiver side, to improve performance, DS-CDMA systems use RAKE receivers to exploit the available path diversity. However, it is difficult for the DS-CDMA RAKE receiver to fully benefit from the path diversity and make efficient use of the received signal energy scattered in the time domain. This is because the multi-path effect that induces path diversity also causes multi-path interference (leading to lowered SIR). As a direct result, BER performance of DS-CDMA is degraded.

In this chapter, we introduce and apply CI codes to DS-CDMA. We investigate the SIR (signal to interference ratio) at the DS-CDMA RAKE receiver when the transmitter uses CI codes, and we compare this to the SIR when Hadamard-Walsh codes are used. We show that the partial cross-correlations of CI codes (after transmission over a multipath fading channel) are independent of phase offsets between different paths.

(When Hadamard-Walsh codes are used, the partial cross-correlations are related to the squared cosine of path phase offsets.) As a direct result, DS-CDMA systems using CI codes demonstrate better performance in term of probability of error than DS-CDMA systems using Hadamard-Walsh codes (and other spreading codes) [44].

4.2 Carrier Interferometry Spreading Codes

In DS-CDMA, each user's information bit is spread by multiplication with a unique N-chip code. User k's transmitted signal corresponds to

$$s_k(t) = \mathrm{Re}[A\sum_{n=-\infty}^{\infty} b_k^{(n)} \sum_{i=0}^{N-1} e^{j\beta_i^k} h(t - iT_c - nT_s)] \tag{4.1}$$

where A is constant to ensure a bit energy of unity, $b_k^{(n)} \in \{-1,+1\}$ is the n^{th} data bit of user k, $g(t)$ represents the chip shape, and $e^{j\beta_i^k}$ (typically +1 or -1) is the i^{th} component of user k's spreading sequence. The total transmitted signal considering all users' signals (and assuming downlink or synchronous uplink communications) is:

$$s(t) = \mathrm{Re}[A\sum_{k=0}^{K-1} \sum_{n=-\infty}^{\infty} b_k^{(n)} \sum_{i=0}^{N-1} e^{j\beta_i^k} h(t - iT_c - nT_s)] \tag{4.2}$$

Traditionally, Hadamard-Walsh (HW) codes are employed as spreading codes to maintain orthogonality between different users, i.e., β_i^k is 0 or π ($e^{j\beta_i^k}$ is +1 or −1) and is chosen according to well-known principles.

Here, we propose a novel group of complex spreading codes for DS-CDMA referred to as Carrier Interferometry (CI) codes. These orthogonal codes are generated by allowing the i^{th} component of user k's spreading sequence, $e^{j\beta_i^k}$, to demonstrate phase offset

$$\beta_i^{(k)} = i \cdot k \frac{2\pi}{N} \tag{4.3}$$

To understand the origins of the CI codes, we first look at one interpretation of the well-known HW codes. There exists a well-known transform in the DSP (digital signal processing) literature known as the Walsh-Hadamard Transform (WHT) [70], which enables any discrete-time signal to be decomposed onto a basis of 1's and −1's. This transform corresponds to the operation

$$\bar{X}_N^{WHT} = \mathbf{W}_{N\times N}^{WHT} \bar{x}_N \tag{4.4}$$

where $\bar{X}_N^{WHT}$ is the WHT of $\bar{x}_N$, and

$$\mathbf{W}_{N\times N}^{WHT} = \begin{bmatrix} W^{WHT}(0,0) & W^{WHT}(0,1) & W^{WHT}(0,2) & \cdots & W^{WHT}(0,N-1) \\ W^{WHT}(1,0) & W^{WHT}(1,1) & W^{WHT}(1,2) & \cdots & W^{WHT}(1,N-1) \\ \cdot & \cdot & \cdot & \cdot & \\ \cdot & \cdot & \cdot & \cdot & \\ W^{WHT}(N-1,0) & W^{WHT}(N-1,1) & & \cdots & W^{WHT}(N-1,N-1) \end{bmatrix} \tag{4.5}$$

Here, $W^{WHT}(p,q) = (-1)^{C_{p,q}}$ where $C_{p,q}$ is selected such that each row corresponds to an orthogonal vector (relative to the other rows). Specifically, each rows of $W^{WHT}_{N\times N}$ corresponds to a HW spreading sequence. Hence, HW codes can be understood as rows of the WHT. This expansion of discrete linear transforms to spreading sequences can be extended to transforms other than the WHT. In general, any discrete linear transform can be represented by a matrix $W_{N\times N}$ and the rows of the matrix can be used as orthogonal spreading sequences. Specifically, in this work, we create a new set of spreading sequences based on the DFT (Discrete Fourier Transform):

$$\bar{X}_N = \mathbf{W}^{DFT}_{N\times N}\bar{x}_N \tag{4.6}$$

where $\bar{X}_N$ is the DFT of $\bar{x}_N$, and $\mathbf{W}^{DFT}_{N\times N}$ corresponds to

$$\mathbf{W}^{DFT}_{N\times N} = \begin{bmatrix} W^{DFT}(0,0) & W^{DFT}(0,1) & W^{DFT}(0,2) & \cdots & W^{DFT}(0,N-1) \\ W^{DFT}(1,0) & W^{DFT}(1,1) & W^{DFT}(1,2) & \cdots & W^{DFT}(1,N-1) \\ \cdot & \cdot & \cdot & \cdot & \\ \cdot & \cdot & \cdot & \cdot & \\ W^{DFT}(N-1,0) & W^{DFT}(N-1,1) & & \cdots & W^{DFT}(N-1,N-1) \end{bmatrix} \tag{4.7}$$

Here, $W^{DFT}(p,q) = e^{j\frac{2\pi}{N}p\cdot q}$. The vector corresponding to one row of the DFT is orthogonal to the vector representing a different row, i.e.,

$$\frac{1}{N}\cdot \mathrm{Re}[\sum_{i=0}^{N-1} e^{j(\beta_i^{(k)}-\beta_i^{(k')})}] = 0, k \neq k' \tag{4.8}$$

Hence, rows of the DFT matrix represent a new set of spreading sequences (corresponding to equation (4.3)). We call these sequences CI spreading sequences, where CI refers to Carrier Interferometry, because when these sequences are applied to distinct harmonics, an interferometry pattern is observed.

One of the important features of CI codes is that there exists a set of CI codes of any integer N (since there exists DFT's of any length N), where traditionally only length $N=2^m$ Hadamard-Walsh codes exist (as WH transform exists only for length 2^m).

4.3 SIR Investigation at the RAKE Receiver

Assuming the signal $s(t)$ of equation (4.2) is transmitted over a multipath fading channel at carrier frequency f_c, the signal arriving at the receiver side corresponds to

$$r(t) = \mathrm{Re}[A\sum_{l=0}^{L-1}\alpha_l \sum_{k=0}^{K-1} \sum_{n=-\infty}^{\infty} b_k^{(n)} \sum_{i=0}^{N-1} e^{j\beta_i^k} h(t - iT_c - nT_s - \tau_l) e^{j(2\pi f_c t + \theta_l)}] + \eta(t) \quad (4.9)$$

where L is the total number of paths; α_l is the fading parameter of the l^{th} path; τ_l is the time delay of the l^{th} path, θ_l is the phase offset of the l^{th} path and is assumed to be an i.i.d. random variable uniformly distributed over $[0,2\pi)$; and $\eta(t)$ is the additive white Gaussian noise. Moreover, we label paths such that $\tau_0 < \tau_1 < \tau_2 < \cdots < \tau_{L-1}$.

Considering the RAKE receiver of Figure 2.2, the m^{th} finger's output for user p corresponds to (for detection of bit n=0)

$$
\begin{aligned}
r_m^p &= \sum_{l=0}^{m-1} \alpha_l \operatorname{Re}[e^{j(\theta_l-\theta_m)} \cdot [\sum_k b_k^{(0)} R_{k,p}(T_s-(\tau_m-\tau_l)) + \sum_k b_k^{(+1)} R_{p,k}(\tau_m-\tau_l)]] \\
&+\alpha_m b_p^{(0)} + \alpha_m \sum_{k\neq n} b_k^{(0)} R_{k,n}(0) \\
&+ \sum_{l=m+1}^{L-1} \alpha_l \operatorname{Re}[e^{j(\theta_l-\theta_m)} \cdot [\sum_k b_k^{(-1)} R_{k,p}(\tau_l-\tau_m) + \sum_k b_k^{(0)} R_{p,k}(T_s-(\tau_l-\tau_m))]] \\
&+\eta_m
\end{aligned}
\tag{4.10}
$$

where $b_k^{(-1)}$ is user k's previous data bit, $b_k^{(+1)}$ is user k's next data bit, and $R_{k,p}(T)$ represents the partial cross-correlation of user k and p at time delay $T = q \cdot T_c, (q \in I)$:

$$R_{k,p}(T) = \frac{1}{N} \sum_{i=0}^{q-1} e^{j(\beta_i^p - \beta_{N-q+i}^k)} \tag{4.11}$$

Specifically, when there is no time delay and when orthogonal spreading codes (Hadamard-Walsh codes or CI codes) are employed

$$R_{k,p}(0) = 0 \qquad\qquad k \neq p \tag{4.12}$$

Assuming orthogonal codes, we rewrite equation (4.10) as

$$
\begin{aligned}
r_m^p &= \alpha_m b_p^{(0)} + \sum_{l=0}^{m-1} \alpha_l \operatorname{Re}[e^{j(\theta_l-\theta_m)} \cdot [\sum_k b_k^{(0)} R_{k,p}(T_s-(\tau_m-\tau_l)) + \sum_k b_k^{(+1)} R_{p,k}(\tau_m-\tau_l)\ ]] \\
&+ \sum_{l=m+1}^{L-1} \alpha_l \operatorname{Re}[e^{j(\theta_l-\theta_m)} \cdot [\sum_k b_k^{(-1)} R_{k,p}(\tau_l-\tau_m) + \sum_k b_k^{(0)} R_{p,k}(T_s-(\tau_l-\tau_m))]] + \eta_m
\end{aligned}
\tag{4.13}
$$

In equation (4.12), the first term represents the desired user's signal contribution in the m^{th} path, and the second term and third term represent the multipath interference (MPI) and the fourth term is the noise, represented by a Gaussian random variable with variance $\sigma_{N_m}^2$.

Thus, the SIR of the RAKE receiver's m^{th} finger's output corresponds to

$$SIR_m = \frac{\alpha_i^2}{\sigma_{MPI\,m}^2 + \sigma_{N\,m}^2} \tag{4.14}$$

where $\sigma_{MPI\,m}^2$ represents the power of MPI in m^{th} finger's output (term two and three in equation (4.13)).

When Hadamard-Walsh (HW) codes are used, $\beta_i^{(k)}$ is 0 or π, and hence equation (4.13) becomes

$$\begin{aligned} r_m^p &= \alpha_m b_p^{(0)} + \sum_{l=0}^{m-1} \alpha_l \cos(\theta_l - \theta_m) \cdot \mathrm{Re}[\sum_k b_k^{(0)} R_{k,p}(T_s - (\tau_m - \tau_l)) + \sum_k b_k^{(+1)} R_{p,k}(\tau_m - \tau_l)\ ] \\ &+ \sum_{l=m+1}^{L-1} \alpha_l \cos(\theta_l - \theta_m) \cdot \mathrm{Re}[\sum_k b_k^{(-1)} R_{k,p}(\tau_l - \tau_m) + \sum_k b_k^{(0)} R_{p,k}(T_s - (\tau_l - \tau_m))] + \eta_m \end{aligned} \tag{4.15}$$

Using a Gaussian approximation, the power of MPI for HW codes can be easily shown to be

$$\sigma_{MPI\,m}^2 = E\left[\sum_{\substack{l=0 \\ l \neq m}}^{L-1} \alpha_l^2 \cos^2(\theta_l - \theta_m) \cdot K \cdot (\mathrm{Re}[e^{j(\beta_p^{(k)} - \beta_q^{(k')})}])^2\right] = K \cdot \sum_{\substack{l=0 \\ l \neq m}}^{L-1} \alpha_l^2 \cos^2(\theta_l - \theta_m) P_{HW}$$

(4.16)

where

$$P_{HW} = E[(\mathrm{Re}[e^{j(\beta_p^k - \beta_q^{k'})}])^2] = E[\cos^2(\beta_p^k - \beta_q^{k'})] = \frac{1}{2}\cdot\cos^2(0) + \frac{1}{2}\cos^2(\pi) = 1 \tag{4.17}$$

Thus, the SIR at the m^{th} finger output in the RAKE receiver for HW codes is

$$SIR_m = \frac{\alpha_l^2}{K\cdot\sum_{\substack{l=0\\l\neq m}}^{L-1}\alpha_l^2\cos^2(\theta_l-\theta_m)+\frac{N_0}{2}} \tag{4.18}$$

When CI codes are used, equation (4.10) becomes

$$\begin{aligned} r_m^p = \alpha_m b_p^{(0)} &+ \sum_{l=0}^{m-1}\alpha_l\{\cos(\theta_l-\theta_m)\cdot\mathrm{Re}[\sum_k b_p^{(0)}R_{k,p}(T_s-(\tau_m-\tau_l))+\sum_k b_k^{(+1)}R_{p,k}(\tau_m-\tau_l)\ ] \\ &\qquad +\sin(\theta_l-\theta_m)\cdot\mathrm{Im}[\sum_k b_k^{(0)}R_{k,p}(T_s-(\tau_m-\tau_l))+\sum_k b_k^{(+1)}R_{p,k}(\tau_m-\tau_l)\ ]\} \\ &+\sum_{l=m+1}^{L-1}\alpha_l\{\cos(\theta_l-\theta_m)\cdot\mathrm{Re}[\sum_k b_k^{(-1)}R_{k,p}(\tau_l-\tau_m)+\sum_k b_k^{(0)}R_{p,k}(T_s-(\tau_l-\tau_m))] \\ &\qquad +\sin(\theta_l-\theta_m)\cdot\mathrm{Im}[\sum_k b_k^{(-1)}R_{k,p}(\tau_l-\tau_m)+\sum_k b_k^{(0)}R_{p,k}(T_s-(\tau_l-\tau_m))]\}+\eta_m \end{aligned}$$

(4.19)

Turning yet again to the Gaussian approximation, the power of MPI when CI codes are used can be shown to correspond to

$$\sigma_{MPI\,m}^{\;2} = E\left[\sum_{\substack{l=0\\l\neq m}}^{L-1}\alpha_l^2K\cdot(\cos^2(\theta_l-\theta_m)\cdot(\mathrm{Re}[e^{j(\beta_p^k-\beta_q^{k'}}])^2+\sin^2(\theta_l-\theta_m)\cdot(\mathrm{Im}[e^{j(\beta_p^k-\beta_q^{k'}}])^2\right]$$

(4.20)

$$\sigma_{MPI\,m}^{\;2} = K \cdot \sum_{\substack{l=0 \\ l \neq m}}^{L-1} \alpha_l^2 (\cos^2(\theta_l - \theta_m) + \sin^2(\theta_l - \theta_m)) P_{CI} \tag{4.21}$$

$$\sigma_{MPI\,m}^{\;2} = K \cdot \sum_{\substack{l=0 \\ l \neq m}}^{L-1} \alpha_l^2 P_{CI} \tag{4.22}$$

where

$$P_{CI} = E[(\mathrm{Re}[e^{j(\beta_p^k - \beta_q^{k'})}])^2] = E[(\mathrm{Im}[e^{j(\beta_p^k - \beta_q^{k'})}])^2] = E[\cos^2(\beta_p^k - \beta_q^{k'})] = E[\cos^2(\phi)] \tag{4.23}$$

Here, ϕ is a discrete random variable with an equal probability of taking one of the values in the set $\{0, \frac{2\pi}{N}, 2 \cdot \frac{2\pi}{N}, \cdots, (N-1) \cdot \frac{2\pi}{N}\}$. Thus,

$$P_{CI} = E[\cos^2(\phi)] = \frac{1}{N} \sum_{i=0}^{N-1} \cos^2(i \cdot \frac{2\pi}{N}) = \frac{1}{2} \tag{4.24}$$

Applying (4.24) to (4.22), and (4.22) to (4.14), the SIR of the RAKE receiver's m^{th} finger output when CI codes are applied at the transmitter can be rewritten as

$$SIR_m = \frac{\alpha_i^2}{K \cdot \sum_{\substack{l=0 \\ l \neq m}}^{L-1} \alpha_l^2 \cdot \frac{1}{2} + \frac{N_0}{2}} \tag{4.25}$$

Comparing equations (4.18) and (4.25), CI codes demonstrates an SIR independent of the phase offset between different paths. On the other hand, when Hadmard-Walsh codes are used, the SIR is related to squared cosine of the phase offset between paths. Even though the average SIR per finger in Hadamard-Walsh codes is the same as that of CI codes (because $E\left[\cos^2(\theta_l-\theta_m)\right]=\frac{1}{2}$), the distribution of SIR over the random variable $\cos(\theta_l-\theta_m)$ causes degradation in the BER performance. (This is not unlike the case of a transmission over flat Rayleigh fading channels: even when the Rayleigh gain has a mean of 1, the performance is far worse than that in an AWGN channel).

All the outputs of RAKE receiver fingers are combined together to create the final decision variable for user p:

$$R^p=\sum_{m=0}^{L-1}W_m r_m^p \tag{4.26}$$

and a hard decision device follows, i.e.,

$$\hat{b}_p^{(0)}=\begin{cases}+1 & \text{if } R^p>0\\ -1 & \text{otherwise}\end{cases} \tag{4.27}$$

If an ML (maximum likelihood) combining is employed as the branch combiner, the combining weights for DS-CDMA/HW and DS-CDMA/CI are different. This is a direct consequence of the difference in SIR branch values of the two systems. For Hadamard-Walsh codes, ML combining corresponds to

$$W_m=\frac{\alpha_m}{K\cdot\sum_{\substack{l=0\\ l\neq m}}^{L-1}\alpha_l^2\cos^2(\theta_l-\theta_m)+\frac{N_0}{2}} \tag{4.28}$$

where for CI codes, ML combining weights are

$$W_m = \frac{\alpha_m}{K \cdot \sum_{\substack{l=0 \\ l \neq m}}^{L-1} \frac{\alpha_l^2}{2} + \frac{N_0}{2}} \tag{4.29}$$

4.4 Simulation Results for DS-CDMA with CI Codes

To test the performance of the novel CI codes and compare it with that of Hadamard-Walsh codes, simulations are performed over frequency selective Rayleigh fading channels. The Hilly Terrain (HT) channel model discussed in section 3.4 is assumed [57]. We assume bandwidth consistent with the GSM standard. That is, we choose chip duration T_c=3.69 μs and hence bandwidth $BW = 270.8kHz$. We also assume a synchronous downlink channel. To make the comparison fair, we assume the processing gains are 32 for both systems (Hadamard-Walsh codes and CI codes) in all simulations.

Figure 4.1 shows the simulation results at a fixed SNR of 15dB, where the x-axis represents system load (number of active users) and the y-axis shows probability of error. Figure 4.2 displays the performance results for a fixed system load (number of active users is 32), where the x-axis represents SNR and the y-axis probability of error.

In both figures, the solid line marked with circles indicates the performance of DS-CDMA system with Hadamard-Walsh codes; the solid line marked with stars indicates DS-CDMA system with CI codes. These results show the novel CI codes notably outperforming Hadamard-Walsh codes. For a 32-user system, CI codes demonstrate as much as 6 dB gain over Hadamard-Walsh codes. Moreover, for a fixed SNR of 15dB, DS-CDMA systems with CI codes support 32 users at the same performance level as a HW system with only 20 users (a 37.5% gain in the network capacity).

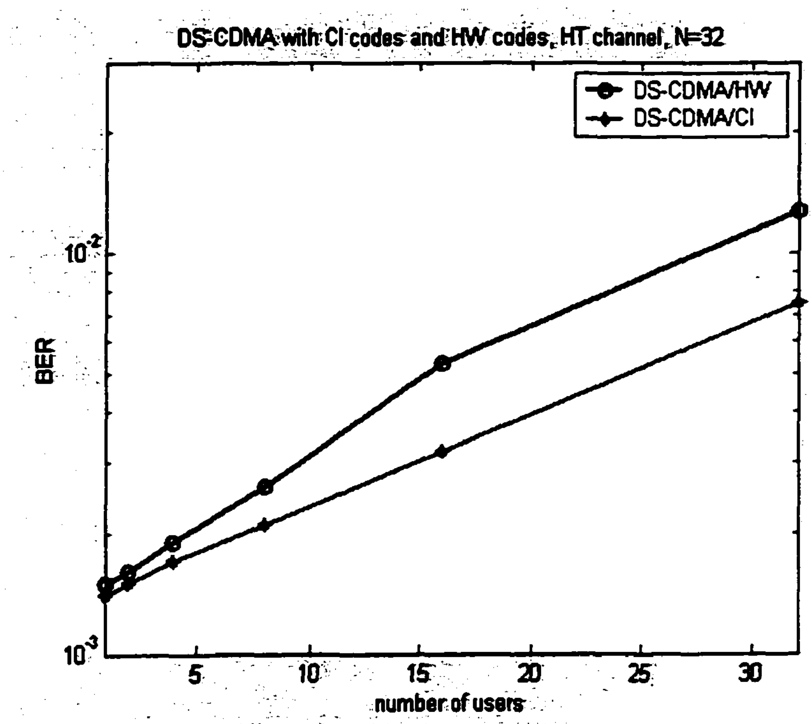

Figure 4.1 Simulation Result 1: DS-CDMA/CI and DS-CDMA/HW in HT Channel, SNR=15dB

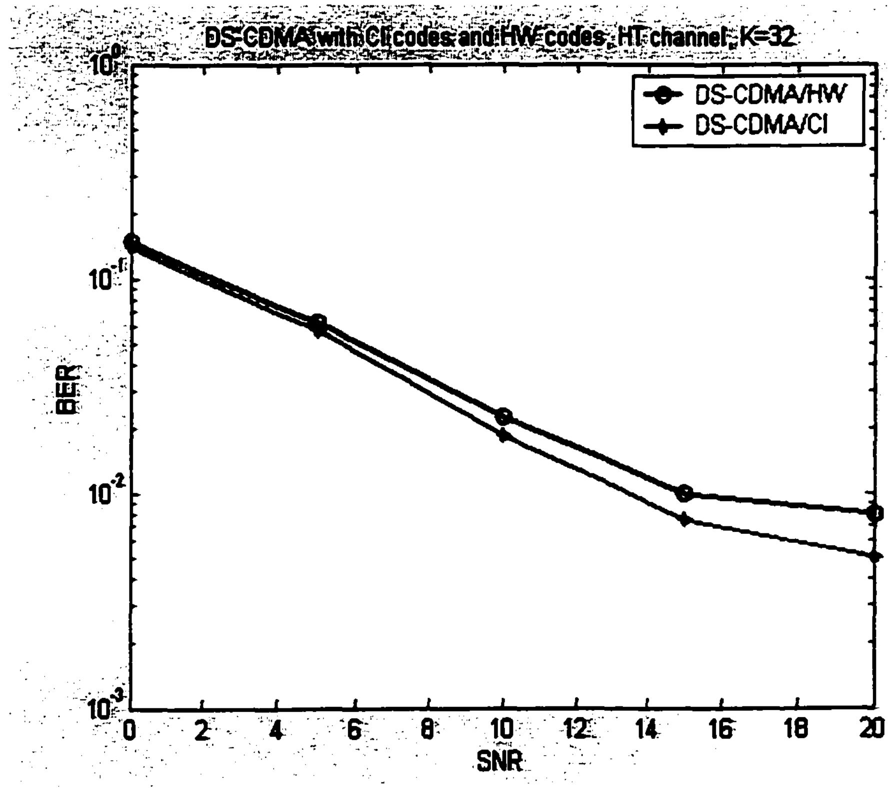

Figure 4.2 Simulation Result 2: DS-CDMA/CI and DS-CDMA/HW in HT Channel, K=32

4.5 High-Capacity DS-CDMA with Two Sets of CI Codes

Traditionally, to increase the network capacity of DS-CDMA systems, pseudo-orthogonal codes (e.g., Gold Codes, Kasami sequences [1]) are employed. Recently, Hadamard-Walsh codes layered with two independent m-sequences has been proposed as "excellent" pseudo-orthogonal codes to increase network capacity [71]. The set of the

HW codes layered with one m-sequence is still an orthogonal set, but the two sets of HW codes are pseudo-orthogonal to each other.

Here, we propose a novel way to increase the network capacity of DS-CDMA systems using CI codes. To increase the number of spreading sequences available in the DS-CDMA system (i.e., to increase the number of users), we use two discrete linear transforms to create two sets of N CI spreading sequences each. We are careful to select these transforms such that we minimize cross-correlation between all $2N$ sequences.

4.5.1 Two Orthogonal CI Codes Set

We allow the first set of N spreading sequences to correspond to the DFT, leading to the CI spreading sequences $\{(1, e^{j\frac{2\pi}{N}k}, e^{j\frac{2\pi}{N}2k}, \cdots, e^{j\frac{2\pi}{N}(N-1)k}), k = 0, 1, \cdots, N-1\}$ shown in (4.3). To create the second set of spreading sequences, we introduce a new discrete linear transform which we refer to as the Offset-DFT (ODFT). As the name suggests, the ODFT is the transform

$$\bar{X}_N^{ODFT} = \mathbf{W}_{N\times N}^{ODFT} \bar{x}_N \tag{4.30}$$

where

$$\mathbf{W}_{N\times N}^{ODFT}=\begin{bmatrix} W^{ODFT}(0,0) & W^{ODFT}(0,1) & W^{ODFT}(0,2) & \cdots & W^{ODFT}(0,N-1) \\ W^{ODFT}(1,0) & W^{ODFT}(1,1) & W^{ODFT}(1,2) & \cdots & W^{ODFT}(1,N-1) \\ \cdot & \cdot & \cdot & \cdot & \\ \cdot & \cdot & \cdot & \cdot & \\ W^{ODFT}(N-1,0) & W^{ODFT}(N-1,1) & & \cdots & W^{ODFT}(N-1,N-1) \end{bmatrix} \quad (4.31)$$

Here, $W^{ODFT}(p,q)=e^{j\frac{2\pi}{N}p\cdot q+q\cdot\theta}$. (This transform corresponds to the DFT of a time delay version of x_N). The rows of the ODFT lead to a new set of N orthogonal spreading sequences, namely

$$\{(1,e^{j\frac{2\pi}{N}k+\theta},e^{j\frac{2\pi}{N}2k+2\theta},\cdots,e^{j\frac{2\pi}{N}(N-1)k+(N-1)\theta}),k=N,N+1,\cdots,2N-1\} \quad (4.32)$$

As in the case for HW codes layered with two m-sequences, each of the CI code sets is still an orthogonal set but the two sets are pseudo-orthogonal to each other. We seek the value of θ minimizing the average cross-correlation between codes in the two CI codes sets (leading to a minimized multi-user interference). First we introduce the root mean square cross-correlation between the two sets

$$CC_{1,2}=[\frac{1}{N^2}\sum_{j=0}^{N-1}\sum_{k=0}^{N-1}(CC_{1,2}(j,k))^2]^{\frac{1}{2}} \quad (4.33)$$

where $CC_{1,2}(j,k)$ represents the cross correlation between j^{th} code from the first CI code set and k^{th} code from the second CI code set, and corresponds to

$$CC_{1,2}(j,k)=\mathrm{Re}\left[\sum_{i=0}^{N-1}e^{j(\beta_i^{(j)}-\beta_i^{(k)})}\right]=\sum_{i=0}^{N-1}\cos[i(\frac{2\pi}{N}j-\frac{2\pi}{N}k-\theta)] \quad (4.34)$$

It is easy to show that, for the two sets of CI codes,

$$\sum_{j=0}^{N-1} (CC_{1,2}(j,k))^2 = \sum_{j=0}^{N-1} (CC_{1,2'}(j,k'))^2 \qquad k \neq k' \tag{4.35}$$

That is, the total cross-correlation between the k^{th} code in second code set and all codes in first code set is identical to the cross-correlation between the $(k')^{th}$ code in second code set and all codes in first code set. Using equation (4.35), we can rewrite equation (4.34) as follows:

$$CC_{1,2} = [\frac{1}{N}\sum_{j=0}^{N-1} (CC_{1,2}(j,0))^2]^{\frac{1}{2}} \tag{4.36}$$

and, using equation (4.33), this becomes

$$CC_{1,2} = [\frac{1}{N}\sum_{j=0}^{N-1} [\sum_{i=0}^{N-1} \cos[i(\frac{2\pi}{N} j - \theta)]]^2]^{\frac{1}{2}} \tag{4.37}$$

Let us now determine the selection of θ that minimizes the root mean square correlation between the two orthogonal CI code sets. To do this, we set

$$\frac{\partial CC_{1,2}}{\partial \theta} = 0 \tag{4.38}$$

Solving equation (4.38), we determine: $\frac{\partial CC_{1,2}}{\partial \theta} = 0$ whenever $\theta = \frac{p\pi}{N}, p = 0,1,2,\cdots$.

Seeking to determine which θ are maxima and which are minima, we calculate the second order partial derivative at $\theta = \frac{p\pi}{N}$ and determine:

$$\frac{\partial CC^2}{\partial^2\theta} > 0 \quad when \quad \theta = \frac{(2p+1)\pi}{N}$$
$$\frac{\partial CC^2}{\partial^2\theta} < 0 \quad when \quad \theta = \frac{2p\pi}{N} \tag{4.39}$$

Hence, $\theta = \frac{2p\pi}{N}$ corresponds to maxima and $\theta = \frac{(2p+1)\pi}{N}$ provides minima. Selecting $p=0$, we choose $\theta = \frac{\pi}{N}$ as our minima.

Hence, if we have one set of N orthogonal users using CI codes, and we want to increase system capacity to $2N$ users, we introduce a second set of N orthogonal users also using CI codes. To best do that, in a minimum interference sense, introduce a second set of CI codes, phase offset by $\theta = \frac{\pi}{N}$ with respect to the first set of CI codes. That is, for $2N$ users on the system, numbered 0 to $2N-1$, the k^{th} user should be assigned the spreading code $\{e^{j\beta_0^{(k)}}, e^{j\beta_1^{(k)}}, \cdots, e^{j\beta_{N-1}^{(k)}}\}$ where

$$\beta_i^{(k)} = i \cdot k \cdot \frac{2\pi}{N} \qquad k = 0,1,\ldots, N-1$$
$$\beta_i^{(k)} = i \cdot k \cdot \frac{2\pi}{N} + i \cdot \frac{\pi}{N} \qquad k = N, N+1,\ldots, 2N-1 \tag{4.40}$$

The total transmitted signal, with a full $2N$ users, is then

$$s(t) = \mathrm{Re}[A\sum_{k=0}^{2N-1}\sum_{n=-\infty}^{\infty} b_n^{(k)} \sum_{i=0}^{N-1} e^{j\beta_i^{(k)}} g(t - iT_c - nT_s)] \tag{4.41}$$

with $\beta_i^{(k)}$ selected according to (4.40).

4.5.2 SIR Investigation at the RAKE Receiver

In this section we characterize the SIR performance (at the receiver) when using a DS-CDMA system with the two sets of CI codes defined by equation (4.39) and (4.40). We compare this to the performance with other spreading codes in DS-CDMA.

Assuming the signal of equation (4.41) is transmitted over a multipath fading channel at carrier frequency f_c, the signal arriving at the receiver side corresponds to

$$r(t) = \mathrm{Re}[A\sum_{l=0}^{L-1}\alpha_l \sum_{k=0}^{K-1}\sum_{n=-\infty}^{\infty} b_n^{(k)} \sum_{i=0}^{N-1} e^{j\beta_i^{(k)}} g(t - iT_c - nT_s - \tau_l) e^{j(2\pi f_c t + \theta_l)}] + \eta(t) \tag{4.42}$$

where L is the total number of paths; K is the total number of users ($K \in [1,2N]$); α_l is the fading parameter of the l^{th} path; τ_l is the time delay of the l^{th} path; θ_l is the phase offset of the l^{th} path and is assumed to be an i.i.d. random variable uniformly distributed over $[0,2\pi)$; and $\eta(t)$ is the additive white Gaussian noise. Moreover, we label paths such that $\tau_0 < \tau_1 < \tau_2 < \cdots < \tau_{L-1}$.

Considering the RAKE receiver, the m^{th} finger's output for user p (using a CI code in the first code set) corresponds to (for detection of bit 0):

$$\begin{aligned}
r_m^p &= \sum_{l=0}^{m-1} \alpha_l \operatorname{Re}[e^{j(\theta_l-\theta_m)} \cdot [\sum_k b_k^{(0)} R_{k,p}(T_s-(\tau_m-\tau_l)) + \sum_k b_k^{(+1)} R_{p,k}(\tau_m-\tau_l)]] \\
&+\alpha_m b_p^{(0)} + \alpha_m \sum_{k\neq n} b_k^{(0)} R_{k,n}(0) \\
&+\sum_{l=m+1}^{L-1} \alpha_l \operatorname{Re}[e^{j(\theta_l-\theta_m)} \cdot [\sum_k b_k^{(-1)} R_{k,p}(\tau_l-\tau_m) + \sum_k b_k^{(0)} R_{p,k}(T_s-(\tau_l-\tau_m))]] \\
&+\eta_m
\end{aligned} \tag{4.43}$$

where $b_k^{(-1)}$ is user k's previous data bit, $b_k^{(+1)}$ is user k's next data bit, and $R_{k,p}(T)$ represents the partial cross-correlation of user k and p at time delay $T = q \cdot T_c, (q \in I)$:

$$R_{k,p}(T) = \frac{1}{N}\sum_{i=0}^{q-1} e^{j(\beta_i^p - \beta_{N-q+i}^k)} \tag{4.44}$$

Specifically, when there is no time delay and when orthogonal codes (HW codes or CI codes) are employed

$$R_{k,n}(0) = 0 \qquad\qquad k \neq n \tag{4.45}$$

Since all the codes in the first CI code set are orthogonal and assuming $K>N$ users on the system, we can rewrite equation (4.43) as

$$r_m^p = \alpha_m b_p + \alpha_m \sum_{k=N}^{K-1} b_k R_{k,p}(0) + \sum_{l=0}^{m-1} \alpha_l \, \mathrm{Re}[e^{j(\theta_l - \theta_m)} \cdot [\sum_k b_k R_{k,p}(T_s - (\tau_m - \tau_l)) + \sum_k b_k^{(+1)} R_{p,k}(\tau_m - \tau_l)\,]]$$

$$+ \sum_{l=m+1}^{L-1} \alpha_l \, \mathrm{Re}[e^{j(\theta_l - \theta_m)} \cdot [\sum_k b_k^{(-1)} R_{k,p}(\tau_l - \tau_m) + \sum_k b_k R_{p,k}(T_s - (\tau_l - \tau_m))]] + \eta_m$$

(4.46)

In equation (4.46), the first term represents the desired user's signal contribution in m^{th} path, the second term represents the pseudo-orthogonal users' intra-path interference (IPI), the thrid term and fourth term represent the multi-path interference (MPI) and the fifth term is the noise, represented by a Gaussian random variable with variance $\sigma_{N_m}^2 = \dfrac{N_0}{2}$.

Thus, the SIR of the RAKE receiver's m^{th} finger's output corresponds to

$$SIR_m = \frac{\alpha_i^2}{\sigma_{IPI_m}^2 + \sigma_{MPI\,m}^2 + \sigma_{N\,m}^2} \tag{4.47}$$

where $\sigma_{IPI\,m}^2$ represents the power of IPI in m^{th} finger's output (term two in equation (4.46)) and $\sigma_{MPI\,m}^2$ represents the power of MPI in m^{th} finger's output (term three and four in equation (4.46)).

When DS-CDMA systems support *2N* users using HW codes layered with two m-sequences, $\beta_i^{(k)}$ is *0* or π, and hence the power of IPI corresponds to

$$\sigma_{IPI_m}^2(HW) = E\left[\alpha_m^2 \cdot \sum_{k=N}^{K-1} \frac{1}{N}\left(\sum_{i=0}^{N-1} \mathrm{Re}\left[e^{j(\beta_i^{(k)} - \beta_i^{(k^*)})}\right]\right)^2\right]$$
$$= \left[\alpha_m^2 \cdot \sum_{k=N}^{K-1} \frac{1}{N} \sum_{i=0}^{N-1} E[\mathrm{Re}\left[e^{j(\beta_i^{(k)} - \beta_i^{(k^*)}}\right]^2]\right] \tag{4.48}$$
$$= (K-N)\alpha_m^2$$

Alternatively, when DS-CDMA system support *2N* users via two sets of CI codes, the power of IPI corresponds to

$$\sigma_{IPI_m}^2(CI) = E\left[\alpha_m^2 \cdot \sum_{k=N}^{K-1} \frac{1}{N}\left(\sum_{i=0}^{N-1} \mathrm{Re}\left[e^{j(\beta_i^{(k)} - \beta_i^{(k^*)})}\right]\right)^2\right]$$
$$= \frac{(K-N)}{N}\alpha_m^2 \cdot E\left[\sum_{i=0}^{N-1} \cos(i \cdot k \cdot \frac{2\pi}{N} - i \cdot (k^* - N) \cdot \frac{2\pi}{N} - i \cdot \frac{\pi}{N})\right] \tag{4.49}$$
$$= \frac{(K-N)}{N}\alpha_m^2$$

Comparing equations (4.48) and (4.49), it is apparent that two sets of orthogonal CI codes demonstrate much lower IPI than two sets of orthogonal HW codes (layered with two m-sequences).

In section 4.3, we demonstrated that the powers of MPI for HW codes and CI codes are:

$$\sigma_{MPI\,m}^{\;2}(HW) = K \cdot \sum_{\substack{l=0 \\ l \neq m}}^{L-1} \alpha_l^2 \cos^2(\theta_l - \theta_m) \tag{4.50}$$

$$\sigma_{MPI\,m}^{\;2}(CI) = K \cdot \sum_{\substack{l=0 \\ l \neq m}}^{L-1} \alpha_l^2 \cdot \frac{1}{2} \tag{4.51}$$

Thus, the SIR at the output of m^{th} finger of a RAKE receiver correspond to

$$SIR_m(HW) = \frac{\alpha_l^2}{(K-N)\cdot\alpha_m^2 + K\cdot\sum_{\substack{l=0\\l\neq m}}^{L-1}\alpha_l^2\cos^2(\theta_l-\theta_m) + \frac{N_0}{2}} \tag{4.52}$$

$$SIR_m(CI) = \frac{\alpha_l^2}{\frac{(K-N)}{N}\cdot\alpha_m^2 + K\cdot\sum_{\substack{l=0\\l\neq m}}^{L-1}\alpha_l^2\cdot\frac{1}{2} + \frac{N_0}{2}} \tag{4.53}$$

where $SIR_m(HW)$ refers to the SIR when $K\in[N+1,2N]$ users are supported using two sets of m-sequences-layered HW codes, and $SIR_m(CI)$ refers to the SIR when $K\in[N+1,2N]$ users are supported via the proposed two sets of CI codes. Comparing equations (4.52) and (4.53), layered CI codes demonstrate an SIR much higher than that of HW codes. As a direct result, DS-CDMA using CI codes to increase capacity to $2N$ users demonstrate much better performance than DS-CDMA system using layered HW codes.

All the outputs of RAKE receiver fingers are combined together to create the final decision variable for user p:

$$R^{(p)} = \sum_{m=0}^{L-1} W_m r_m^p \tag{4.54}$$

and a hard decision device follows, i.e.,

$$\hat{b}_p = \begin{cases} +1 & \text{if } R^{(p)} > 0 \\ -1 & \text{otherwise} \end{cases} \tag{4.55}$$

If an ML (maximum likelihood) combining is employed as the branch combiner, the combining weights for DS-CDMA/HW and DS-CDMA/CI are different. This is a direct consequence of the difference in SIR branch values of the two systems. For Hadamard-Walsh codes, ML combining weights correspond to

$$W_m = \frac{\alpha_m}{(K-N)\cdot\alpha_m^2 + K\cdot\sum_{\substack{l=0 \\ l\neq m}}^{L-1}\alpha_l^2\cos^2(\theta_l-\theta_m)+\frac{N_0}{2}} \tag{4.56}$$

where as for CI codes, ML combining weights are

$$W_m = \frac{\alpha_m}{\frac{(K-N)}{N}\cdot\alpha_m^2 + K\cdot\sum_{\substack{l=0 \\ l\neq m}}^{L-1}\frac{\alpha_l^2}{2}+\frac{N_0}{2}} \tag{4.57}$$

4.5.3 Channel Modeling and Simulation Results

To test the performance of the novel CI codes and compare it with that of Hadamard-Walsh codes, simulations are performed over frequency selective Rayleigh fading channels. The Hilly Terrain (HT) channel model described in section 3.4 is assumed [57]. We assume bandwidth consistent with the GSM standard. That is, we choose chip duration T_c=3.69 μs and hence $BW = 270.8kHz$. We assume a synchronous downlink channel. To make the comparison fair, we assume the processing gains are N=32 for both systems (Hadamard-Walsh and CI) in all simulations.

Figure 4.3 shows the simulation results at a fixed SNR of 15dB, where the x-axis represents system load (number of active users) and the y-axis shows probability of error. In the figure, the solid line marked with stars indicates the performance of DS-CDMA system with two sets of Hadamard-Walsh codes (each layered by a unique m-sequence); the solid line marked with dots indicates the performance of a DS-CDMA system using typical pseudo-orthogonal codes (in this case, two sets of Gold codes are used); and the solid line marked with circles indicates the proposed DS-CDMA system with two sets of CI codes. These results show the novel CI codes notably outperforming two sets of Hadamard-Walsh codes as well as traditional pseudo-orthogonal codes. The BER of a DS-CDMA with CI codes supporting 64 users is the same as the BER of DS-CDMA with HW codes supporting only 36 users (and close to the performance of DS-CDMA with HW codes supporting 32 users).

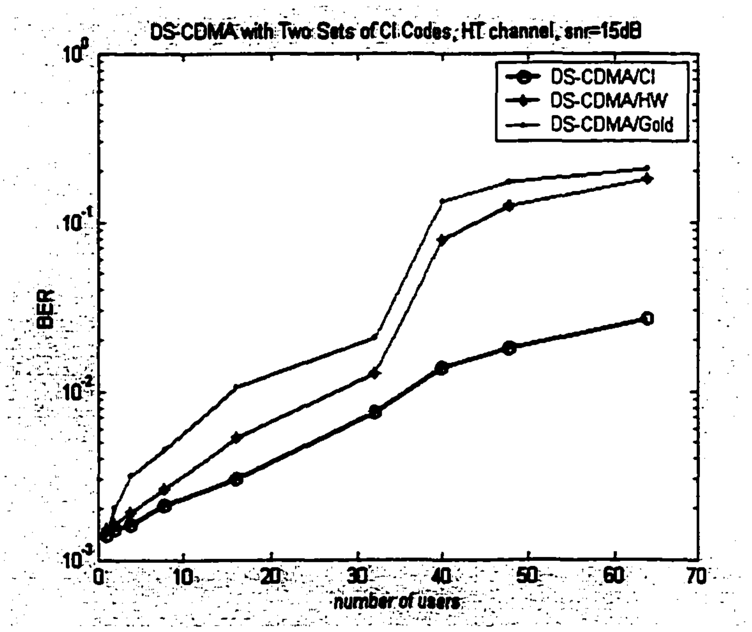

Figure 4.3: Simulation Result 1: DS-CDMA/CI and DS-CDMA/HW in HT Channel, SNR=15dB

4.6 Conclusions

In this work, novel orthogonal complex CI spreading codes for DS-CDMA are proposed. These CI codes introduce MPI whose variance is independent of phase offsets between different paths, and as a direct result, achieve better BER performance relative to that of HW codes. Simulation over Hilly Terrain channels indicates that the novel CI codes can notable outperform Hadamard-Walsh codes (and other spreading codes). Furthermore, two orthogonal CI codes sets (with minimum cross correlation between sets) are introduced for the DS-CDMA system. In this way, $2N$ users may be supported in a system with a processing gain of N. These CI codes demonstrate much lower intra-path interference, and improved signal-to-interference ratio, relative to other proposed pseudo-orthogonal codes, and as a direct result, achieve better BER performance. Simulation over Hilly Terrain channels indicates that the novel CI codes can strongly outperform traditional pseudo-orthogonal coding methods while doubling network capacity. Moreover, as stated in section 2, CI codes can be designed for any processing gain N (unlike HW codes which requires $N=2^m$).

Chapter 5 Ultra Wideband DS-CDMA via CI Chip Shaping

One important requirement for next generation wireless communication systems is the ability to support a wide range of high rate data services. Despite advances in efficient modulation and multiple access technologies, very high data rate transfer will still require ultra-wide frequency bands. Traditional DS-CDMA systems operate over one single continuous bandwidth, and with the limited spectrum available from the FCC auctioned off in small blocks, it will not be possible for DS-CDMA to operate over a contiguous ultra-wide frequency band.

This chapter demonstrates how our novel CI chip shaping scheme (Chapter 3), designed specifically for DS-CDMA systems, enables DS-CDMA to operate over non-adjacent frequency bands in a way that is identical to its operation if all these bands are made contiguous [43]. That is, we now add the ability to operate over non-adjacent bands to the benefits of CI chip shaping – in addition to its very high performance (by exploiting frequency diversity instead of path diversity) and ability to double network capacity. With the exception of the chip shape and a receiver design which operates over non-contiguous bands, this new system retains all the features of a traditional DS-CDMA system.

5.1 Introduction to Ultra Wideband Communication

Today's growing need for wireless spectrum stems not only from an increase in number of wireless phone accounts, but also from industry plans to offer more and more services over these phones. With over 50% of the 1.2 billion wireless phones in the world by 2003 expected to be Internet ready, and the demand for voice, data and video links on the rise, ultra wide-band links will be the only way to support this diverse range of demands.

One obstacle to such future development is the lack of contiguous ultra-wide bandwidth available to communication companies. The frequency spectrum, a very scarce resource, has (for the most part) already been allocated to different companies in small blocks, and as such no company owns a contiguous wide bandwidth.

DS-CDMA (as developed in existing standards including IS-95, CDMA 2000, and WCDMA) has been and is being deployed around the world. No one wants to throw out all these existing DS-CDMA systems and standards. But, at present, DS-CDMA cannot efficiently support ultra-wideband communication without a large continuous bandwidth, and none is available.

On the other hand, MC-DS-CDMA (multi-carrier DS-CDMA) [72-78] may be able to support ultra-wideband communication over non adjacent bands, by operating narrow band DS-CDMA over each non-contiguous band. Here, to maintain orthogonality between different users, orthogonal spreading sequences on each narrow band. Thus, the total number of users is bound by the processing gain of single band, and not the total processing gain of all frequency bands. This is unacceptable in a wireless system where spectrum is a scarce commodity.

Specifically, because DS-CDMA chip shapes such as the sinc and raised cosine chip shape occupy a continuous bandwidth, DS-CDMA must occupy a single contiguous bandwidth. If N non-adjacent bands are available, then, at present, DS-CDMA must be implemented to operate independently over each of the N bands, losing the benefits inherent in using all bands as a part of a single multiple access transmission system.

In Chapter 3, we present novel CI chip shaping scheme which brings significant performance and network capacity benefits to DS-CDMA. Specifically, by employing Carrier Interferometry (CI) chip shaping in DS-CDMA (and calling the system CI/DS-CDMA), we enabled DS-CDMA receivers to exploit frequency diversity and as such enabled these receivers to better exploit the received signal energy. The CI chip shape corresponded to the linear combining of N orthogonal (and adjacent) carriers.

In this chapter, we introduce another innovation to CI chip shaping which allows chip shapes to operate over non-contiguous bands simultaneously [43]. Specifically, we loosen the requirement on the CI chip shape - replacing the requirement that it be made up of N orthogonal and adjacent carriers by the less rigid requirement that it be made up of N orthogonal carriers (which need not be adjacent). This enables DS-CDMA to operate over multiple frequency bands that are non-adjacent in the same manner that it would operate if all bands were indeed adjacent. Moreover, because the fades over non-adjacent frequency bands are independent, more diversity is available to this DS-CDMA system, providing further performance improvement.

5.2 Transmitter for CI/DS-CDMA Over Non-Adjacent Frequency Bands

In Chapter 3, we defined that the CI chip shape as

$$h(t) = \sum_{n=0}^{N-1} A e^{j2\pi n\Delta f t} \tag{5.1}$$

and used chip shape of the form

$$h(t - iT_c) = \sum_{n=0}^{N-1} A e^{j2\pi n\Delta f (t - iT_c)} \tag{5.2}$$

We now introduce a new notation, namely

$$h_i(t) = h(t - iT_c) = \sum_{n=0}^{N-1} Ae^{j2\pi n\Delta f t - n\theta_i} \tag{5.3}$$

where

$$\theta_i = i\frac{2\pi}{N}, i = 0,1,\ldots N-1 \tag{5.4}$$

We now expand over definition of the CI chip shape to ensure its operability over non-adjacent frequency bands. Specifically, we generalize our chip shape by replacing $n\Delta f$ by f_n, i.e.,

$$h_i(t) = \sum_{n=0}^{N-1} A\cos(2\pi f_n t + n\theta_i)g(t) \tag{5.5}$$

where f_p and f_q $(p \neq q)$ are chosen such that carriers are orthogonal over duration T_s. While one solution is the selection (characteristics of the CI chip shape in (5.1)) $f_n = n\Delta f$, many other solutions exist. For example, consider the case of four non-adjacent frequency bands (Figure 5.1), each with a processing gain of *N=16*, which together could form a system with an *N=64* processing gain. We can create a chip shape to exploit the benefits of the full *N=64* processing gain system, by using the chip shape in (5.5) with e.g.

$$f_n = \begin{cases} n\Delta f & n = 0,1,2,\cdots\cdots,15 \\ (n+16)\Delta f & n = 16,17,18,\cdots\cdots 31 \\ (n+32)\Delta f & n = 32,33,34,\cdots\cdots 47 \\ (n+48)\Delta f & n = 48,49,50,\cdots\cdots 63 \end{cases} \tag{5.6}$$

Figure 5.1 illustrates this CI chip shape in the frequency domain, and Figure 5.2 plots the chip in the time domain. From this simple example, it is apparent how we can create a chip shape that occupies four non-adjacent frequency bands simultaneously, and offer the benefits of a *4N* processing gain DS-CDMA system.

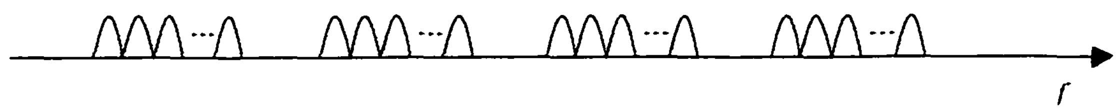

Figure 5.1 CI Chip Shape Over Non-Adjacent Frequency Bands in Frequency Domain

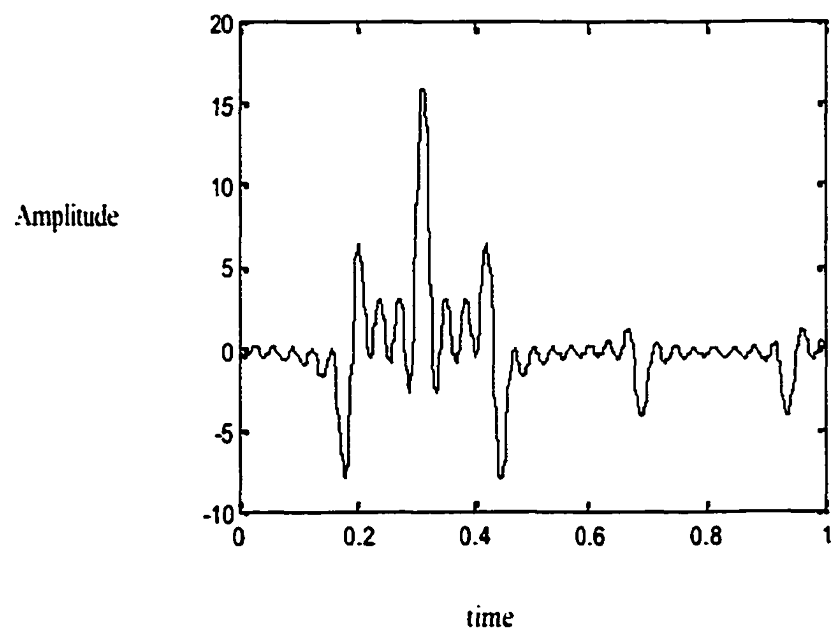

Figure 5.2 CI Chip Shape Over Non-Adjacent bands in Time Domain

Using equation (5.5), we can rewrite user k's transmitted signal as

$$
\begin{aligned}
s^{(k)}(t) &= b_k \sum_{i=0}^{N-1} \beta_i^{(k)} h_i(t) \\
&= b_k \sum_{i=0}^{N-1} \beta_i^{(k)} \sum_{n=0}^{N-1} A \cdot \cos(2\pi f_c t + 2\pi f_n t + n\theta_i) g(t) \\
&= b_k \sum_{i=0}^{N-1} \beta_i^{(k)} \sum_{n=0}^{N-1} A \cdot \cos(2\pi f_c t + 2\pi f_n t + ni\frac{2\pi}{N}) g(t)
\end{aligned}
\tag{5.7}
$$

In the case of a chip shape designed to occupy non-adjacent frequencies as shown in Figure 5.2, the chip shape $h_i(t)$ can be generated using four 16 point IFFTs, or as shown in Figure 5.3(b). The overall transmitter is designed as shown in Figure 5.3(a).

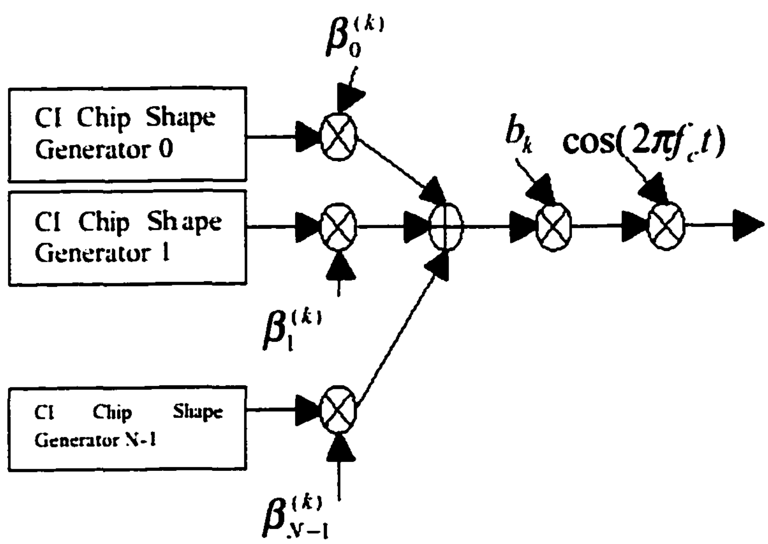

(a) Transmitter

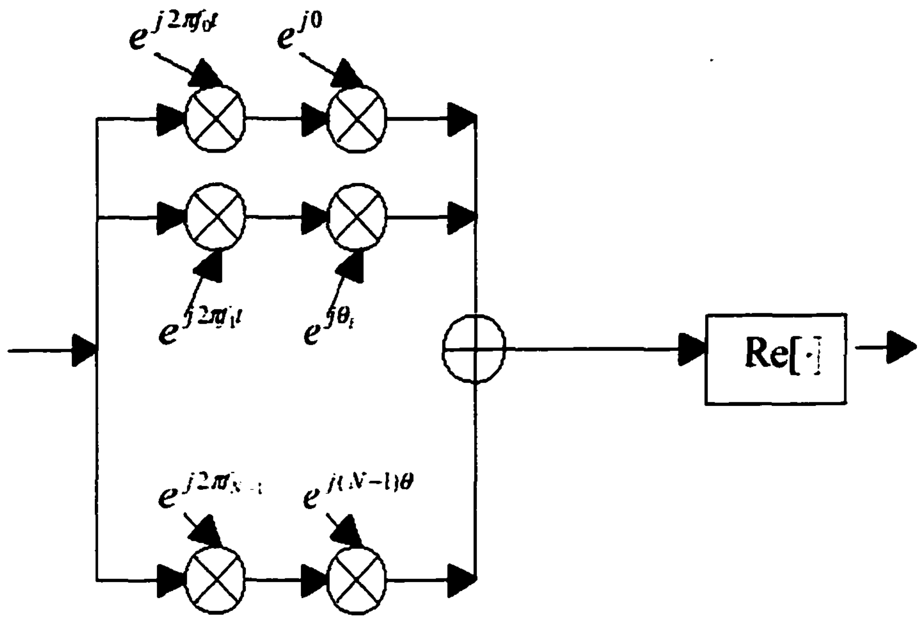

(b) CI Chip Shape Generator *I*

Figure 5.3 Transmitter for CI/DS-CDMA Over Non-adjacent Frequency Bands

(a) Transmitter

(b) CI Chip Shape Generator *i*

The total transmitted signal for K users in downlink (or synchronized uplink) communication is:

$$S(t) = \sum_{k=0}^{K-1} b_k \sum_{i=0}^{N-1} \beta_i^{(k)} \sum_{n=0}^{N-1} \cos(2\pi f_c t + 2\pi f_n t + ni2\pi / N) g(t) \tag{5.8}$$

5.3 Receiver for CI/DS-CDMA Over Non-Adjacent Frequency Bands

In most Rayleigh fading channels used for wideband communication, frequency selectivity exists over the entire bandwidth, but not over individual carriers in the multi-carrier chip shape. Hence, each frequency component making up the CI/DS-CDMA chip shape experiences a unique flat fade. That is, the received signal in the fading channel is characterized by (assuming the transmit signal of equation (5.8)):

$$r(t)=\sum_{k=0}^{K-1} b_k \sum_{i=0}^{N-1} \beta_i^{(k)} \sum_{n=0}^{N-1} \alpha_n \cos(2\pi f_c t+2\pi f_n t-ni2\pi/N+\phi_n)g(t)+\eta(t) \tag{5.9}$$

where α_n is the gain and φ_n the phase offset in the n^{th} carrier of the CI pulse (due to the channel fade), and $\eta(t)$ represents additive white Gaussian noise. To simplify the analysis, exact phase synchronization is assumed.

For the l^{th} user, the CI/DS-CDMA receiver detects the m^{th} chip as shown in Figure 5.4(b). Here, the m^{th} chip is separated into its N carrier components. As shown in Chapter 3, each chip and each carrier contributes a decision variable $r_{m,n}$ corresponding to

$$r_{m,n}^{(l)}=\sum_{k=0}^{K-1} b_k \sum_{i=0}^{N-1} \beta_i^{(k)} \alpha_n \cos(nm2\pi/N-ni2\pi/N)+\eta_{m,n} \tag{5.10}$$

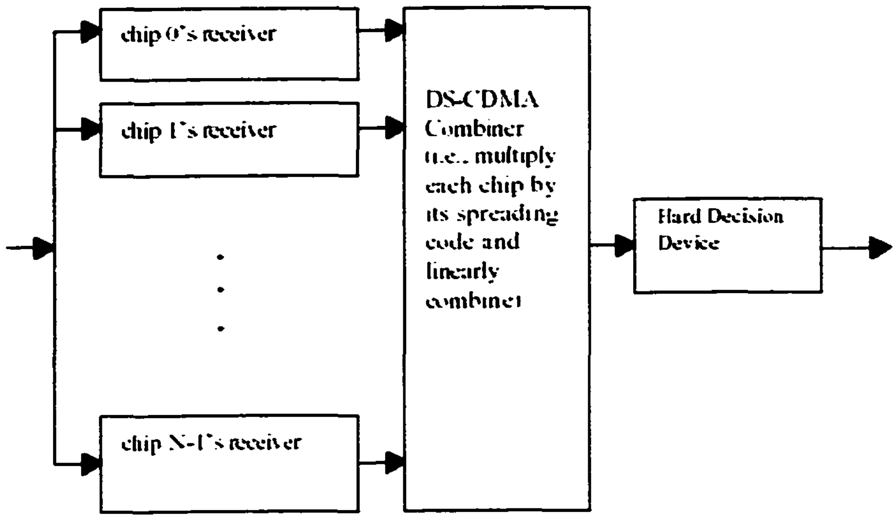

(a) Receiver

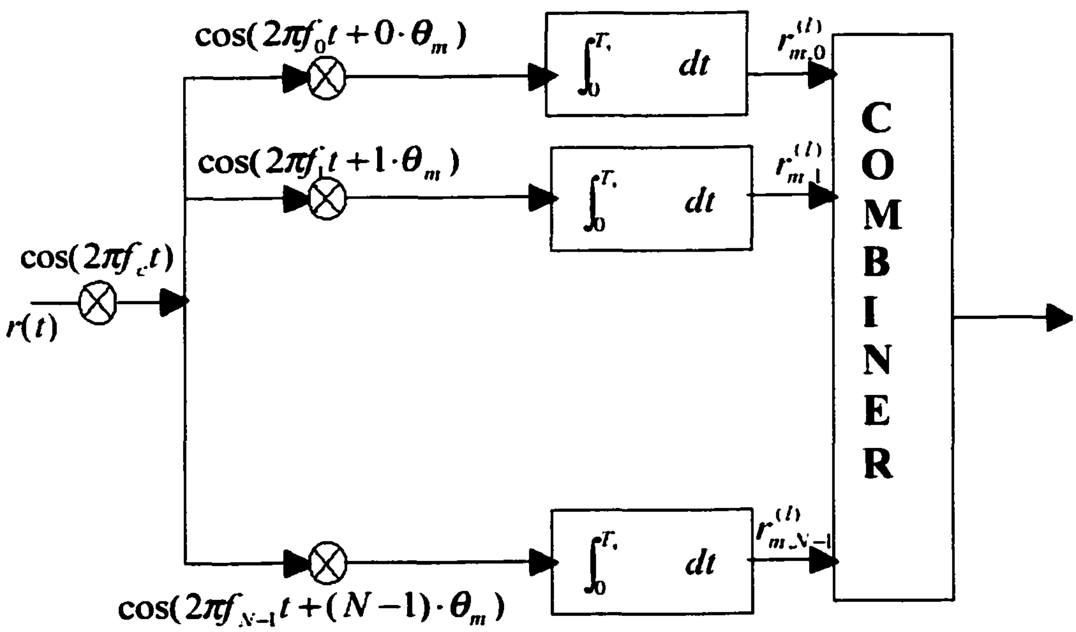

(b) Chip m's receiver

Figure 5.4 Receiver for CI/DS-CDMA over Non-adjacent Frequency Bands

(a) Receiver

(b) Chip *m*'s receiver

The same MMSE frequency combining and time combining are employed as described in Chapter 3 to create the final decision variable.

5.4 Channel Model and Simulation Results

Again, we use the Hilly Terrain (HT) channel described in section 3.4 to assess the performance of the proposed ultra wideband DS-CDMA system [57].

Simulations are performed assuming that a total of $N=32$ subcarriers. Specifically, the CI/DS-CDMA system with non-adjacent frequency bands is assumed to operate over 4 non-contiguous frequency bands, each consisting of 8 adjacent subcarriers. These four frequency bands are far enough from one another that the fades over each band are independent. Benchmark results are generated using the following systems: (1) a traditional DS-CDMA system using N=32 Hadamard-Walsh codes and operating over contiguous bandwidth and (2) a CI/DS-CDMA system using $N=32$ carriers that are contiguous. We assume a synchronous downlink (or uplink) channel.

Figure 5.5 presents bit error probability (BER) versus SNR for fully loaded systems and Figure 5.6 presents the BER versus number of users for fixed SNR=10dB. The curve marked with circles represents the performance of traditional DS-CDMA, while the curves marked with asterisks represents the performance of CI/DS-CDMA over adjacent frequency bands and the curves marked with dots represents the performance of CI/DS-CDMA system over non-adjacent frequency bands.

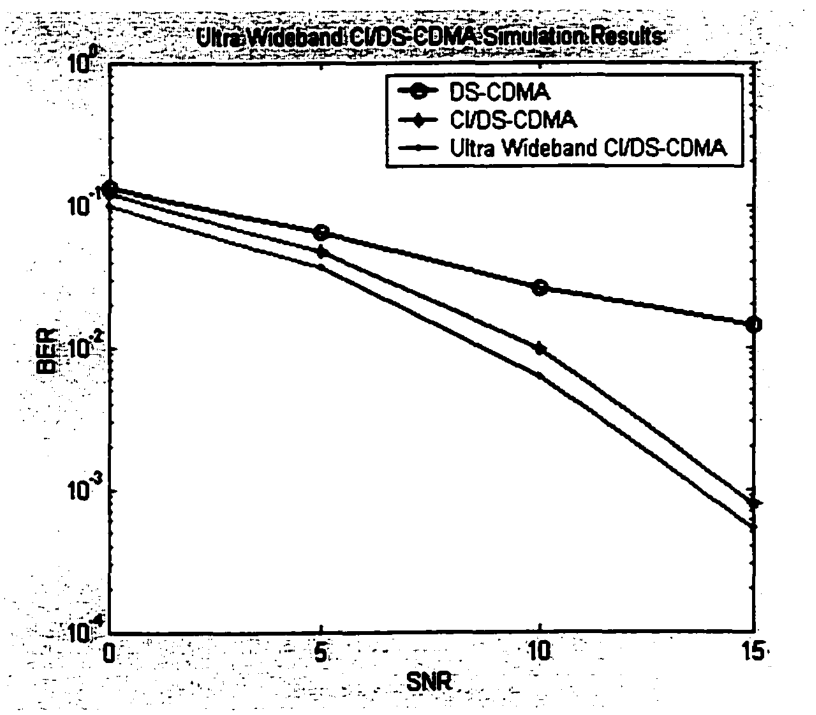

Figure 5.5 BER performance of non-adjacent CI/DS-CDMA

BER vs SNR, Fully Loaded, HT channel

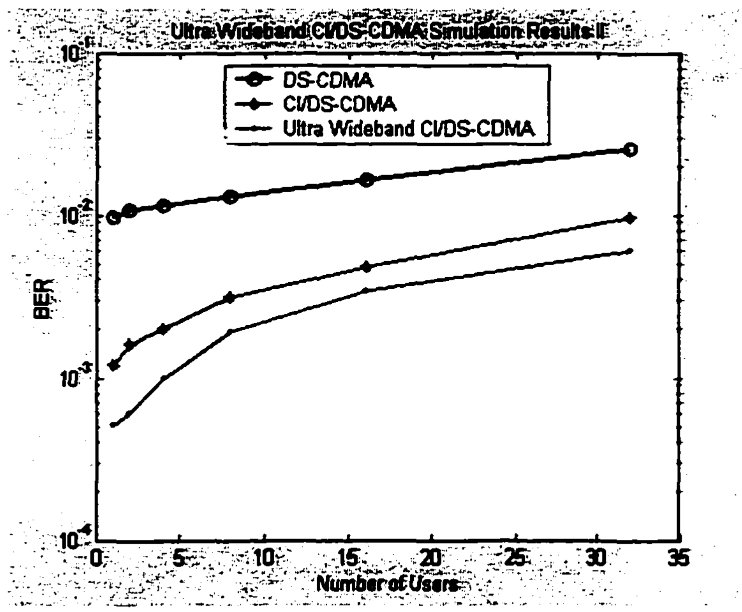

Figure 5.6 BER performance of non-adjacent CI/DS-CDMA
BER vs Number of Users, SNR=10dB, HT channel

These results confirm that CI/DS-CDMA operating over non-adjacent frequency bands exploits more frequency diversity than CI/DS-CDMA operating over adjacent frequency bands (providing better performance). Of course, both systems outperform traditional DS-CDMA dramatically.

5.5 Conclusions

In this chapter the novel CI chip shaping method is investigated further and shown to support ultra wide-band DS-CDMA over non-adjacent frequency bands. This

CI/DS-CDMA scheme does not require a RAKE receiver. Instead, using suitable combining strategies at the receiver, the system exploits frequency diversity benefits that are inherent in such multi-carrier chip shaping. Simulation results show dramatically improved BER performance when this architecture is applied, when compared to that offered by a conventional DS-CDMA system and a CI/DS-CDMA system operating over adjacent frequency bands. Moreover, unlike the MC-DS-CDMA alternative, which only supports N' users where N' is the number of users available in one of the non-contiguous frequency bands, ultra wideband CI/DS-CDMA supports $N = LN'$ users, where L is the number of non-contiguous bands.

Chapter 6 Short-term DS-CDMA Receiver Improvements

As mentioned in Chapter 2, tapped delay line RAKE receivers are commonly used to achieve path diversity gains in DS-CDMA systems. Here, Maximum Ratio Combining (MRC) across paths is typically considered the optimal combining scheme when fading parameters can be perfectly tracked. Lee and Milstein [72] noted that MRC is not optimal because different diversity branches have different MAI power. However, Lee and Milstein's combining scheme used inaccurate estimator of the MAI power. In this chapter, the optimal combining scheme for DS-CDMA RAKE receivers, based on the maximum likelihood criteria, is derived. Simulation over Rayleigh frequency selective fading channels indicates the benefits over other combining schemes [79].

While the performance benefits available (to DS-CDMA) by improving RAKE receivers are small when compared to the benefits of using CI chip shape (Chapter 3) or CI codes (Chapter 4), this work is important because it provides a short-term solution to poor DS-CDMA performance. This solution can be used until CI codes and CI chip shapes are embraced by academic and industrial communities.

6.1 Introduction

In current DS-CDMA systems, tapped delay line RAKE receivers are commonly employed to achieve path diversity gain (Figure 2.2). In a frequency-selective multipath channel with L separable paths, the RAKE receiver provides up to L^{th}-order diversity.

In RAKE receivers, each "finger" extracts one of the separable multipaths, and the fingers' outputs are then combined to exploit path diversity and overcome multi-path effects. Maximum Ratio Combining (MRC) is typically considered the optimal combining scheme when fading parameters can be tracked [1][2]. However, MRC is the optimal method of combining if and only if the MAI (multiple access interference) in different diversity branches (i.e., different "fingers") is independent and identically distributed (i.i.d.). This is simply not the case in DS-CDMA. This was first observed by Lee and Milstein in [72], where an improved combining scheme (referred to here as MRC2) is derived. However, we have determined that Lee and Milstein's MRC2 is still not optimal, a direct result of inaccurate assumptions regarding the power of the MAI term.

In this chapter, we present an optimal combining scheme for RAKE receivers based on maximum likelihood criteria and accurate estimation of MAI power (hereafter referred to as MRC3). Simulation over Rayleigh multi-path fading channels shows the novel combining scheme outperforming traditional MRC as well as MRC2. It is important to note that this novel combining scheme does not require any additional information (beyond that required by MRC and MRC2).

6.2 Maximum Likelihood Combining Scheme for DS-CDMA RAKE Receiver

Recall from Chapter 2, equation (2.9), in n^{th} user's DS-CDMA RAKE receiver, the m^{th} finger's output corresponds to

$$\begin{aligned} r_m^{(n)} &= \alpha_m b_n \\ &+ \sum_{l=0}^{m-1} \alpha_l \cos(\theta_l - \theta_m)[\sum_k b_k R_{k,n}(T_s - (\tau_m - \tau_l)) + \sum_k b_k^{(+1)} R_{n,k}(\tau_m - \tau_l)\ ] \\ &+ \sum_{l=m+1}^{L-1} \alpha_l \cos(\theta_l - \theta_m)[\sum_k b_k^{(-1)} R_{k,n}(\tau_l - \tau_m) + \sum_k b_k R_{n,k}(T_s - (\tau_l - \tau_m))] \\ &+ \eta_m \end{aligned} \tag{6.1}$$

All decision variables $r_m^{(n)}$ are combined across paths (i.e., index m) to exploit the path diversity gain and create a final decision statistic for user n, $R^{(n)}$. Mathematically, this corresponds to

$$R^{(n)} = \sum_{m=0}^{L-1} W_m r_m^{(n)} \tag{6.2}$$

A hard decision device follows, i.e.,

$$\hat{b}_n = \begin{cases} +1 & \text{if } R^{(n)} > 0 \\ -1 & \text{else} \end{cases} \tag{6.3}$$

Maximum Ratio Combining (MRC) is typically treated as the combining method providing the best performance; here, the weights W_m of equation (6.2) correspond to:

$$W_m = \alpha_m \tag{6.4}$$

However, MRC is the optimal method of combining only when the MAI in different diversity branches (i.e., different "fingers") is independent and identically distributed (i.i.d.). In [72], Lee and Milstein demonstrated that the MAI of each RAKE finger's output has a different power, and hence MRC is not optimal.

Considering the second term and the third term in equation (6.1) as MAI, and estimating its power, Lee and Milstein present a new version of MRC (MRC2), where

$$W_m = \frac{\alpha_m}{\frac{K}{N}\sum_{\substack{l=0 \\ l \neq m}}^{L-1} \frac{\alpha_l^2}{2} + \frac{N_0}{2}} \tag{6.5}$$

However, the combining with weights from equation (6.5) fails to take into account: (1) information regarding the phase θ_l, which is tracked at the receiver and (2) the presence of b_n in terms two and three of equation (6.1). Thus, the estimation of MAI power in MRC2 is not accurate. As a result, MRC2 is not truly optimal. With this in mind, we rederive the combining weights (creating MRC3) as follows. First, rewrite equation (6.1) by separating out the b_n component in the second and third term, i.e.,

$$\begin{aligned} r_m &= \alpha_m b_n \\ &+ \sum_{l=0}^{m-1} \alpha_l \cos(\theta_l - \theta_m) b_n R_{n,n}(T_s - (\tau_m - \tau_l)) + \sum_{l=m+1}^{L-1} \alpha_l \cos(\theta_l - \theta_m) b_n R_{n,n}(T_s - (\tau_l - \tau_m)) \\ &+ \sum_{l=0}^{m-1} \alpha_l \cos(\theta_l - \theta_m)[\sum_{k \neq n} b_k R_{k,n}(T_s - (\tau_m - \tau_l)) + \sum_k b_k^{(+1)} R_{n,k}(\tau_m - \tau_l)\ ] \\ &+ \sum_{l=m+1}^{L-1} \alpha_l \cos(\theta_l - \theta_m)[\sum_k b_k^{(-1)} R_{k,n}(\tau_l - \tau_m) + \sum_{k \neq n} b_k R_{n,k}(T_s - (\tau_l - \tau_m))] + \eta_m \end{aligned} \tag{6.6}$$

From equation (6.6), we can clearly see that the desired data b_n is contained in the first three terms, and the power of the MAI is determined by the fourth and fifth term. That is,

$$r_m = Z_m^S + Z_m^{MAI} + \eta_m \tag{6.7}$$

where Z_m^S is the contribution of the total desired signal (the first three terms in equation (6.6)), and Z_l^{MAI} is the contribution of MAI (the fourth term and the fifth term in equation (6.6)).

Using (1) equation (6.7), (2) the Maximum Likelihood Criteria, and (3) approximating MAI as a Gaussian random variable, the optimal combining scheme for the RAKE receiver (MRC3) is easily shown to correspond to

$$W_m = \frac{|Z_m^S|}{R_{m,m}} \tag{6.8}$$

where

$$\begin{aligned} R_{m,m} &= E[\eta_m \eta_m] + E\left[Z_m^{MAI} Z_m^{MAI} \mid \vec{\alpha}_m\right] \\ &= \frac{N_0}{2} + \frac{1}{N} \sum_{\substack{l=0 \\ l \neq m}}^{L-1} \left(K - 1 + \frac{|\tau_l - \tau_m|}{T_s}\right) \alpha_l^2 \cos^2(\theta_l - \theta_m) \end{aligned} \tag{6.9}$$

Finally, the resulting weights in equation (6.2) correspond to:

$$W_m = \frac{\alpha_m + \sum_{l=0}^{m-1} \alpha_l \cos(\theta_l - \theta_m) R_{n,n}(T_s - (\tau_m - \tau_l)) + \sum_{l=m+1}^{L-1} \alpha_l \cos(\theta_l - \theta_m) R_{n,n}(T_s - (\tau_l - \tau_m))}{\frac{1}{N} \sum_{\substack{l=0 \\ l \neq m}}^{L-1} \left(K - 1 + \frac{|\tau_l - \tau_m|}{T_s}\right) \alpha_l^2 \cos^2(\theta_l - \theta_m) + \frac{N_0}{2}} \tag{6.10}$$

These weights require amplitude, phase, and delay tracking for each multipath, typically available in DS-CDMA.

6.3 Channel Model and Simulation Results

To test the performance of the novel combining scheme (MRC3) and compare it with other combining schemes, simulations are performed over Rayleigh frequency selective fading channels. MRC, MRC2 and MRC3 are simulated for a DS-CDMA system with a processing gain of 128 and chip time $0.2\mu s$. The Hilly Terrain (HT) channel model is assumed. For such a DS-CDMA system, the HT channel is a multipath fading channel with six paths [57]. The power and time delay of each path are shown in Table 3.1.

Figure 6.1 shows the simulation results at a fixed SNR of 10dB, where the x-axis represents system load (number of active users) and the y-axis shows probability of error. Figure 6.2 displays the results for a fixed system load (number of active users is 32), where the x-axis represents SNR and the y-axis probability of error. In both figures, the solid line marked with circles indicates MRC performance; the solid line marked with stars indicates MRC2 performance; and the solid line marked with dots presents MRC3 results. These results show the novel combining scheme (MRC3) notably outperforming MRC and MRC2. For a 32 user system, MRC3 demonstrates as much as a 10dB gain over MRC and 5 dB gain over MRC2.

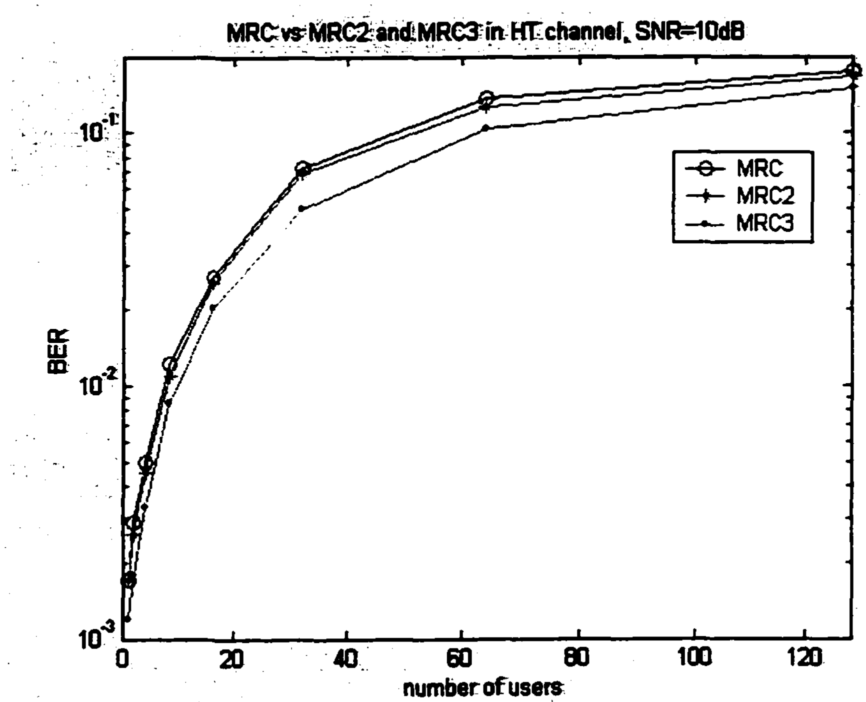

Figure 6.1 Simulation results in HT channel (fixed SNR=10dB)

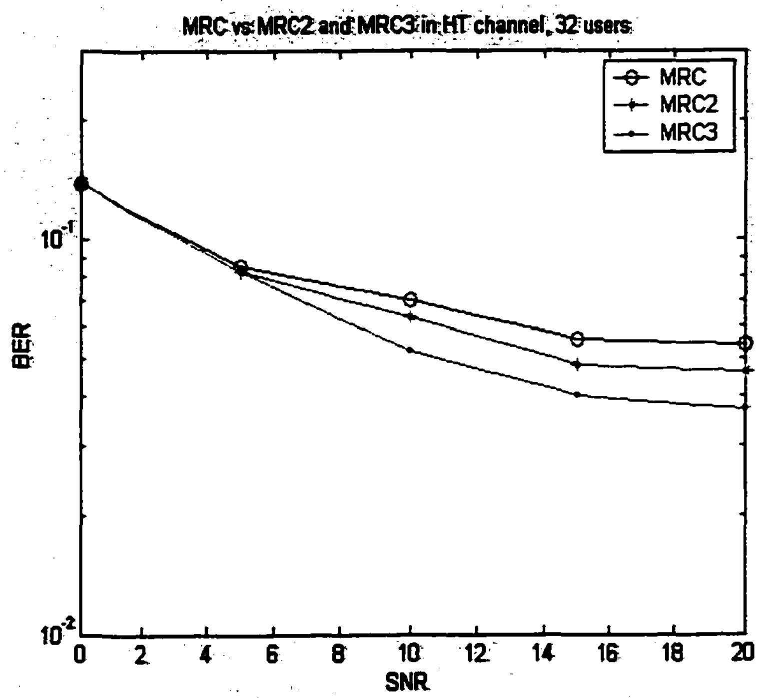

Figure 6.2 Simulation results in HT channel (fixed system load=32 users)

6.4 Conclusions

In this chapter, a novel maximum likelihood combining scheme for the DS-CDMA RAKE receiver is proposed. Based on accurate estimation of MAI power in every diversity branch (RAKE finger), the optimal ML combining is derived.

Simulation over Hilly Terrain channels indicates that the novel combining scheme can strongly outperform other combining schemes. It is important to note that (1) the proposed combining scheme does not require any additional information relative to traditional MRC and (2) the added computation load is very small.

Chapter 7 Applications of the Technology: The IEEE 802.11b WLAN Standard

WLANs (Wireless Local Area Networks) promise to combine the mobile connectivity of the wireless world with the speed and robustness of current wired systems. With IEEE 802.11, WLANs are emerging that support a variety of data types as well as rates. This chapter introduces an application of novel Carrier Interferometry chip-shaping technology to the DSSS implementation of IEEE 802.11 WLAN [46][47]. This application is capable of improving performance and increasing the throughput of the current DSSS system. It is shown that, the proposed system supports four times the throughput of the traditional DSSS system, while simultaneously achieving a 2dB performance gain at a probability of error of 10^{-3}.

7. 1 Introduction

Wireless Local Area Networks (WLANs) have been at the center of intense research, development, and standardization efforts since the early 1990's. The growing interest has stemmed from two primary considerations: low cost of maintenance and expansion (i.e., elimination of new cabling, reduced time to deploy, and increased physical space) and the popularity of devices like portable computers and personal digital assistants (PDA's).

In 1997, IEEE created the 802.11 standard, a specification for wireless LANs operating in the 2.4 GHz ISM band [80]. This standard specifies two wireless Physical Layers, one based upon Direct Sequence Spread Spectrum (DSSS), and the other upon Frequency Hopped Spread Spectrum (FHSS).

The DSSS portion of the IEEE 802.11 standard utilizes an 11-chip pseudonoise (PN) Barker code combined with Differential Binary Phase Shift Keying (DBPSK) or Differential Quadrature Phase Shift Keying (DQPSK) to achieve 1 and 2 Mbps data rates. Here, an incoming 1 MHz symbol rate is spread to an 11 Mchip/s chipping rate, widening the data to a larger 22 MHz bandwidth.

In this chapter, staying within the IEEE 802.11 DSSS standard, we introduce our novel CI (Carrier Interferometry) chip shaping described in Chapter 3 to the DSSS architecture. By applying CI chip shapes in the DSSS's specified 11 chip Baker sequence, it is shown that the 22 MHz channel bandwidth supports twice the throughput *and* improves probability of error performance, outperforming traditional DSSS by approximately 4 dB at a BER of 10^{-3}.

7.2 IEEE 802.11 DSSS Physical Layer Specifications

IEEE 802.11 divides the 2.4 GHz ISM band into 14 channels. In the United States, only 11 of these 14 are used, with Channel 1's center frequency set to 2.412 GHz, Channel 2's center frequency set to 2.417 GHz, up to Channel 11's center frequency set at 2.462 GHz. While 11 channels are available, only three channels operate at any one time, with each pair separated by at least 30 MHz. This ensures little to no interference between channels.

In each of the three channels in use, information bits are modulated utilizing either DBPSK or DQPSK, allowing the system to transmit at 1 or 2 Mbps respectively. Next, the data is spread to a larger bandwidth by application of an 11-chip pseudonoise Barker sequence, selected because of its good autocorrelation properties. The Barker sequence corresponds to:

$$(+1, -1, +1, +1, -1, +1, +1, +1, -1, -1, -1) \tag{7.1}$$

At the receiver, a despreading process and peak detection device are used to extract the strongest multipath component, and a decision device determines the transmitted signal. More expensive designs include the use of multi-tap RAKE receivers prior to the decision device (see Chapter 2).

7.3 CI-DSSS: Application of CI Chip Shape to 802.11 DSSS

The CI chip-shaping filter, when applied to IEEE's 802.11 DSSS standard, creates chip shapes corresponding to the linear combination of 11 subcarriers, equally spaced within the 22 *MHz* bandwidth. Figure 7.1(a) demonstrates the CI chip shape in the frequency domain, and Figure 7.1(b) shows one period of the corresponding chip shape in the time domain. As is evident from Figure 7.1(b), one period of the CI chip shape is similar in time to the *sinc*(.) chip shape.

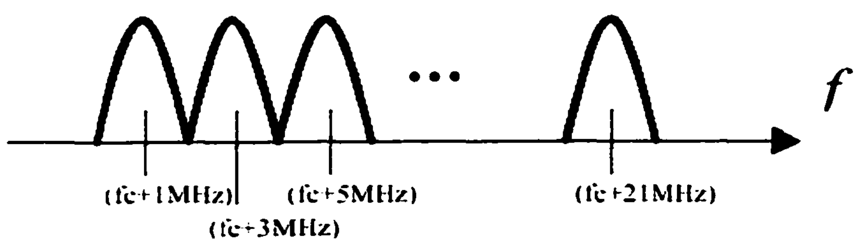

(a): CI Chip Shape in the frequency domain

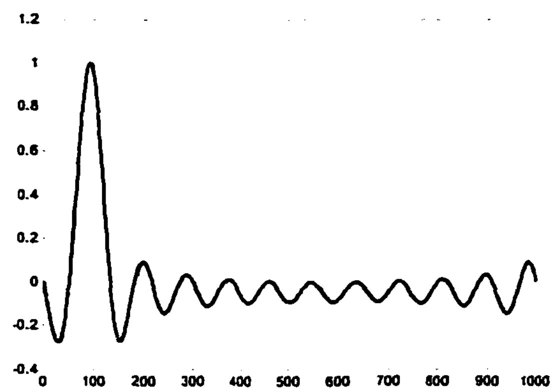

(b): CI Chip Shape in the time domain

Figure 7.1 CI Chip Shape for 802.11 DSSS

Mathematically, the CI chip shape (generated using FFT's) for 802.11 DSSS application corresponds to

$$h(t) = \sum_{n=0}^{10} A e^{j2\pi n \Delta f t} \tag{7.2}$$

where A is a constant to ensure a code energy (after spreading) of unity, $N = 11$ is the number of chips, and $\Delta f = 2/T_s$ (T_s being the symbol duration of $1\text{x}10^{-6}$ sec in 802.11 DSSS), i.e., $\Delta f = 2$ MHz.

The spreading sequence (+1's and −1's), corresponding to the Barker sequence, is modulated using the CI chip shaping filter to create the Barker code as follows (denoted here as $X^{CI}(t)$):

$$X^{CI}(t) = A\sum_{i=0}^{10} \beta_i \, h(t - iT_c) \cdot g(t) \tag{7.3}$$

where $h(t)$ is the CI chip shape of equation (7.2), β_i is the i^{th} element of the Barker sequence shown in equation (7.1), $g(t)$ is a unit amplitude rectangular waveform of duration T_s, and A is a constant ensuring code energy is unity.

As mentioned in Chapter 3, by utilizing the CI shape, we create a chip-shape that in the time domain demonstrates a shape similar to that of the well-known *sinc*(.) waveform, but in the frequency domain is easily decomposed into its 11 subcarriers. At the receiver, a frequency combining strategy can be utilized, whereby each chip is decomposed into its 11 carriers and frequency combining is deployed to exploit a frequency diversity benefit. Specifically, a frequency selectivity typically exists over the entire bandwidth, whereas a flat fade exists over each of the 11 carriers used to create the CI chip shape. Hence, through use of a frequency combining strategy such as the Minimum Mean Squared Error (MMSE) or Maximum Likelihood (ML) combiner, the 11 carriers that make up the CI chip shape can be combined to exploit the frequency diversity available in the channel. This leads to notable performance benefits as shown in section 7.5.

Moreover, CI chip shaping offers a second advantage over the IEEE 802.11 DSSS standard: a throughput benefit. Specifically, in a 22 MHz bandwidth, with a symbol rate of $R = 1/T_s = 1$ MHz, it is well known that there exists 22 orthogonal carriers (with a frequency spacing of $\Delta f = 1/T_s = 1$ MHz). Referring to Figure 7.1(a), it is evident that only 11 of these carriers are used in the proposed CI chip shape (with a frequency spacing of $\Delta f = 2$ MHz). That is, referring to Figure 7.2, only the carriers marked *Set 1* are used in 802.11's DSSS with CI chip shaping. We propose the introduction of a second set of 11 CI chips, which supports a second data stream of rate 1 MHz, created by the 11 carriers designated as *Set 2* of Figure 7.2. That is, with 22 orthogonal carriers available in the 22 MHz band, we use one set of 11 carriers to create CI chips for one DSSS transmission, and a second set of 11 carriers to create new CI chips for a second transmission. These two respective transmissions are frequency orthogonal to one another, and therefore cause zero interference while coexisting.

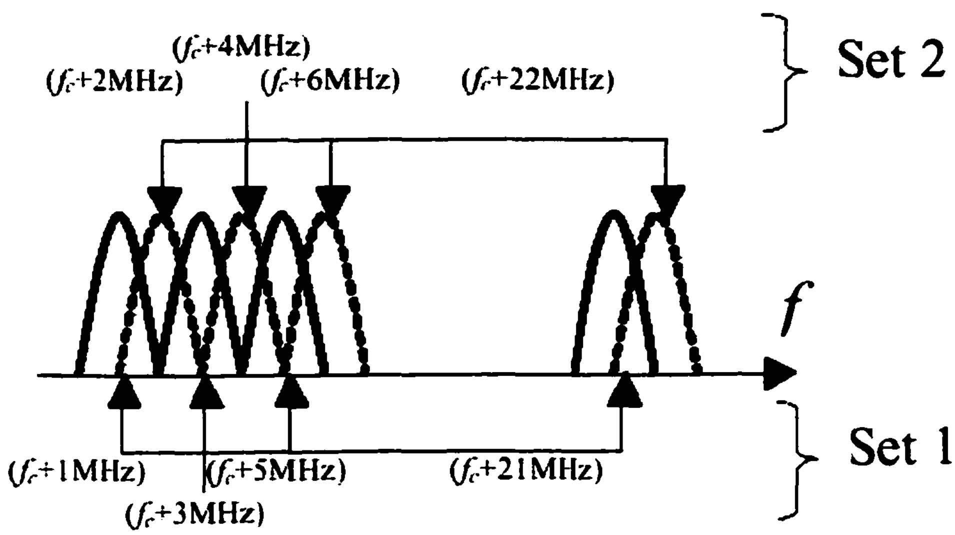

Figure 7.2 Orthogonal Carrier Sets

7.4 CI-DSSS WLAN Transmitter and Receiver Models

Figure 7.3 depicts the transmitter for the proposed CI-DSSS WLAN architecture when one set of orthogonal frequencies, Set 1 (Figure 7.2), are used to transmit a 1 MHz data stream. An analogous design is used to send the second 1MHz data stream with carriers from Set 2 (Figure 7.2). Referring to Figure 7.3, (1) the CI chip $h(t)$ is created by a linear combining of the 11 carriers, (2) the code is then generated by creating chips $h(t)$, $h(t-T_c)$,...., $h(t-10T_c)$ and applying the Barker sequence (as in equation (7.3)), (3) the data is applied to the code stream, then time limited by $g(t)$, and finally, (4) the signal is modulated to the center frequency.

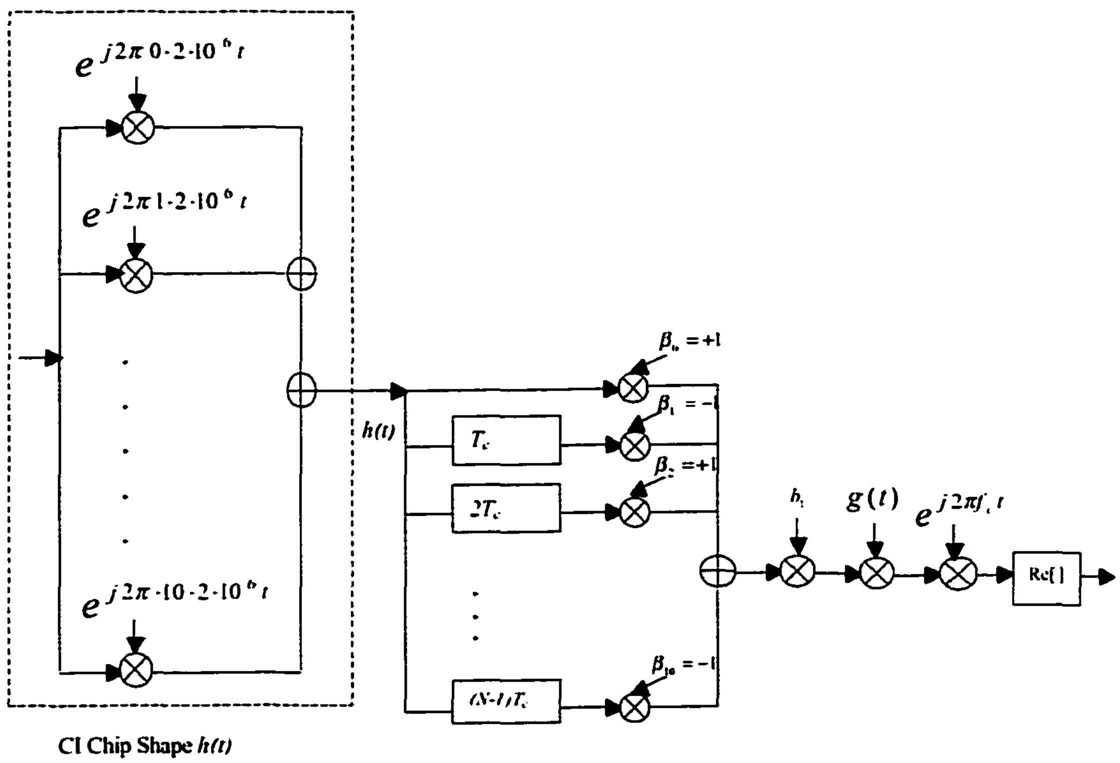

Figure 7.3 CI-DSSS Transmitter for one set of chips

The mathematical representation of this signal is therefore:

$$s\,(t) = b\,A\sum_{i=0}^{10}\beta_i \cdot \sum_{n=0}^{10}\cos\big(2\pi f_c t + 2\pi\, n\,\Delta f\big(t - iT_c\big)\big)\cdot g(t) \tag{7.4}$$

Considering the second set of 11 chips created using orthogonal frequencies (Set 2), define the new CI chip shape on carrier set 2 as

$$h_2(t) = \sum_{n=0}^{10} A e^{j(\frac{2n+1}{2})2\pi\,\Delta f\,t} \tag{7.5}$$

and rename the original CI chip shape on carrier set 1, $h(t)$, as $h_1(t)$:

$$h_1(t) = h(t) = \sum_{n=0}^{10} A e^{j2\pi n\Delta f t} \tag{7.6}$$

The spreading sequences modulated using these CI chip shapes correspond to

$$X_1^{CI}(t) = A\sum_{i=0}^{10}\beta_i\; h_1(t - iT_c)\cdot g(t) \tag{7.7}$$

and

$$X_2^{CI}(t) = A\sum_{i=0}^{10}\beta_i\; h_2(t - iT_c)\cdot g(t) \tag{7.8}$$

Using $X_1^{CI}(t)$ and $X_2^{CI}(t)$, two bit streams can be supported. The output with both chip sets summed together is:

$$X^{CI}(t) = b_1 X_1^{CI}(t) + b_2 X_2^{CI}(t) \tag{7.9}$$

$$X^{CI}(t) = b_1 A \sum_{i=0}^{10} \beta_i \; h_1(t - iT_c) \cdot g(t) + b_2 A \sum_{i=0}^{10} \beta_i \; h_2(t - iT_c) \cdot g(t) \tag{7.10}$$

The corresponding transmitted signal is then

$$\begin{aligned} S(t) &= b_1 A \sum_{i=0}^{10} \beta_i \cdot \sum_{n=0}^{10} \cos\left(2\pi f_c t + 2\pi n \Delta f\left(t - iT_c\right)\right) \cdot g(t) \\ &+ b_2 A \sum_{i=0}^{10} \beta_i \sum_{n=0}^{10} \cos(2\pi f_c t + 2\pi \; n\Delta f(t - iT_c) + 2\pi \frac{\Delta f}{2} t) g(t) \end{aligned} \tag{7.11}$$

where b_1 is a bit from the first 1 MHz stream spread by the first set of orthogonal carriers of Figure 2, b_2 is a bit from the second data stream spread by the second set of orthogonal carriers of Figure 2, and $T_c = 2/N\Delta f$.

The received signal after transmission through a frequency selective fading channel is thus:

$$\begin{aligned} r(t) &= b_1 A \sum_{i=0}^{10} \beta_i \cdot \sum_{n=0}^{10} \alpha_n \cos(2\pi f_c t + 2\pi n \Delta f t - ni \frac{2\pi}{N} + \phi_n) g(t) \\ &+ b_2 A \sum_{i=0}^{10} \beta_i \sum_{n=0}^{10} \alpha_n' \cos(2\pi f_c t + 2\pi n \Delta f t + 2\pi \frac{\Delta f}{2} t - ni \frac{2\pi}{N} + \phi_n') g(t) + \eta(t) \end{aligned} \tag{7.12}$$

where, α_n is the channel fade on the n^{th} carrier of Set 1, α_n' is the channel fade on the n^{th} carrier of Set 2, ϕ_n is the phase offset through the channel on the n^{th} carrier of Set 1, and ϕ_n' is the phase offset of the channel for the n^{th} carrier of Set 2.

Figure 7.4(a) presents the overall receiver architecture for processing the received data stream present on frequency Set 1, while Figure 7.4(b) elaborates on the MMSE frequency combining scheme utilized in each branch of Figure 7.4(a). The frequency recombining performed in Figure 7.4(b) allows for exploitation of the frequency diversity in the channel. An analogous receiver operation is used to detect the incoming data stream on frequency Set 2.

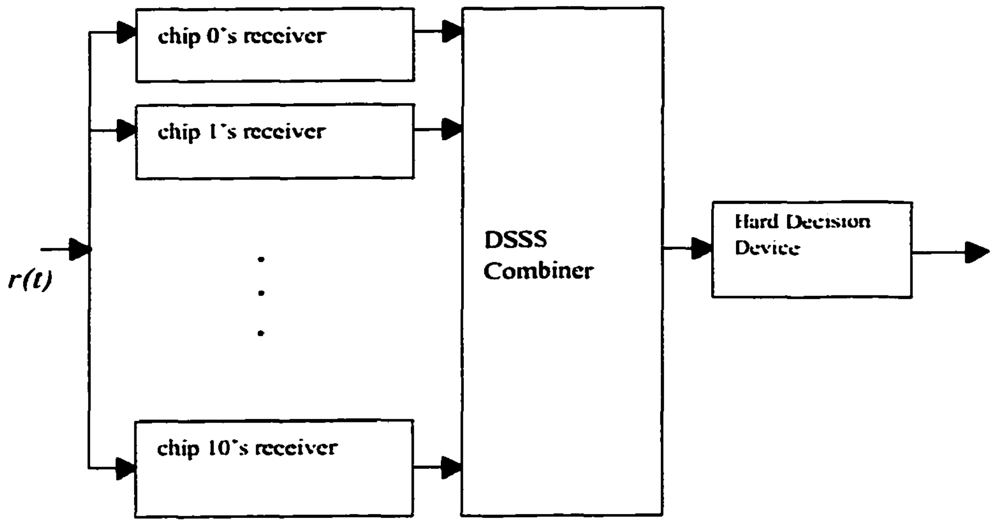

(a) Receiver structure

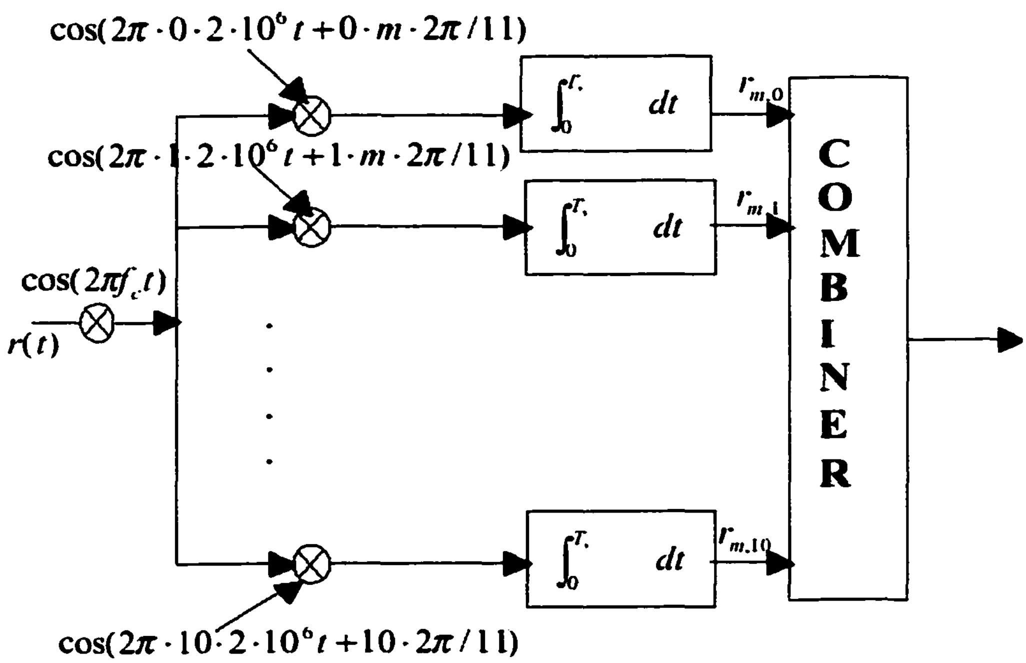

(b) Chip *m*'s receiver

Figure 7.4 CI-DSSS Receiver

Referring now to Figures 7.4(a) and 7.4(b), the incoming bit stream is split into N = 11 streams, and each is processed by the chip receiver of Figure 7.4(b). Here, detection of the m^{th} chip is performed as described in Chapter 4 and summarized next. First, the m^{th} chip is separated into its N orthogonal carrier components. Each of the m^{th} chip's carriers contributes a decision variable $r_{m,n}$, corresponding to

$$r_{m,n} = bA\beta_m\alpha_n + b\ A\alpha_n\sum_{\substack{i=0\\ i\neq m}}^{10}\beta_i\ \cos(nm\frac{2\pi}{N} - ni\frac{2\pi}{N}) + \eta_{m,n} \tag{7.13}$$

From here, the MMSE combining scheme is employed to recombine the $r_{m,n}$ terms in (7.13) across carriers to minimize interchip interference (the second term in equation (7.12)) and noise (the third term in equation (7.12)), leading to:

$$R_m = \sum_{n=0}^{10} r_{m,n}\frac{\alpha_n}{P_n\alpha_n^2 + N_0/2} \tag{7.14}$$

where the value of P_n refers to

$$P_n = \sum_{i=0}^{10}\cos^2(n(m-i)\frac{2\pi}{N}) = \begin{cases}\frac{11}{2} & n = 1,2,\ldots,10\\ 11 & n = 0\end{cases} \tag{7.15}$$

After the MMSE frequency combining of (7.14) and (7.15), we refer to Figure 7.4(a) which shows a final decision variable for the bit generated by combining the R_m 's across chips in the usual DSSS dispreading fashion:

$$D = \sum_{m=0}^{10} R_m \beta_m \tag{7.16}$$

That is, each chip decision variable R_m is multiplied by m^{th} chip's spreading value (see the m^{th} value in equation (7.1)) and combined together. A hard decision is then made on this recombined D, outputting the bit's value. By processing the signal in the frequency domain and not in the time domain, i.e., by exploiting frequency diversity and not path diversity, we achieve notable performance benefits.

7.5 Channel Model and Simulation Results

To emulate typical WLAN channels, simulations were performed utilizing the UMTS indoor channel models "Channel A" and "Channel B." These define the path models for the indoor channel at delay spreads (T_m) of 35 ns and 100 ns respectively, and match delay spreads for typical office environments [81][82]. As a benchmark for comparison, we simulated the traditional DSSS WLAN with a 4-fingered and a 6-fingered RAKE receiver (for Channel A and Channel B respectively). These two channel models are defined as a transversal filter with time varying coefficients whose average power is determined by the multipath power delay profile (PDP) given in Table 7.1 and Table 7.2.

Tap No.	$\tau(ns)$	Average power (dB)
1	0	0.0
2	50	-3.0
3	110	-10.0
4	170	-18.0
5	290	-26.0
6	310	-32.0

Table 7.1 Multipath Power Delay Profiles for UMTS Channel A

Tap No.	$\tau(ns)$	Average power (dB)
1	0	0.0
2	100	-3.6
3	200	-7.2
4	300	-10.8
5	500	-18.0
6	700	-25.2

Table 7.2 Multipath Power Delay Profiles for UMTS Channel B

This performance was compared to that of our DSSS WLAN with CI chip-shaping (referred to below as CI-DSSS WLAN). Our emulated CI system has twice the throughput of the benchmark traditional 802.11 DSSS system.

Figure 7.5 and Figure 7.6 compare bit error rate (BER) versus signal-to-noise ratio (SNR) for DBPSK DSSS WLAN and DBPSK CI-DSSS WLAN in both Channel A and B. While the DSSS data rate is 1 Mbps, the CI-DSSS data rate is 2 Mbps, achieved by incorporation of the second set of orthogonal chips. From Figures 7.5 and 7.6, even with twice the throughput, CI-DSSS outperforms DSSS by approximately 4 dB at a BER of 10^{-3} in Channel A, and approximately 3 dB in Channel B at BER of 10^{-3}. These performance benefits are conservative estimates, since, in creating these results, benchmark DSSS receivers are based on 4 and 6 fingered RAKE (complex and expensive). (Typically, one or two path RAKE receivers are deployed in DSSS WLAN.)

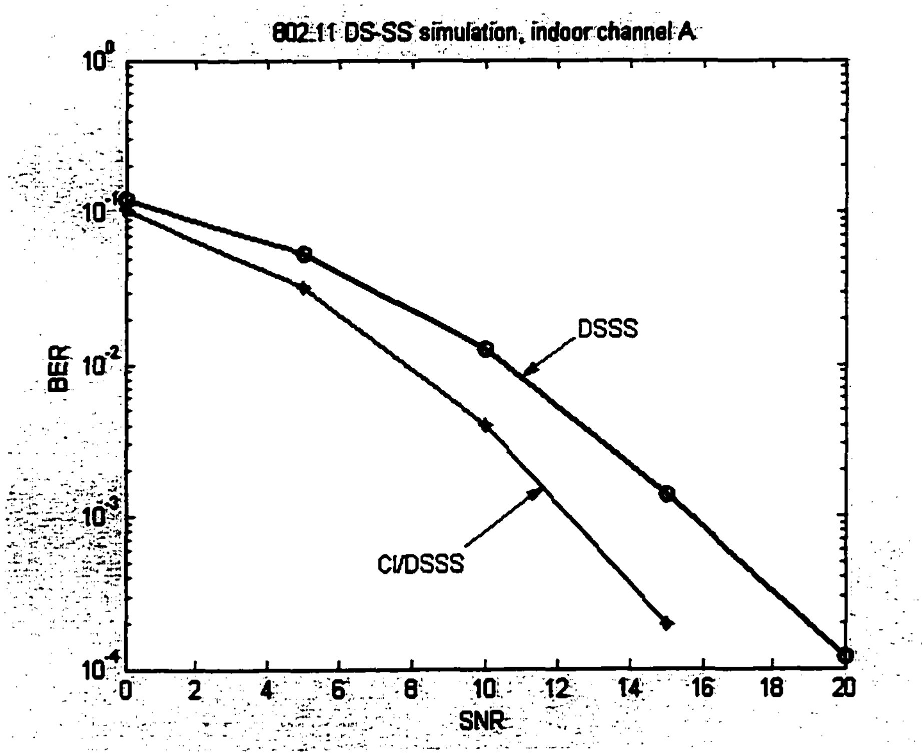

Figure 7.5 Simulation Results for Channel A

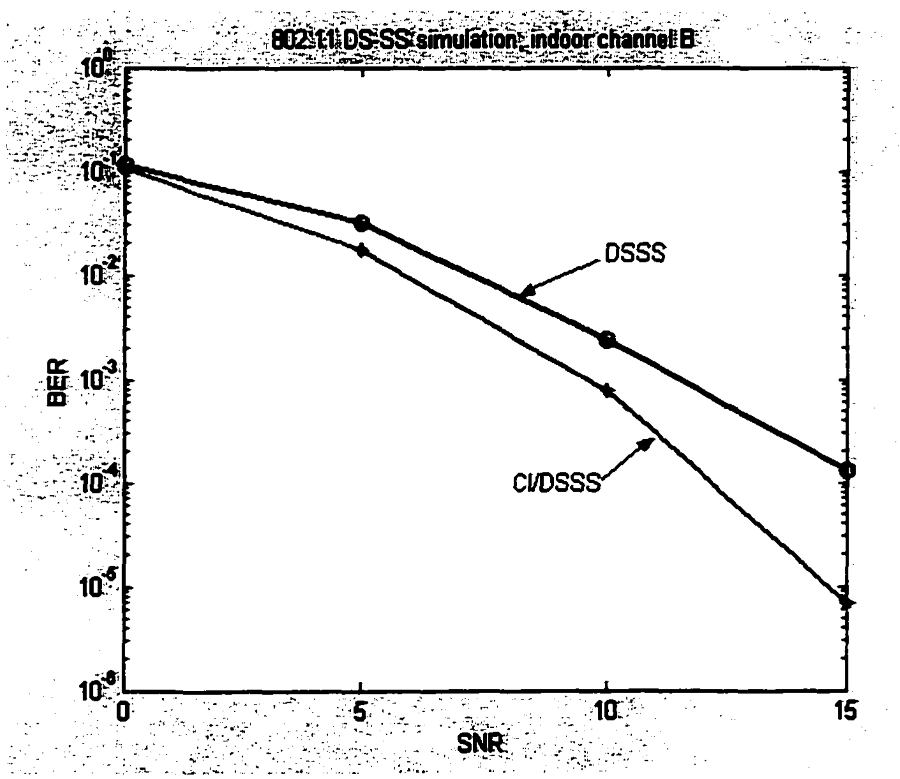

Figure 7.6 Simulation Results for Channel B

7.6 PO-CI-DSSS: High-Performance IEEE 802.11 DSSS WLAN via CI Chip Shaping with Quadruple Throughput

In earlier sections, we applied novel CI chip shapes into the IEEE 802.11 DSSS WLAN scenario and showed how this leads to a doubling in throughput. Specifically, when CI chip shapes are used, two spreading codes are available (as opposed to the usual one spreading code), namely

$$X_1^{CI}(t) = A\sum_{i=0}^{10} \beta_i \; h_1(t - iT_c)\cdot g(t) \tag{7.17}$$

where

$$h_1(t) = h(t) = \sum_{n=0}^{10} Ae^{j2\pi n\Delta f t} \tag{7.18}$$

and

$$X_2^{CI}(t) = A\sum_{i=0}^{10} \beta_i \; h_2(t - iT_c)\cdot g(t) \tag{7.19}$$

where

$$h_2(t) = \sum_{n=0}^{10} Ae^{j(\frac{2n+1}{2})2\pi\Delta f t} \tag{7.20}$$

In this section, we further exploit the CI chip shaping strategy, allowing us to again double the throughput, for a total throughput gain of four times that of traditional IEEE 802.11 DSSS WLAN. Specifically, we propose to again double the throughput of the CI-DSSS system by introducing a pseudo-orthogonal chip set (described in section 3.6), creating what we term PO-CI-DSSS (pseudo-orthogonal CI-DSSS). When doing this, the novel PO-CI-DSSS system supports four times the throughput of the traditional

DSSS system, while simultaneously achieving a 2dB performance gain at a probability of error of 10^{-3}. The details follow.

As discussed in section 3.6, there exists a novel way to further double the throughput of the CI-DSSS system: introduce pseudo-orthogonal chip sets (in time). By doing so, the novel CI-DSSS system supports four times the throughput of the traditional DSSS system. Specifically, consider the first orthogonal subcarrier set, characterized by equations (7.17) and (7.18). It is easily shown that a second set code can be created that is highly (but pseudo) orthogonal to this code, namely

$$X_1^{PO\text{-}CI}(t) = \sum_{i=0}^{10} \beta_i \; h(t - iT_c - \frac{T_c}{2}) \cdot g(t) \tag{7.21}$$

That is, it turns out that the code created by delaying the CI chips by a duration of $T_c/2$ is highly orthogonal to the code created with CI chips with a zero delay offset. Using this pseudo-orthogonal code, and calling the resulting system PO-CI-DSSS (pseudo-orthogonal CI-DSSS), we can now support four simultaneous transmission, each using one of the four codes

$$X_1^{CI}(t) = \sum_{i=0}^{10} \beta_i \; h_1(t - iT_c) \cdot g(t) \tag{7.22}$$

$$X_1^{PO\text{-}CI}(t) = \sum_{i=0}^{10} \beta_i \; h_1(t - iT_c - \frac{T_c}{2}) \cdot g(t) \tag{7.23}$$

$$X_2^{CI}(t) = \sum_{i=0}^{10} \beta_i \; h_2(t - iT_c) \cdot g(t) \tag{7.24}$$

$$X_2^{PO-CI}(t) = \sum_{i=0}^{10} \beta_i \; h_2(t - iT_c - \frac{T_c}{2}) \cdot g(t) \tag{7.25}$$

The transmitter for the proposed CI-DSSS WLAN architecture when the code $X_1^{CI}(t)$ is used to transmit a 1 MHz data stream is exactly the same as shown in Figure 7.3. An analogous design is used to send the second, third and fourth 1 MHz data stream with code $X_1^{PO-CI}(t)$, $X_2^{CI}(t)$, and $X_2^{PO-CI}(t)$. Referring to Figure 7.3, (1) the CI chip $h_1(t)$ is created by a linear combining of the 11 carriers, (2) the code is then generated by creating chips $h_1(t)$, $h_1(t-T_c)$,..., $h_1(t-10T_c)$ and applying the Barker sequence (as seen in equation (7.1)), (3) the data is applied to the code stream, then time limited by $g(t)$, and finally, (4) the signal is modulated to the center frequency. The mathematical representation of this signal is therefore:

$$s(t) = \mathrm{Re}\{bX_1^{CI}(t)e^{j2\pi f_c t}g(t)\} \tag{7.26}$$

$$s(t) = b\; A\sum_{i=0}^{10} \beta_i \cdot \sum_{n=0}^{10} \cos\left(2\pi f_c t + 2\pi\; n\; \Delta f\left(t - iT_c\right)\right) \cdot g(t) \tag{7.27}$$

Considering the second set of 11 chips created using orthogonal frequencies (Set 2), the output with both chip sets summed together is:

$$s(t) = \mathrm{Re}\{(b_1 X_1^{CI}(t) + b_2 X_2^{CI}(t))e^{j2\pi f_c t}g(t)\} \tag{7.28}$$

$$S(t) = \mathrm{Re}\{(b_1 A\sum_{i=0}^{10} \beta_i h_1(t - iT_c)g(t) + b_2 A\sum_{i=0}^{10} \beta_i h_2(t - iT_c))e^{j2\pi f_c t}\} \tag{7.29}$$

Finally, with the codes generated using delayed CI (equation (7.23) and (7.25)), four data bits are sent through the channel simultaneously:

$$s(t) = \mathrm{Re}\{(b_1 X_1^{CI}(t) + b_2 X_x^{CI}(t) + b_3 X_1^{PO-CI}(t) + b_4 X_2^{PO-CI}(t))e^{j2\pi f_c t} g(t)\} \quad (7.30)$$

$$\begin{aligned} S(t) = \mathrm{Re}\{(&b_1 A \sum_{i=0}^{10} \beta_i\, h_1(t - iT_c) \cdot g(t) + b_2 A \sum_{i=0}^{10} \beta_i\, h_2(t - iT_c) g(t) \\ &+ b_3 A \sum_{i=0}^{10} \beta_i h_1(t - iT_c - T_c/2) \cdot g(t) + b_4 A \sum_{i=0}^{10} \beta_i h_2(t - iT_c - T_c/2) \cdot g(t)) e^{j2\pi f_c t}\} \end{aligned}$$

(7.31)

where b_1 is a bit from the first 1 MHz stream, b_2 is a bit from the second data stream, and so on.

Using the $h_1(t)$ and $h_2(t)$ of equation (7.18) and (7.20) leads to:

$$\begin{aligned} S(t) = &\, b_1 A \sum_{i=0}^{10} \beta_i \cdot \sum_{n=0}^{10} \cos\big(2\pi f_c t + 2\pi\ n\Delta f\big(t - iT_c\big)\big) \cdot g(t) \\ &+ b_2 A \sum_{i=0}^{10} \beta_i \sum_{n=0}^{10} \cos(2\pi\, f_c t + 2\pi\ n\Delta f(t - iT_c) + 2\pi \frac{\Delta f}{2}(t - iT_c)) \cdot g(t) \\ &+ b_3 A \sum_{i=0}^{10} \beta_i \sum_{n=0}^{10} \cos(2\pi f_c t + 2\pi n\Delta f(t - iT_c - T_c/2)) \cdot g(t) \\ &+ b_4 A \sum_{i=0}^{10} \beta_i \sum_{n=0}^{10} \cos(2\pi f_c t + 2\pi n\Delta f(t - iT_c - T_c/2) + 2\pi \frac{\Delta f}{2}(t - iT_c)) \cdot g(t) \end{aligned}$$

(7.32)

The received signal after transmission through a frequency selective fading channel is thus:

$$
\begin{aligned}
r(t) &= b_1 A\sum_{i=0}^{10}\beta_i \cdot\sum_{n=0}^{10}\alpha_{n,1}\cos\left(2\pi f_c t+2\pi\ n\Delta f\left(t-iT_c\right)+\phi_{n,1}\right)\cdot g(t)\\
&+b_2 A\sum_{i=0}^{10}\beta_i \sum_{n=0}^{10}\alpha_{n,2}\cos(2\pi f_c t+2\pi\ n\Delta f(t-iT_c)+2\pi\frac{\Delta f}{2}(t-iT_c)+\phi_{n,2})\cdot g(t)\\
&+b_3 A\sum_{i=0}^{10}\beta_i \sum_{n=0}^{10}\alpha_{n,1}\cos(2\pi f_c t+2\pi n\Delta f(t-iT_c-T_c/2)+\phi_{n,1})\cdot g(t)\\
&+b_4 A\sum_{i=0}^{10}\beta_i \sum_{n=0}^{10}\alpha_{n,2}\cos(2\pi f_c t+2\pi n\Delta f(t-iT_c-T_c/2)+2\pi\frac{\Delta f}{2}(t-iT_c)+\phi_{n,2})\cdot g(t)\\
&+\eta(t)
\end{aligned}
\tag{7.33}
$$

or, expressing the delays as phase offsets,

$$
\begin{aligned}
r(t) &= b_1 A\sum_{i=0}^{10}\beta_i \cdot\sum_{n=0}^{10}\alpha_{n,1}\cos\left(2\pi f_c t+2\pi n\,\Delta f t-ni2\pi/N+\phi_{n,1}\right)\cdot g(t)\\
&+b_2 A\sum_{i=0}^{10}\beta_i \sum_{n=0}^{10}\alpha_{n,2}\cos(2\pi f_c t+2\pi n\Delta f t-ni2\pi/N+2\pi\frac{\Delta f}{2}t-i\pi/N+\phi_{n,2})\cdot g(t)\\
&+b_3 A\sum_{i=0}^{10}\beta_i \sum_{n=0}^{10}\alpha_{n,1}\cos(2\pi f_c t+2\pi n\Delta f t-ni2\pi/N-n\pi/N+\phi_{n,1})\cdot g(t)\\
&+b_4 A\sum_{i=0}^{10}\beta_i \sum_{n=0}^{10}\alpha_{n,2}\cos(2\pi f_c t+2\pi n\Delta f t-ni2\pi/N-n\pi/N+2\pi\frac{\Delta f}{2}t-i\pi/N+\phi_{n,2})\cdot g(t)\\
&+\eta(t)
\end{aligned}
\tag{7.34}
$$

where $\alpha_{n,1}$ is the channel fade on the n^{th} carrier of frequency Set 1; $\alpha_{n,2}$ is the channel fade on the n^{th} carrier of frequency Set 2; $\phi_{n,1}$ is the phase offset through the channel on the n^{th} carrier of frequency Set 1, and $\phi_{n,2}$ is the phase offset of the channel for the n^{th} carrier of frequency Set 2, and $\eta(t)$ is the additive Gaussian noise.

Figure 7.4(a) presents the overall receiver architecture for processing the first data stream, i.e, the data stream on code $X_1^{CI}(t)$. Figure 8.4(b) elaborates on the frequency combining scheme utilized in each branch of Figure 7.4(a). Analogous receiver operations are used to detect the incoming data streams on the other codes ($X_1^{PO-CI}(t)$, $X_2^{CI}(t)$ and $X_2^{PO-CI}(t)$). The frequency recombining performed by the receiver in Figure 8.4(b) exploits the frequency diversity in the channel.

Referring now to Figures 7.4(a) and 7.4(b), the incoming bit stream is split into $N = 11$ streams, and each is processed by the chip receiver of Figure 7.4(b) (where, detection of the m^{th} chip is performed). First, the m^{th} chip is separated into its N orthogonal carrier components. Each of the m^{th} chip's carriers contributes a decision variable $r_{m,n}$ for b_1 corresponding to

$$\begin{aligned} r_{m,n} &= b_1 A\beta_m\alpha_n + b_1 A\alpha_n \sum_{\substack{i=0 \\ i\neq m}}^{10} \beta_i \cos(nm\frac{2\pi}{N} - ni\frac{2\pi}{N}) \\ &+ b_3 A\alpha_n \sum_{i=0}^{10} \beta_i \cos(nm\frac{2\pi}{N} - ni\frac{2\pi}{N} - n\frac{\pi}{N}) + \eta_{m,n} \end{aligned} \tag{7.35}$$

Next, the MMSE combining scheme is employed to recombine the $r_{m,n}$ terms in (7.35) across carriers to minimize interchip interference (the second and third terms in equation (7.35)) and noise (the fourth term in equation (7.35)), leading to:

$$R_m = \sum_{n=0}^{10} r_{m,n} \frac{\alpha_n}{2P_n\alpha_n^2 + N_0/2} \tag{7.36}$$

where the value of P_n refers to

$$P_n = \sum_{i=0}^{10} \cos^2(n(m-i)\frac{2\pi}{N}) = \begin{cases} \frac{11}{2} & n = 1,2,\ldots,10 \\ 11 & n = 0 \end{cases} \tag{7.37}$$

After the MMSE frequency combining of (7.36) and (7.37), we refer to Figure 7.4(a), where a final decision variable for the bit is generated by combining the R_m's across chips in the usual DSSS despreading fashion:

$$D = \sum_{m=0}^{10} R_m \beta_m \tag{7.38}$$

That is, each chip decision variable R_m is multiplied by m^{th} chip's spreading value (see the m^{th} value in equation (7.1)) and combined together. A hard decision is then made on this recombined D, outputting the bit's value. By processing the signal in the frequency domain and not in the time domain, i.e., by exploiting frequency diversity and not path diversity, we achieve notable performance benefits while supporting four times throughput relative to traditional 802.11 DSSS standard.

As above, to emulate typical WLAN channels, simulations were performed utilizing the UMTS indoor channel models "Channel A" and "Channel B." These define the path models for indoor channels with delay spreads (T_m) of 35 *ns* and 100 *ns* respectively (matching delay spreads for typical office environments). As a benchmark for comparison, we simulated both the traditional DSSS WLAN with a 4-fingered and a 6-fingered RAKE receiver (for Channel A and Channel B respectively) and we simulated CI-DSSS WLAN without pseudo-orthogonal chips. This performance was compared to that of our high throughput DSSS WLAN with CI chip-shaping and pseudo-orthogonal chips (referred to below as PO-CI-DSSS WLAN). Our emulated CI system has four times the throughput of the benchmark traditional 802.11 DSSS system, and is constructed as described above.

Figure 7.7 and Figure 7.8 compare bit error rate (BER) versus signal-to-noise ratio (SNR) for DBPSK DSSS WLAN, DBPSK CI-DSSS WLAN and DBPSK PO-CI-DSSS WLAN in both Channel A and B. While the DSSS data rate is 1 Mbps, the CI-DSSS data rate is 2 Mbps, and the PO-CI-DSSS data rate is 4 Mbps, achieved by incorporation of the pseudo-orthogonal chips and the second set of orthogonal carriers. From Figure 7.7 and Figure 7.8, even with four times the throughput, PO-CI-DSSS still outperforms DSSS by approximately 2 dB at a BER of 10^{-3} in Channel A, and approximately 1 dB in Channel B at BER of 10^{-3}. These performance benefits are conservative estimates, since, in creating these results, benchmark DSSS receivers are based on 4 and 6 fingered RAKE (complex and expensive). (Typically, one or two path RAKE receivers are deployed in DSSS WLAN.) We also observe that little performance is lost relative to CI-DSSS proposed in section 8.3-8.5, but a doubling in throughput is achieved.

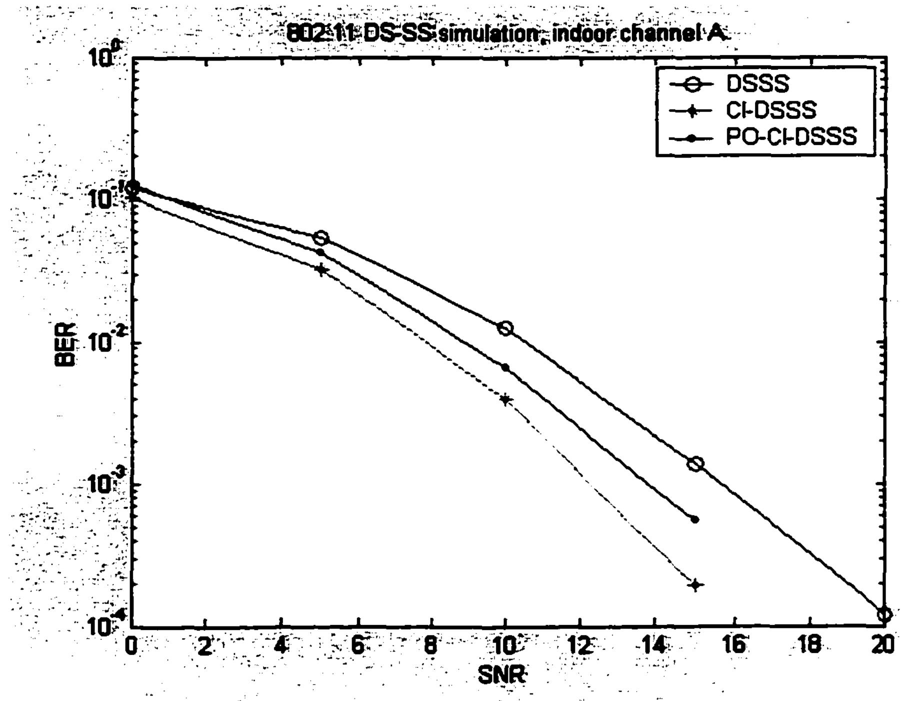

Figure 7.7 **Simulation Results of PO-CI-DSSS for Channel A**

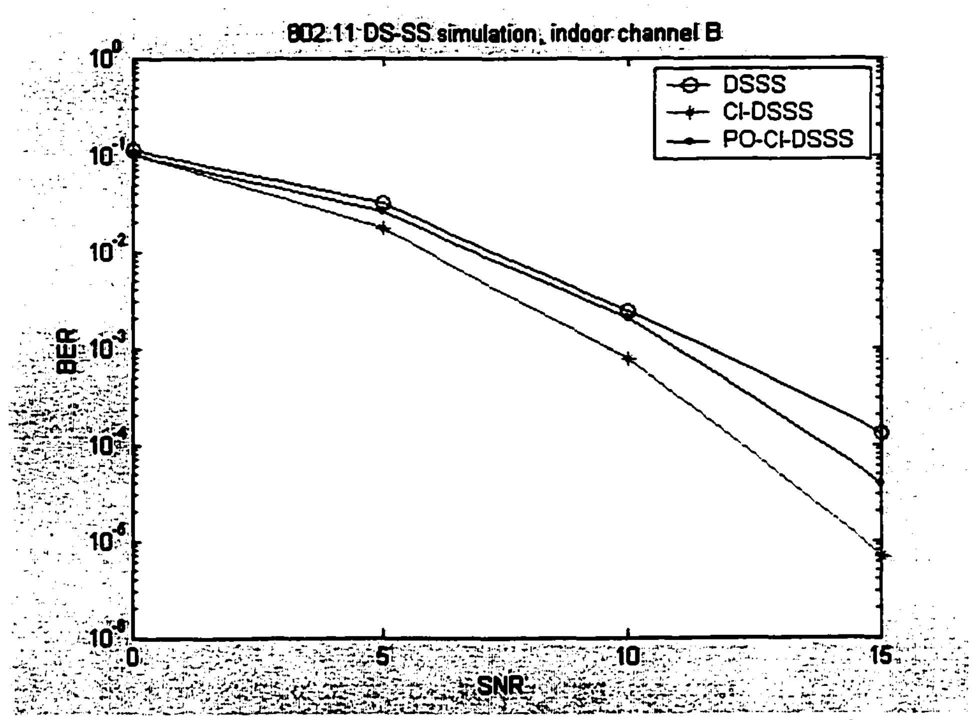

Figure 7.8 **Simulation Results of PO-CI-DSSS for Channel B**

7.7 Conclusions

In this chapter, we propose CI-DSSS which, when compared to traditional DSSS, offers significant improvement in terms of both performance and throughput. Specifically, we have shown how applying CI chip-shaping and frequency recombining (described in Chapter 3) enables 3 dB performance gain and a doubling of data rate over traditional 802.11 DSSS WLAN. The cost of added transmitter complexity is minimal when compared to these substantial gains.

Furthermore, we apply both pseudo-orthogonal chips (described in section 3.6) and a second set of orthogonal carriers in DSSS which, when compared to traditional DSSS, offers *very* significant improvement in terms of throughput (while achieving a performance *gain*). Specifically, we have shown how our this work enables a *quadrupling* of data rate over traditional 802.11 DSSS WLAN while achieving a 2dB performance gain at probability of error of 10^{-3}. The cost of added transmitter complexity is minimal when compared to these substantial gains. By implementing the proposed CI-DSSS at the physical layer, IEEE's 802.11 WLAN becomes a high-performance, high-throughput connection.

Part III

MC-CDMA

Chapter 8 Introduction to MC-CDMA and CI/MC-CDMA

MC-CDMA (multi-carrier code vision multiple access) has emerged as a powerful alternative to current DS-CDMA in wireless communications. Instead of spreading the signal in the time domain as in DS-CDMA, MC-CDMA spreads the signal in frequency domain. Specifically, in MC-CDMA, each user's data is transmitted simultaneously over multiple narrowband subcarriers, with the subcarriers encoded with a unique orthogonal (or pseudo-orthogonal) spreading code.

After transmission through a multipath fading channel (or equivalently a frequency selective fading channel), the orthogonality between MC-CDMA signals is lost. However, by decomposing the MC-CDMA signal into each and every frequency component (i..e, subcarrier) and carefully recombining them, frequency diversity can be exploited. It has been shown that the frequency diversity exploited in MC-CDMA leads to larger SIR (signal to interference ratio) compared to a RAKE receiver in current DS-CDMA systems (which exploits path diversity).

Moreover, by introducing the novel CI (carrier interferometry) codes described in Chapter 4 into MC-CDMA, other authors have created a novel version of the MC-CDMA system: CI/MC-CDMA (carrier interferometry multi-carrier code vision multiple access) [49][83-86]. With lower cross correlation properties in frequency selective channels (relative to traditional spreading codes used for MC-CDMA systems), CI/MC-CDMA demonstrates better BER performance than conventional MC-CDMA systems [49][83][84]. Moreover, by introducing offset CI codes (with minimum correlation to CI codes) as pseudo-orthogonal codes, CI/MC-CDMA systems have been shown to double the network capacity of conventional MC-CDMA systems with negligible performance loss [85].

In this chapter, we briefly review the concept of MC-CDMA, its transmitter structure, receiver structure, and its performance improvements over DS-CDMA. Additionally, we review CI/MC-CDMA and show how this novel version of MC-CDMA is able to significantly improve the performance and network capacity of current MC-CDMA systems. (It is important to note that CI/MC-CDMA is not being presented as innovation research conducted as part of this thesis – however, the improvement to it, found in Chapter 9-11, do represent an important contribution to the filed.)

8.1 Introduction to MC-CDMA

First proposed in 1993, MC-CDMA has received a great deal of attention and has been considered a strong alternative to DS-CDMA for next generation mobile communications [25-38].

The block diagram representation of the MC-CDMA transmitter is shown in Figure 8.1. Much like in DS-CDMA, the MC-CDMA transmitter for user k spreads the original data stream via a spreading code $c_k(t)$. However, the spreading code $c_k(t)$ is applied in the frequency domain instead of the time domain. Each user is allocated a unique spreading code (typically orthogonal in both the downlink and synchronous uplink).

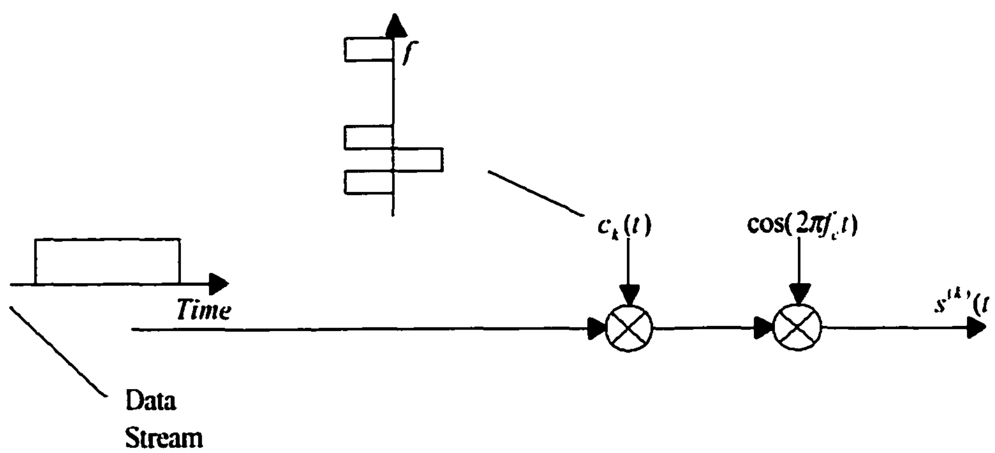

Figure 8.1 Conceptual Transmitter for MC-CDMA

Mathematically, in an MC-CDMA system, the k^{th} user's transmission corresponds to

$$s^k(t) = \mathrm{Re}\{b_k c_k(t) e^{j2\pi f_c t}\} \tag{8.1}$$

where b_k is user k's information bit (assumed +1 or −1 for ease in presentation), and $c_k(t)$ is user k's spreading code, which in MC-CDMA systems refers to

$$c_k(t) = \sum_{i=0}^{N-1} e^{j\beta_i^{(k)}} e^{j2\pi i\Delta f t} \cdot g(t) \tag{8.2}$$

Here, N is processing gain, i.e., the total number of narrowband carriers in the MC-CDMA code; $e^{j\beta_i^k}$ is the i^{th} value in user k's spreading sequence, typically +1 or −1 ($\beta_i^{(k)}$ is 0 or π) in accordance with known spreading codes such as Hadamard-Walsh codes; $i\Delta f$ is the frequency position of the i^{th} frequency component (typically $\Delta f = 1/T_s$, where T_s is symbol duration, to ensure carrier orthogonality); and $g(t)$ is a rectangular waveform of unity height which time-limits the code to one symbol duration T_s.

Including code creation in the MC-CDMA transmitter side, we can redraw Figure 8.1 in a more detailed manner, as shown in Figure 8.2:

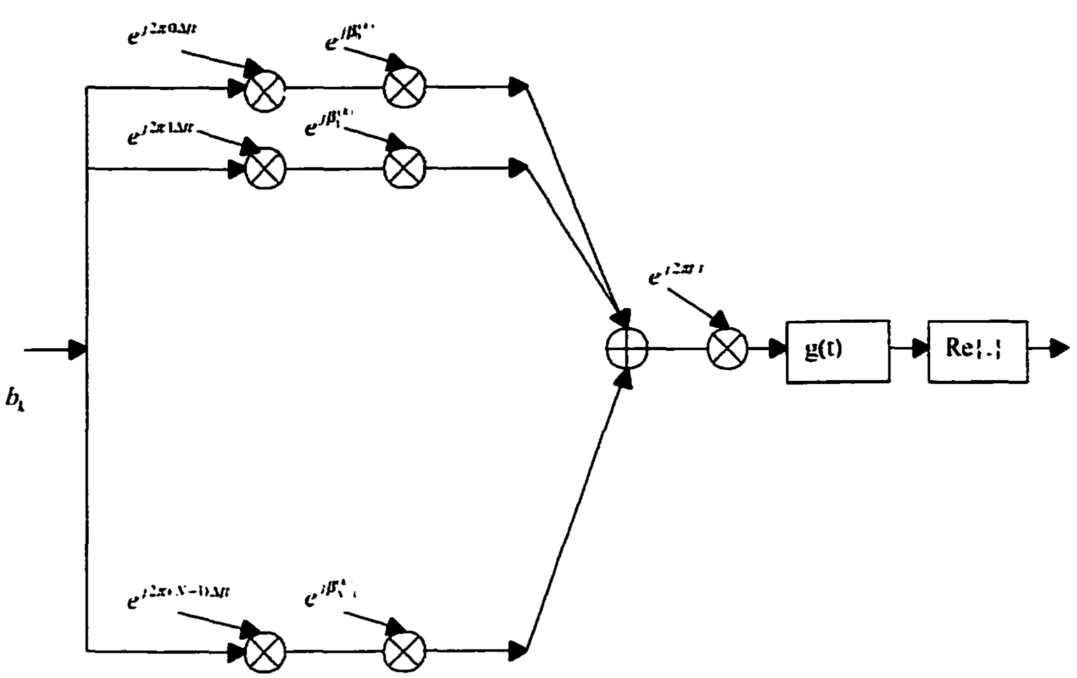

Figure 8.2 Transmitter for MC-CDMA

The total transmit signal considering all K users' signals (and assuming downlink or synchronous uplink communications):

$$S(t)=\sum_{k=0}^{K-1} b_k \operatorname{Re}\left\{\sum_{i=0}^{N-1} e^{j\beta_i^{(i)}} e^{j2\pi f_c t} e^{j2\pi i\Delta f t}\right\}\cdot g(t) \tag{8.5}$$

After transmission through a multipath fading channel, the frequency selectivity over the entire bandwidth is resolved by the narrowband carriers, i.e., each of the N narrowband carriers experience a unique flat fade. The received signal in MC-CDMA thus corresponds to

$$r(t)=\sum_{k=0}^{K-1} b_k \operatorname{Re}\left\{\sum_{i=0}^{N-1} \alpha_i e^{j\beta_i^{(i)}} e^{j2\pi f_c t} e^{j2\pi i\Delta f t} e^{j\theta_i}\right\}\cdot g(t)+\eta(t) \tag{8.6}$$

where K is the number of users occupying the system, α_i is the gain of the i^{th} subcarrier and ϕ_i the phase offset of the i^{th} subcarrier due to the channel, and $\eta(t)$ represents AWGN.

The MC-CDMA receiver for user l is shown in Figure 8.3.

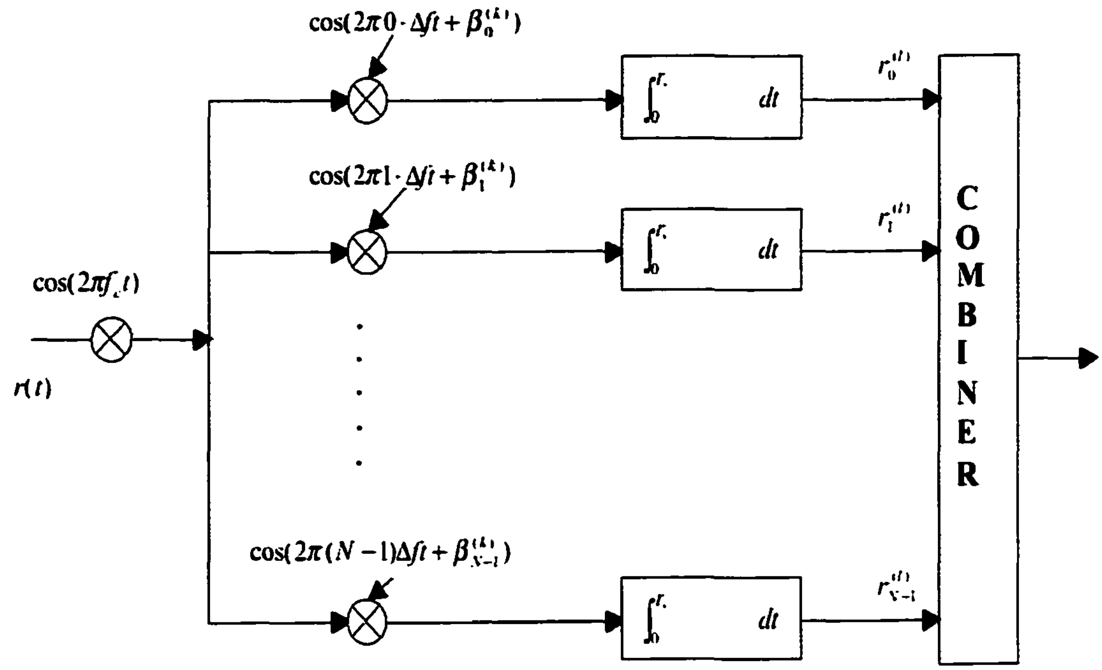

Figure 8.3 MC-CDMA Receiver for user l

Here, the received signal is decomposed into its N orthogonal carriers and despread by user l's spreading code. The i^{th} carrier generates the decision variable (assuming ideal phase synchronization)

$$r_i^{(l)} = \alpha_i b_l + \alpha_i \sum_{\substack{k=0 \\ k\neq l}}^{K-1} b_k \operatorname{Re}[e^{j(\beta_i^{(k)}-\beta_i^{(l)})}] + \eta_i \tag{8.7}$$

Here, η_i is a Gaussian random variable with 0 mean and variance $\frac{N_0}{2}$. Next, a suitable combining strategy is used to linearly combine the $r_i^{(l)}$ terms and create a final decision variable. It has been shown in literatures that MMSEC (minimized mean square error combining) produces the best performances in terms of bit error rate. Employing MMSEC in MC-CDMA results in the decision variable

$$R^{(l)} = \sum_{i=0}^{N-1} r_i^{(l)} \frac{\alpha_i}{K\alpha_i^2 + N_0/2} \tag{8.8}$$

A hard decision device follows to make the final decision:

$$\hat{b}_l = \begin{cases} +1 & \mathit{if}\ R^{(l)} > 0 \\ -1 & \mathit{else} \end{cases} \tag{8.9}$$

From the above receiver design, we observe MC-CDMA receivers exploit frequency diversity in the frequency selective channel by separating carriers and recombining them (while DS-CDMA RAKE receiver use correlators to resolve multiple paths and create path diversity) (Chapter 2). In DS-CDMA case, large inter-path interferences on each RAKE finger significantly decrease the performance. As MC-CDMA receivers avoid this damaging effect, MC-CDMA receivers outperform DS-CDMA RAKE receivers significantly.

Figure 8.4 shows a typical MC-CDMA and DS-CDMA BER versus signal to noise ratio (SNR) curve in the hilly terrain (HT) channel. Figure 8.5 shows the same result in typical urban (TU) channel [57]. The processing gain is N=32 and the system is fully loaded: the high error floor due to the multipath interference in DS-CDMA is avoided in MC-CDMA.

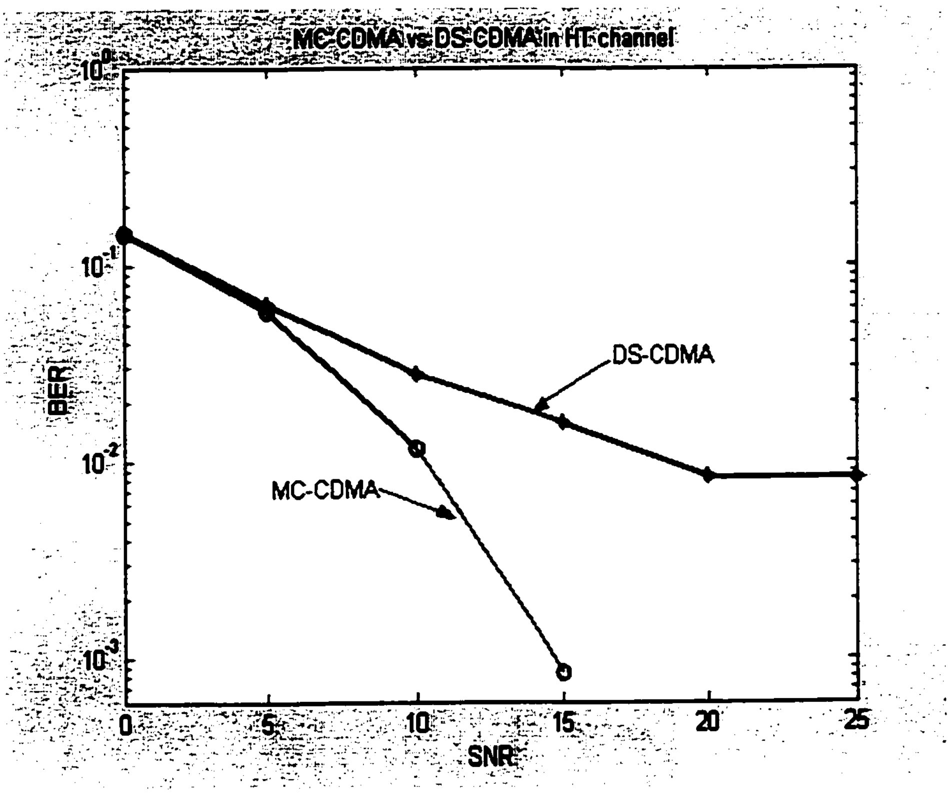

Figure 8.4 Performance of MC-CDMA and DS-CDMA in HT Channel

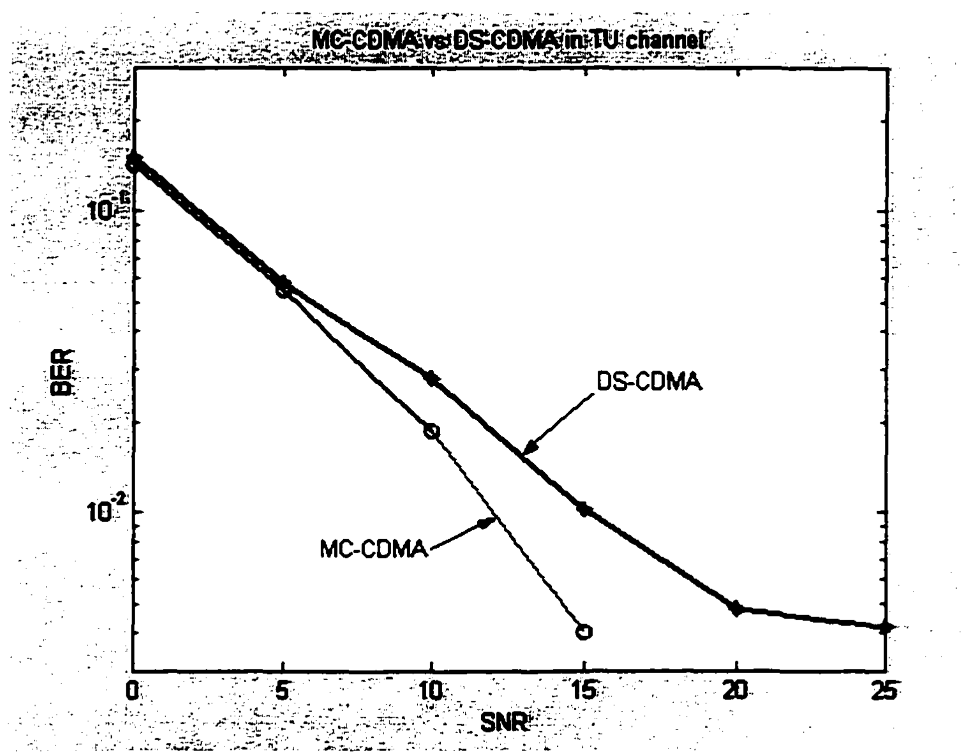

Figure 8.5 Performance of MC-CDMA and DS-CDMA in TU Channel

8.2 Introduction to CI/MC-CDMA

In Chapter 4, we proposed Carrier Interferometry (CI) spreading codes derived from the DFT and applied these to DS-CDMA systems. These CI codes, a novel set of orthogonal codes, can also be applied to MC-CDMA systems. These CI/MC-CDMA systems have recently been presented in the literatures [49][83-86].

Traditionally, Hadamard-Walsh codes are employed to MC-CDMA systems as spreading codes to maintain orthogonality between different users, i.e., $\beta_i^{(k)}$ is *0* or π and is chosen according to well-known principles.

Described in Chapter 4, the orthogonal CI codes are generated by allowing the i^{th} component of user k's spreading sequence, $e^{j\beta_i^k}$, to demonstrate phase offset

$$\beta_i^{(k)} = i \cdot k \frac{2\pi}{N} \tag{8.10}$$

The novel orthogonal spreading codes are called CI spreading codes, where CI refers to Carrier Interferometry, because when these codes are applied to distinct harmonics, an interferometry pattern is observed.

When CI codes are applied as spreading codes in the MC-CDMA system, CI/MC-CDMA results. The transmitter and receiver structures of CI/MC-CDMA systems are identical to those in Figure 8.2 and Figure 8.3; the only update is the change in spreading code from +1 and −1 values to values from (8.10). The impact of this change is detailed next.

User k's transmitted signal in CI/MC-CDMA corresponds to

$$s^{(k)}(t) = b_k \operatorname{Re}\left\{ \sum_{i=0}^{N-1} e^{j \cdot i \cdot k \frac{2\pi}{N}} e^{j2\pi f_c t + 2\pi i \Delta f t} \right\} \cdot g(t) \tag{8.11}$$

and the total transmit signal with K users is

$$S(t)=\sum_{k=0}^{K-1} b_k \operatorname{Re}\left\{\sum_{i=0}^{N-1} e^{j\cdot i\cdot k\frac{2\pi}{N}} e^{j2\pi f_c t} e^{j2\pi i\Delta f t}\right\}\cdot g(t) \tag{8.12}$$

After transmission over a frequency selective fading channel (in downlink or synchronized uplink), the received CI/MC-CDMA signal corresponds to

$$r(t)=\operatorname{Re}\Big[\sum_{k=0}^{K-1} b_k \sum_{i=0}^{N-1} \alpha_i e^{j\phi_i} e^{j\cdot i\cdot k\frac{2\pi}{N}} e^{j2\pi i\Delta f t} e^{j2\pi f_c t} g(t)\Big]+\eta(t) \tag{8.13}$$

where K is the total number of users utilizing the system, α_i is the gain and φ_i the phase offset in the i^{th} carrier, and $\eta(t)$ represents additive white Gaussian noise. Again, to simplify the analysis, exact phase synchronization is assumed.

The output in the i^{th} subcarrier of l^{th} user's receiver corresponds to the decision variable

$$r_i^{(l)}=\alpha_i b_l+\alpha_i \sum_{\substack{k=0\\ k\neq l}}^{K-1} b_k \operatorname{Re}\big[e^{j\cdot i\cdot(k-l)\frac{2\pi}{N}}\big]+\eta_i \tag{8.14}$$

Now let's investigate the SIR at the i^{th} carrier component [48][49]. The SIR at the i^{th} carrier component corresponds to

$$SIR_i^{CI}=\frac{\alpha_i^2}{\sigma_{I\,i}^{\,2}+\sigma_{N\,i}^{\,2}}=\frac{\alpha_i^2}{(K-1)\alpha_i^2 P_i+N_0/2} \tag{8.15}$$

where $\sigma_{I\,i}^{\,2}$ represents the power of MAI (2[nd] term) in the i^{th} carrier, $\sigma_{N\,i}^{\,2}$ represents the power of additive noise in i^{th} carrier component; and

$$P_i = E[(\mathrm{Re}[e^{j(\beta_i^{(k)}-\beta_i^{(l)})}])^2] \qquad k \neq l \tag{8.16}$$

$$P_i = E[\cos^2(\beta_i^{(k)} - \beta_i^{(l)})] \tag{8.17}$$

$$P_i = E[\cos^2(i\frac{2\pi}{N}(k-l))] \tag{8.18}$$

$$P_i = \sum_{n=1}^{N-1}\frac{1}{N-1}\cos^2(\frac{2\pi}{N}in) \tag{8.19}$$

$$P_i = \frac{1}{N-1}\sum_{n=1}^{N-1}\frac{1}{2}[1+\cos(\frac{4\pi}{N}in)] \tag{8.20}$$

$$P_i = \frac{1}{2(N-1)}(N-1+\sum_{n=1}^{N-1}\mathrm{Re}[e^{j\frac{4\pi}{N}in}]) \tag{8.21}$$

$$P_i = \begin{cases} \frac{1}{2(N-1)}(N-1+\frac{e^{j\frac{4\pi}{N}i}(1-e^{j\frac{4\pi}{N}i(N-1)})}{1-e^{j\frac{4\pi}{N}i}}) & i \neq 0, N/2 \\ 1 & i = 0, N/2 \end{cases} \tag{8.22}$$

$$P_i = \begin{cases} (N/2-1)/(N-1) & i \neq 0, N/2 \\ 1 & i = 0, N/2 \end{cases} \tag{8.23}$$

Let's investigate the SIR at the i^{th} carrier component for a traditional MC-CDMA systems with Hadamard-Walsh codes. The SIR at the i^{th} carrier component of MC-CDMA systems with HW codes corresponds to

$$SIR_i^{HW} = \frac{\alpha_i^2}{\sigma_{Ii}^2 + \sigma_{Ni}^2} = \frac{\alpha_i^2}{(K-1)\alpha_i^2 P_i^{HW} + N_0/2} \tag{8.24}$$

where for Hadamard-Walsh codes

$$P_i^{HW} = E[\cos^2(\beta_i^{(k)} - \beta_i^{(l)})] = 1 \tag{8.25}$$

Comparing equations (8.15) and (8.23) with equation (8.24) and (8.25), it is clear that CI codes introduces a lower power MAI per branch than their Hadmard-Walsh counterpart. Specifically, the power of the MAI terms when using CI codes is approximately half ($(N/2-1)/(N-1) \approx \frac{N/2}{N} = \frac{1}{2}$) that present in Hadamard-Walsh codes.

The reduced MAI per decision variable $r_i^{(l)}$ leads to a reduced MAI in the final decision variable $R^{(l)}$, regardless of whether $R^{(l)}$ is generated using MMSEC, EGC or MLC (maximum likelihood combining) criteria. For example, when EGC is applied,

$$R^{(l)} = \sum_{i=0}^{N-1} \alpha_i b_l + \sum_{i=0}^{N-1} \alpha_i \sum_{\substack{k=0 \\ k \neq l}}^{K-1} b_k \operatorname{Re}\left[e^{j(\beta_i^{(k)} - \beta_i^{(l)})}\right] + \sum_{i=0}^{N-1} \eta_i \tag{8.26}$$

The power of MAI within the final decision variable $R^{(l)}$ is

$$\sigma_I^2 = \sum_{i=0}^{N-1} \alpha_i^2 (K-1) P_i \tag{8.27}$$

Hence,

$$\sigma_{I\,CI\,Codes}^2 = \sum_{i=0}^{N-1} \alpha_i^2 (K-1) P_i \approx \frac{1}{2} \sum_{i=0}^{N-1} \alpha_i^2 (K-1) = \frac{1}{2} \sigma_{I\,HW\,Codes}^2 \tag{8.28}$$

Referring to equation (8.28), reduced MAI power leads directly to a higher SIR, and, as a result, higher performances observed with CI codes.

We simulate both CI/MC-CDMA and MC-CDMA (with Hadamard-Walsh codes) in the downlink to compare the performances of these two systems. We assume a slow frequency-selective Rayleigh fading channel. The number of carriers is set to N=32 and, characteristic of a typical CDMA communication environment, the total bandwidth is selected as four times coherence bandwidth, i.e., $BW=4(\Delta f)_c$. Figure 8.6 shows the simulation results for a fully loaded MC-CDMA system at different SNRs (signal to noise ratios) and Figure 8.7 shows performance results with different loads (the number of active users) at SNR=10dB. The line marked with circles represents MC-CDMA with Hadamard-Walsh codes, while the line marked with stars represents MC-CDMA with CI codes. Both MC-CDMA and CI/MC-CDMA systems employ MMSE combining. It is apparent from these figures that MC-CDMA with CI codes outperforms its Hadamard-Walsh counterpart, as suggested by the SIR calculation.

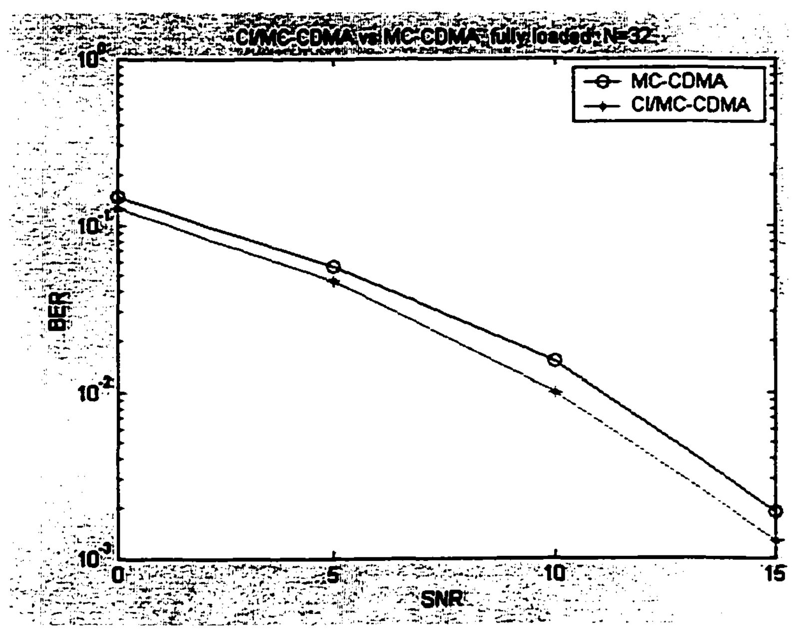

Figure 8.6 **Simulation Result 1 of CI/MC-CDMA and MC-CDMA**

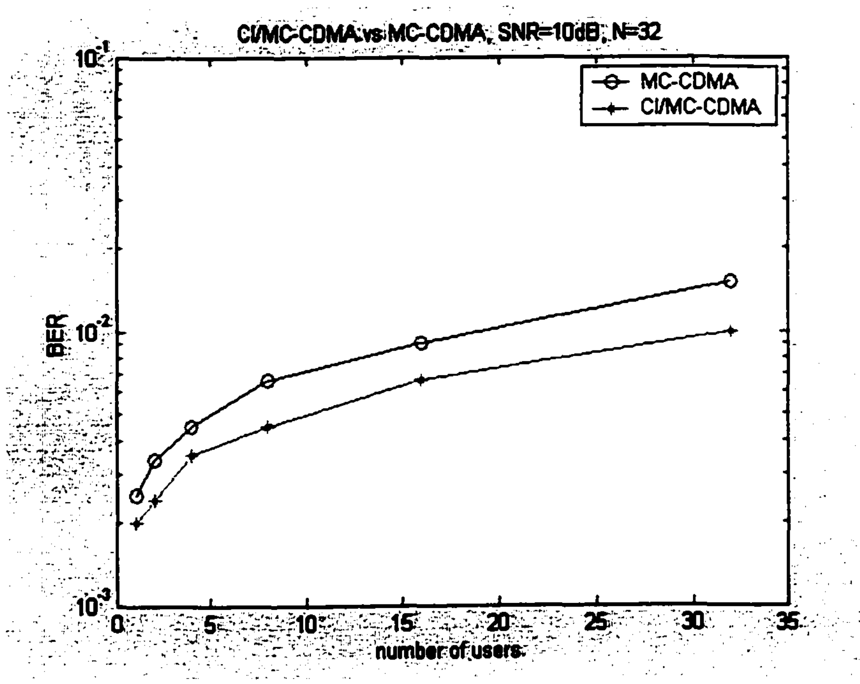

Figure 8.7 **Simulation Result 2 of CI/MC-CDMA and MC-CDMA**

8.3 High-Capacity CI/MC-CDMA

In Chapter 4, we also derived Offset CI codes, a second set of N codes which demonstrated a minimum cross correlation with respect to CI codes. We applied Offset CI codes alongside the original CI codes in DS-CDMA systems to double the network capacity. In work presented by other authors Offset CI codes and CI codes have now been applied into MC-CDMA systems. As a direct result, the network capacity of MC-CDMA systems has been doubled with negligible performance loss [85]. We review this work here.

The Offset CI codes are defined as

$$\beta_i^{(k)} = i \cdot k \cdot \frac{2\pi}{N} + i \cdot \frac{\pi}{N} \qquad k = N, N+1, \ldots, 2N-1 \tag{8.29}$$

and the usual CI codes refer to

$$\beta_i^{(k)} = i \cdot k \cdot \frac{2\pi}{N} \qquad k = 0, 1, \ldots, N-1 \tag{8.30}$$

Together, we have two sets of N spreading sequences which can be used to support $2N$ users in an MC-CDMA system with process gain N. Because the crosscorrelation between Offset CI codes and CI codes is minimized, the performance degradation introduced by Offset CI codes is negligible.

The total transmitted signal with $2N$ users in the system corresponds to

$$S(t)=\sum_{k=0}^{2N-1} b_k \operatorname{Re}\left\{\sum_{i=0}^{N-1} e^{j\beta_i^{(l)}} e^{j2\pi f_c t} e^{j2\pi i\Delta f t}\right\}\cdot g(t) \tag{8.31}$$

where $\beta_i^{(k)}$ is selected as shown in equations (8.29) and (8.30).

At the receiver side, the received signal is characterized by

$$r(t)=\sum_{k=0}^{K-1} b_k \sum_{i=0}^{N-1} \alpha_i \cos(2\pi f_c t+2\pi i\Delta f t+\beta_i^{(k)}+\phi_i)g(t)+\eta(t) \tag{8.32}$$

Using the receiver structure of Figure 8.3, the received signal is first decomposed into its subcarrier components and then despread, outputting $\bar{r}=(r_0^{(l)},r_1^{(l)},...,r_{N-1}^{(l)})$ where

$$r_i^{(l)}=\alpha_i b_l+\sum_{\substack{k=0\\k\neq l}}^{K-1} \alpha_i b_k \cos[\,\beta_i^{(k)}-\beta_i^{(l)}]+\eta_i \tag{8.33}$$

Minimized mean square error combining is employed to combine the $r_i^{(l)}$'s.

The multipath fading channel models used to assess the performance of the double capacity CI/MC-CDMA system are the Hilly Terrain (HT) channel and Typical Urban (TU) channel described in Chapter 3 [57].

Simulations are performed assuming that a total of $N=32$ carriers. Benchmark results are generated using the following systems: (1) a traditional MC-CDMA system receiver using N=32 Hadamard-Walsh codes and (2) traditional MC-CDMA using pseudo-orthogonal codes where the first *33* users use one set of Gold codes and next *32* users use a second set of Gold codes (for a total capacity of K=65 users). We assume a synchronous downlink channel.

Figure 8.8 presents bit error probability (BER) versus the number of users for SNR=10dB in the HT channel and Figure 8.9 presents these results in the TU channel at SNR=15dB. The curve marked with asterisks represents the performance of traditional MC-CDMA with Hadamard-Walsh codes, while the curves marked with circles represents the performance of CI/MC-CDMA, and the curves marked with dots represents the performance of traditional MC-CDMA with Gold codes (supporting up to *65* users). In CI/MC-CDMA, the first *32* users are supported using the first orthogonal group of spreading codes, and the next *32* users are supported using the second orthogonal group of spreading codes.

These curves demonstrate that the use of this novel scheme to increase capacity offers tremendous performance benefits over the use of traditional MC-CDMA system with pseudo-orthogonal codes for increased capacity. *Without any loss of performance*, capacity increases of 50% can be supported (Figure 8.8, Figure 8.9), and there are *negligible* performance losses even when capacity increases by 100%.

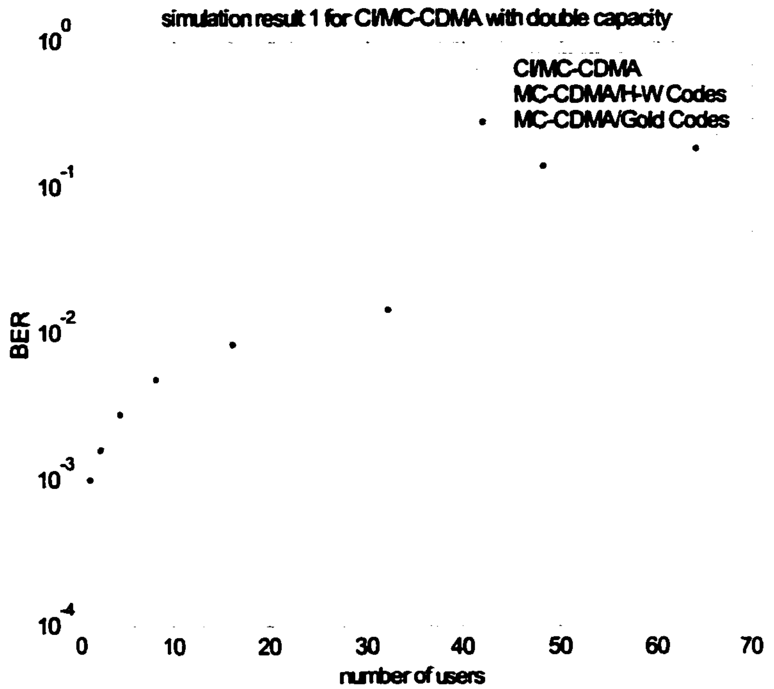

Figure 8.8 **Simulation Results of High Capacity CI/MC-CDMA**

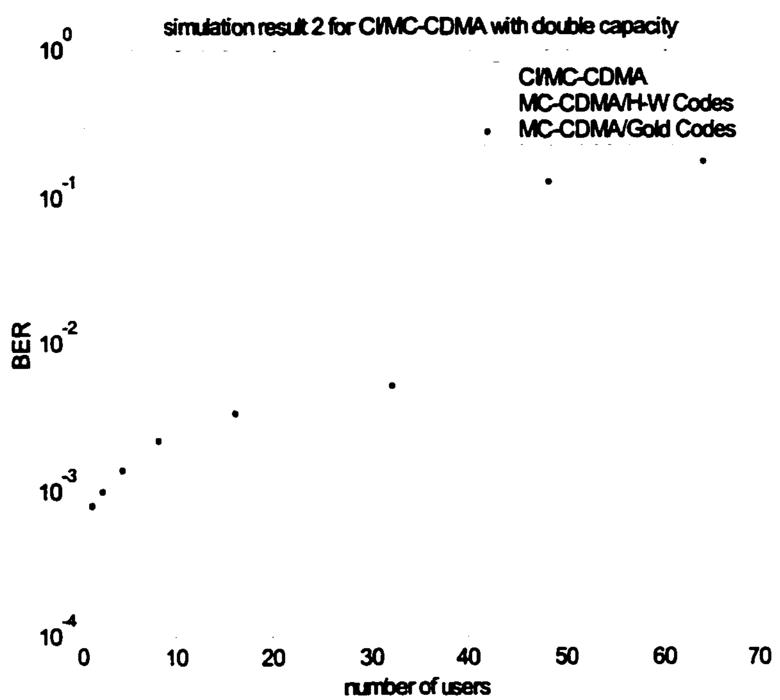

Figure 8.9 **Simulation Results 2 of High Capacity CI/MC-CDMA**

8.4 Conclusions

In this chapter, we reviewed MC-CDMA and CI/MC-CDMA: explaining the transmitter structure and receiver structure, analyzing the SIR; and showing the performance improvements (in terms of both bit error rate and network capacity). In the chapters that follow, we discuss innovations in MC-CDMA and CI/MC-CDMA systems.

Chapter 9 Maximum Likelihood Combining Receiver for MC-CDMA and CI/MC-CDMA

In this chapter, the maximum likelihood combining (MLC) scheme for MC-CDMA and CI/MC-CDMA is derived [48][49]. This scheme is optimal from the standpoint of minimizing the probability of error performance. It is shown that MLC is very close to MMSEC in a fully loaded system, justifying the selection of MMSEC over other combining schemes. However, when the load is small (as measured by number of users), MLC is shown to outperform MMSEC (and all other combining schemes).

9.1 MLC Receiver for MC-CDMA

As discussed in Chapter 8, in MC-CDMA, multiple users share the same N carriers for transmission, but are assigned orthogonal or pseudo-orthogonal codes to guarantee their separatablity at the receiver. In MC-CDMA receivers, each received symbol (sent on N subcarriers) is decomposed into its carrier components, and a combining technique is employed to (1) minimize noise, (2) minimize MAI (Multiple Access Interference), (3) optimize frequency diversity benefits or (4) perform some combination of (1) to (3).

Specifically, the most commonly used combiners in MC-CDMA are: (1) EGC (Equal Gain Combining), where carrier components are summed together to minimize noise; (2) ORC (Orthogonality Restoring Combining), where MAI is eliminated at the cost of noise enhancement; (3) MRC (Maximum Ratio Combining), where frequency diversity benefits are exploited without concern for MAI; and (4) MMSEC (Minimized Mean Square Error Combining), where a mean square error measure between the transmitted symbol and the estimated one is minimized. MMSEC is widely considered the best combining scheme based on probability of error performance. However, prior to this work, no one has established the "goodness" of MC-CDMA MMSE combiners. Here, we evaluate the truly optimal ML combiner, and, in showing how close it is to the MMSE combiner performance, justify the continued use of MMSEC.

Recall in the MC-CDMA receiver, the output in the i^{th} subcarrier of l^{th} user's receiver corresponds to the decision variable

$$r_i^{(l)} = \alpha_i b_l + \alpha_i \sum_{\substack{k=0 \\ k \neq l}}^{K-1} b_k \operatorname{Re}[e^{j(\beta_i^{(k)} - \beta_i^{(l)})}] + \eta_i \tag{9.1}$$

where $b_k \in \{+1,-1\}$, K is the number of users occupying the system, α_i is the gain of the i^{th} subcarrier and ϕ_i the phase offset of the i^{th} subcarrier due to the channel, and $\eta(t)$ represents AWGN.

Next at the receiver side, a suitable linear combining scheme is used to create a decision variable for user k, i.e, the receiver generates

$$R^{(l)} = \sum_{i=0}^{N-1} W_i \cdot r_i^{(l)} \tag{9.2}$$

In MMSEC, the decision variable $R^{(l)}$ is created using weights

$$W_i = \frac{\alpha_i}{K\alpha_i^2 + N_0/2} \tag{9.3}$$

Finally, this decision variable enters a hard decision device which selects

$$\tilde{b}_k = \begin{cases} +1 & \text{if } R^{(l)} > 0 \\ -1 & \text{otherwise} \end{cases} \tag{9.4}$$

Let's determine the optimal combining scheme for MC-CDMA systems. Given $\bar{r}^{(l)} = \{r_0^{(l)}, r_1^{(l)}, \cdots, r_{N-1}^{(l)}\}$, the maximum likelihood criteria requires a decision based on

$$P(\bar{r}^{(l)} \mid b_l = 1) >< P(\bar{r}^{(l)} \mid b_l = -1) \tag{9.5}$$

where $><$ means if the term on the right is greater than the one on the left, output bit -1; otherwise decide +1.

Assuming no knowledge of the other users' spreading codes, the MAI of different carriers (the second term in equation (9.1)) can be viewed as independent from one carrier to another, in which case

$$P(\bar{r} \mid b_l) = \prod_{i=1}^{N} P(r_i^{(l)} \mid b_l) = \prod_{i=1}^{N} P(\eta_i' = r_i^{(l)} - \alpha_i b_l) \tag{9.8}$$

where η_i' is a random variable with mean 0 and variance

$$\sigma_i^2 = E\left[(\alpha_i \sum_{\substack{k=0 \\ k \neq l}}^{K-1} b_k \operatorname{Re}[e^{j(\beta_i^{(k)} - \beta_i^{(l)})}] + \eta_i)^2 \right] \tag{9.9}$$

$$\sigma_i^2 = E\left[(\alpha_i \sum_{\substack{k=0 \\ k \neq l}}^{K-1} b_k \operatorname{Re}[e^{j(\beta_i^{(k)} - \beta_i^{(l)})}])^2 \right] + E\left[\eta_i^2\right] \tag{9.10}$$

$$\sigma_i^2 = (K-1)\alpha_i^2 E\left[\operatorname{Re}[e^{j(\beta_i^{(k)} - \beta_i^{(l)})}]^2\right] + \frac{N_0}{2} \tag{9.11}$$

Since $\beta_i^{(k)} = 0$ or π,

$$E\left[\operatorname{Re}[e^{j(\beta_i^{(k)} - \beta_i^{(l)})}]^2\right] = E\left[\cos^2(\beta_i^{(k)} - \beta_i^{(l)})\right] = \frac{1}{2}\cdot\cos^2(0) + \frac{1}{2}\cdot\cos^2(\pi) = 1 \tag{9.12}$$

Thus,

$$\sigma_i^2 = (K-1)\alpha_i^2 + \frac{N_0}{2} \tag{9.13}$$

Employing the Gaussian approximation of MAI with variance characterized by equation (9.13), and using log's in (9.5), the maximum likelihood decision rule in (9.5) corresponds to:

$$\log P(\bar{r}|b_l = 1) \gtrless \log P(\bar{r}|b_l = -1) \tag{9.14}$$

$$\sum_i \log\frac{1}{\sqrt{2\pi\sigma_i^2}} - \sum_i \left[\frac{(\alpha_i - r_i^{(l)})^2}{2\sigma_i^2}\right] \gtrless \sum_i \log\frac{1}{\sqrt{2\pi\sigma_i^2}} - \sum_i \left[\frac{(-\alpha_i - r_i^{(l)})^2}{2\sigma_i^2}\right] \tag{9.15}$$

$$\sum_i \frac{\alpha_i r_i^{(l)}}{\sigma_i^2} \gtrless 0 \tag{9.16}$$

Using equation (9.13), we get

$$\sum_i \frac{\alpha_i r_i^{(l)}}{(K-1)\alpha_i^2 + \frac{N_0}{2}} \gtrless 0 \tag{9.17}$$

Restating equation (9.17) in a form consistent with equation (9.2) and (9.4), the ML criteria corresponds to the weighted combining of equation (9.2) (followed by the hard decision of (9.4)), where weights correspond to

$$W_i^{MLC} = \frac{\alpha_i}{(K-1)\alpha_i^2 + N_0/2} \tag{9.18}$$

Comparing MLC in equation (9.18) and MMSEC in equation (9.3), it is apparent that the only difference is the K in MMSEC weights replaced by *(K-1)* in MLC weights. In a fully loaded system, i.e., when K is large, replacing K with *(K-1)* makes little difference. This adequately explains the high probability of error performance observed in MMSEC. However, when the load is small, MLC notably outperforms MMSEC (and all other combining schemes).

To test our maximum likelihood combining for MC-CDMA and compare it to MMSEC combining results, we use the Hilly Terrain (HT) channel described in Chapter 3 [57]. Simulations are performed assuming a total of $N=32$ carriers.

Figure 9.1 presents bit error probability (BER) versus the number of users for SNR=10dB in the HT channel. Both MLC and MMSEC results are shown in Figure 9.1. It is apparently from this figure that MLC outperforms MMSEC when system load is small.

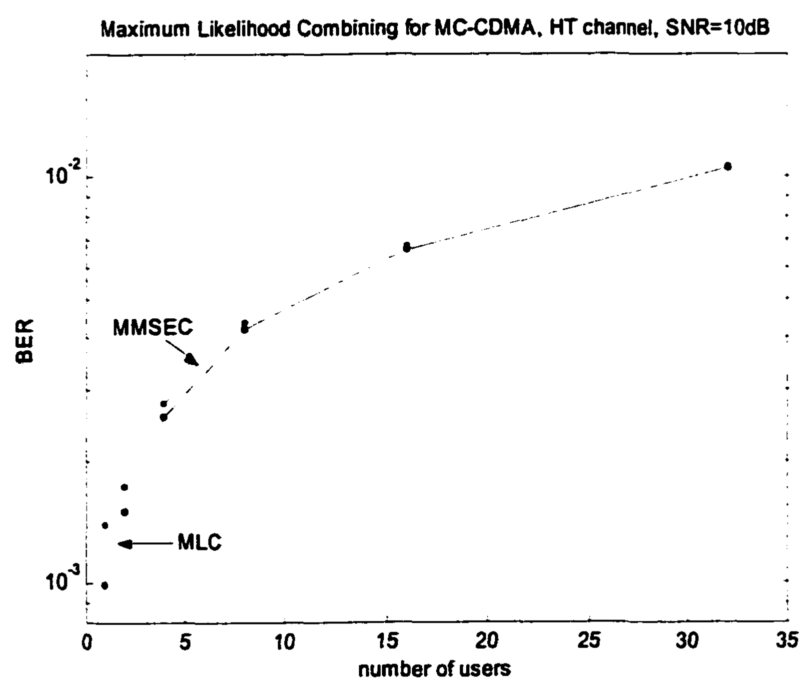

Figure 9.1 Simulation Results for MC-CDMA with MLC

9.2 MLC for CI/MC-CDMA

We now extend our MLC receiver from MC-CDMA to CI/MC-CDMA. Recall in the CI/MC-CDMA receiver, the output in the i^{th} subcarrier of l^{th} user's receiver corresponds to the decision variable

$$r_i^{(l)} = \alpha_i b_l + \alpha_i \sum_{\substack{k=0 \\ k \neq l}}^{K-1} b_k \operatorname{Re}[e^{j \cdot i \cdot (k-l)\frac{2\pi}{N}}] + \eta_i \tag{9.19}$$

where K is the number of users occupying the system and corresponds to a value between 1 and $2N$, α_i is the gain of the i^{th} subcarrier and ϕ_i the phase offset of the i^{th} subcarrier due to the channel, and $\eta(t)$ represents AWGN.

Similar to MC-CDMA, it has been shown that MMSEC outperforms the other combining schemes (e.g., EGC, ORC) in terms of bit error rate. However, we seek to establish the "goodness" of MMSEC by comparing it to the theoretically optimal ML criteria.

It has been shown the MMSE combining for CI/MC-CDMA corresponds to

$$R^{(l)} = \sum_{i=0}^{N-1} W_i \cdot r_i^{(l)} \tag{9.20}$$

where

$$W_i = \frac{\alpha_i}{KP_i'\alpha_i^2 + N_0/2} \tag{9.21}$$

and

$$P_i' = \begin{cases} 1/2 & i \neq 0, N/2 \\ 1 & i = 0, N/2 \end{cases} \tag{9.22}$$

Now we determine the MLC for CI/MC-CDMA. Like MC-CDMA case, we begin with

$$P(\bar{r} \mid b_l = 1) \gtrless P(\bar{r} \mid b_l = -1) \tag{9.23}$$

Also assuming no knowledge of the other users' spreading codes, the MAI on different carriers (the second term in equation (9.19)) can be viewed as independent from one carrier to another, in which case

$$P(\bar{r} \mid b_l) = \prod_{i=1}^{N} P(r_i^{(l)} \mid b_l) = \prod_{i=1}^{N} P(\eta_i' = r_i^{(l)} - \alpha_i b_l) \tag{9.24}$$

where η_i' is a random variable with mean 0 and variance

$$\sigma_i^2 = (K-1)\alpha_i^2 E\left[\mathrm{Re}[e^{j(\beta_i^{(k)} - \beta_i^{(l)})}]^2\right] + \frac{N_0}{2} \tag{9.25}$$

Notice that $E[(\mathrm{Re}[e^{j(\beta_i^{(k)} - \beta_i^{(l)})}])^2]$ is the expectation for $k \neq l$, thus we have

$$P_i = E[(\mathrm{Re}[e^{j(\beta_i^{(k)}-\beta_i^{(l)})}])^2] \qquad k \neq l \tag{9.26}$$

$$P_i = E[\cos^2(\beta_i^{(k)} - \beta_i^{(l)})] \tag{9.27}$$

$$P_i = \begin{cases} (N/2-1)/(N-1) & i \neq 0, N/2 \\ 1 & i = 0, N/2 \end{cases} \tag{9.28}$$

Using a Gaussian approximation of MAI with a variance provided by equation (9.28), and using log's in (9.23), the maximum likelihood decision rule corresponds to:

$$\log P(\bar{r}|b_l = 1) >< \log P(\bar{r}|b_l = -1) \tag{9.29}$$

$$\sum_i \log \frac{1}{\sqrt{2\pi\sigma_i^2}} - \sum_i [\frac{(\alpha_i - r_i^{(l)})^2}{2\sigma_i^2}] >< \sum_i \log \frac{1}{\sqrt{2\pi\sigma_i^2}} - \sum_i [\frac{(-\alpha_i - r_i^{(l)})^2}{2\sigma_i^2}] \tag{9.30}$$

$$\sum_i \frac{\alpha_i r_i^{(l)}}{\sigma_i^2} >< 0 \tag{9.31}$$

Using equation (9.25) and (9.28), we get

$$\sum_i \frac{\alpha_i r_i^{(l)}}{(K-1)P_i\alpha_i^2 + \frac{N_0}{2}} >< 0 \tag{9.32}$$

Representing equation (9.32) in terms consistent with equation (9.20), Maximum Likelihood Combining weights correspond to

$$W_i^{MLC} = \frac{\alpha_i}{(K-1)P_i\alpha_i^2 + N_0/2} \tag{9.33}$$

where

$$P_i = \begin{cases} (N/2-1)/(N-1) & i \neq 0, N/2 \\ 1 & i = 0, N/2 \end{cases} \tag{9.34}$$

Comparing MLC in equation (9.33) and (9.34) and MMSEC in equation (9.21) and (9.22), it is apparent that the only difference is (1) the K in MMSEC weights replaced by $(K\text{-}1)$ in MLC weights and (2) the P_i' in MMSEC weights is replaced by P_i in MLC weights. Notice that when N is large P_i is very close to P_i' and, in a near-fully loaded system, i.e., with K a big number, replacing K with $(K\text{-}1)$ makes little difference. This adequately explains the high probability of error performance observed in MMSEC. However, when the load is small, MLC notably outperforms MMSEC (and all other combining schemes).

To test our maximum likelihood combining for MC-CDMA and compared it to MMSEC combining results, we use Hilly Terrain (HT) channel described in Chapter 3 [57]. Simulations are performed assuming that a total of $N=32$ carriers.

Figure 9.2 presents bit error probability (BER) versus the number of users for SNR=10dB in the HT channel. Both MLC and MMSC results are shown in Figure 9.1. It is apparently from this figure that MLC outperforms MMSEC when system load is small.

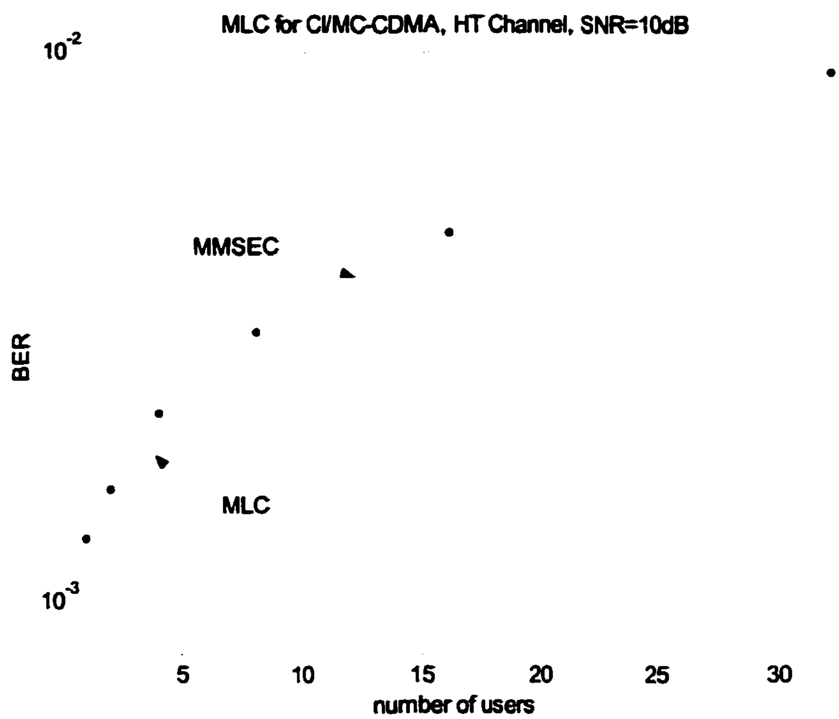

Figure 9.2 Simulation Results for CI/MC-CDMA with MLC

9.3 Conclusions

In this chapter, the maximum likelihood combining (MLC) schemes for MC-CDMA and CI/MC-CDMA are derived. These schemes are optimal from the standpoint of minimizing the probability of error performance. It is shown that MLC is very close to MMSEC in a fully loaded system, justifying the selection of MMSEC over other combining schemes.

Chapter 10 FD-MC-CDMA: A Frequency-based Multiple Access Architecture for High Performance Wireless Communication

MC-CDMA has demonstrated high performance in frequency selective fading channels due to the ability to exploit frequency diversity. But MC-CDMA also suffers from the large MAI.

In this chapter, we propose FD-MC-CDMA, a novel multiple access architecture, - intended to exploit frequency diversity while minimizing MAI [51]. Here, instead of sending all users' information bits over all carriers, smaller sets of carriers are employed to support smaller numbers of users (without loss in network capacity). Simulation results show that FD-MC-CDMA outperforms MC-CDMA and FDMA in frequency selective fading channels.

Furthermore, a truly optimal multi user detection receiver (based on the maximum likelihood (ML) criteria) is employed in FD-MC-CDMA to optimize system performance [52]. Of practical interest is the fact that the complexity of an ML MUD in FD-MC-CDMA is low, a direct consequence of FD-MC-CDMA's division of users into small subsets. Simulation results show FD-MC-CDMA with optimal ML MUD significantly outperforming traditional MC-CDMA and FDMA in frequency selective fading channels, while offering a comparable system complexity.

10.1 FD-MC-CDMA

As discussed in previous chapters, MC-CDMA is considered a strong candidate for next generation wireless, as it supports large diversity gains and demonstrates the potential for high network capacity. Specifically, in MC-CDMA, high diversity gains are achieved by allowing transmitters to send information on N multiple carriers simultaneously, and using receivers that separate the signal into carrier components to exploit frequency diversity. However, MC-CDMA has to tolerate large MAI (multiple access interference) when the number of active users in the system is high. Generally, the performance of the MC-CDMA system is never-than-less limited by the amount of MAI.

On the other hand, FDMA (Frequency Division Multiple Access) completely avoids MAI by allocating each user a unique, orthogonal transmission frequency.

However, with such a transmission, no frequency diversity gains can be achieved at the receiver. As a result, FDMA systems suffer severe performance degradation in fading channels.

Here, we consider a frequency based multiple access architecture which combines the best elements of FDMA and MC-CDMA to simultaneously exploit frequency diversity and minimize the MAI.

In a typical frequency selective fading channel, the fade over each subcarrier is considered flat and the fades over different subcarriers are different. However, the fades over different subcarriers are not independent: there exists a certain amount of cross correlation between the fades over different subcarriers. This cross correlation can be characterized using the coherence bandwidth of the fading channel. As a direct result, the amount of diversity available over the channel is L, which is (much) less than N.

Combining FDMA and MC-CDMA [51][52][87],

(1) the N subcarriers are divided into a few groups;

(2) each group contains L non-contiguous subcarriers;

(3) each user's information bit is sent over L non-contiguous subcarriers instead of all N subcarriers;

(4) the L subcarriers are separated by large frequency bands and have approximately independent fades; (Thus, the frequency diversity exploited

by each user is approximately the same as that of transmitting over all N subcarriers.)

(5) each group of L carriers supports no more than L users. (Thus, the MAI observed at the receiver side decreases dramatically.)

As a result of (a) full diversity benefits and (b) lowered MAI, the performance of the novel multiple access architecture is improved. Moreover, this novel scheme not only outperforms traditional MC-CDMA (as well as FDMA), but also decreases the computational load at the receiver. Additionally, it offers the flexibility of providing different users with different QOS. Details follow.

Recall in a traditional MC-CDMA system, the k^{th} user's transmission corresponds to

$$S(t)=\sum_{k=0}^{K-1} b_k \,\mathrm{Re}\left\{\sum_{i=0}^{N-1} A_i e^{j\beta_i^{(k)}} e^{j2\pi f_c t} e^{j2\pi i\Delta f t}\right\}\cdot g(t) \tag{10.1}$$

where b_k is user k's information bit, Δf is the frequency separation between neighboring carriers, f_c is the transmission frequency, and $e^{j\beta_i^k} = +1$ or -1 in accordance with known spreading codes such as Hadmard-Walsh codes.

Typically, fading channels in wireless systems demonstrate an L fold frequency diversity, where L is in the order of 2, 3 or 4. We assume L=4 for ease in presentation. To build a multiple access system exploiting this L=4 fold diversity, while minimizing MAI, we: rather than allowing all users to share all the N carriers, we support small sets of L=4 users sharing a set of L=4 carriers via MC-CDMA. That is, the k^{th} user in a set of 4 users transmits $S(t)=\sum_{k=0}^{K-1} b_k \operatorname{Re}\left\{\sum_{i=0}^{N-1} A_i e^{j\beta_i^{(k)}} e^{j2\pi f_c t} e^{j2\pi i \Delta f t}\right\} \cdot g(t)$ (as shown in equation (10.1)) where (1) $e^{j\beta_i^k}=+1$ or -1 and (2) $A_i=1$ at L=4 values of i and $A_i=0$ elsewhere.

Specifically, for L=4 fold diversity and N=32 carriers; $\{A_i e^{j\beta_i^k}=\pm 1, i=1,9,17,25\}$ and 0 otherwise for one set of four users; $\{A_i e^{j\beta_i^k}=\pm 1, i=2,10,18,26\}$ and 0 otherwise for another set of four users; and so on. This is shown in Figure 11.1. Generally,

$$A_i e^{j\beta_i^k}=\begin{cases}\pm 1, & i=\left\lfloor \frac{k}{N/L}\right\rfloor+1,\ \left\lfloor \frac{k}{N/L}\right\rfloor+\frac{N}{L}+1,\ \cdots,\ \left\lfloor \frac{k}{N/L}\right\rfloor+(L-1)\cdot\frac{N}{L}+1 \\ 0 & otherwise\end{cases} \tag{10.2}$$

where $\lfloor x \rfloor$ presents the closest integer less than or equal to x.

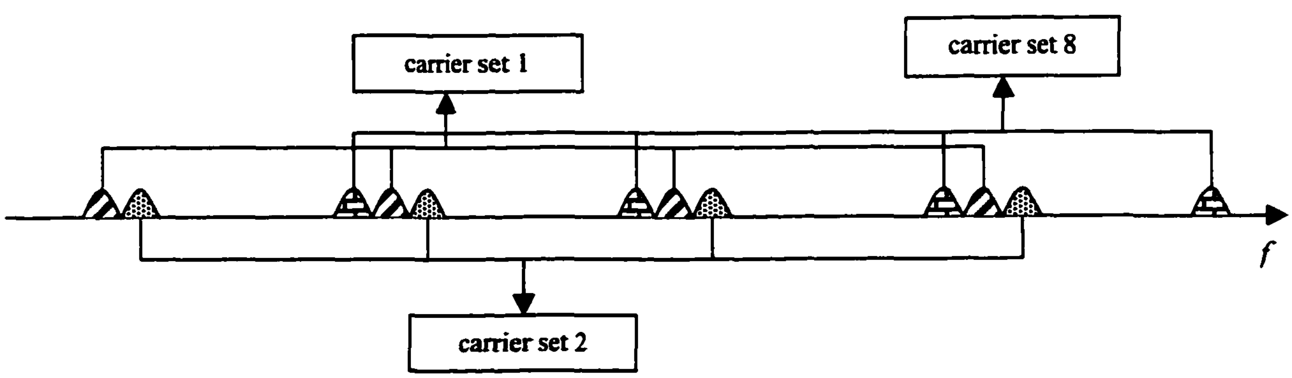

Figure 10.1 MC-CDMA with FDMA: N=32 carriers, L=4 fold diversity

A total of N/L (e.g., 32/4=8) sets of L=4 carriers are used concurrently to maintain the total capacity of the system. Different sets of L=4 carriers are frequency division multiplexed such that the 4 users of one subset do not interfere with users of another set. For each set of L=4 carriers, a set of length 4 Hadamard-Walsh codes are used as the spreading codes.

The transmitter structure for user 1 in our example is presented in Figure 10.2.

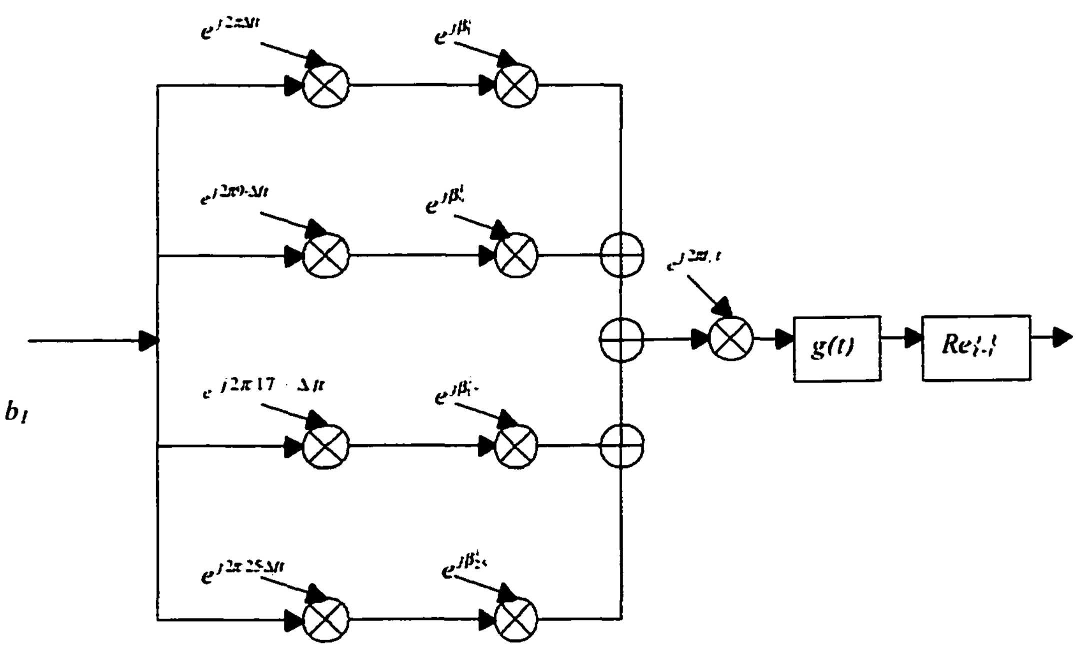

Figure 10.2 FD-MC-CDMA transmitter for user 1

After transmission through a frequency selective fading channel, the received signal corresponds to

$$r(t) = \sum_{k=0}^{K-1} b_k \operatorname{Re}[\sum_{i=0}^{N-1} \alpha_i A_i e^{j\beta_i^{(k)}} e^{j(2\pi f_i t+\phi_i)}]g(t) + \eta(t) \quad (10.3)$$

where α_i is the gain and φ_i the phase offset in the i^{th} subcarrier, and $\eta(t)$ represents additive white Gaussian noise.

User 1's receiver in an FD-MC-CDMA system is shown in Figure 10.3. Here, the received signal is decomposed into its L information-bearing carriers and despread by user 1's spreading code.

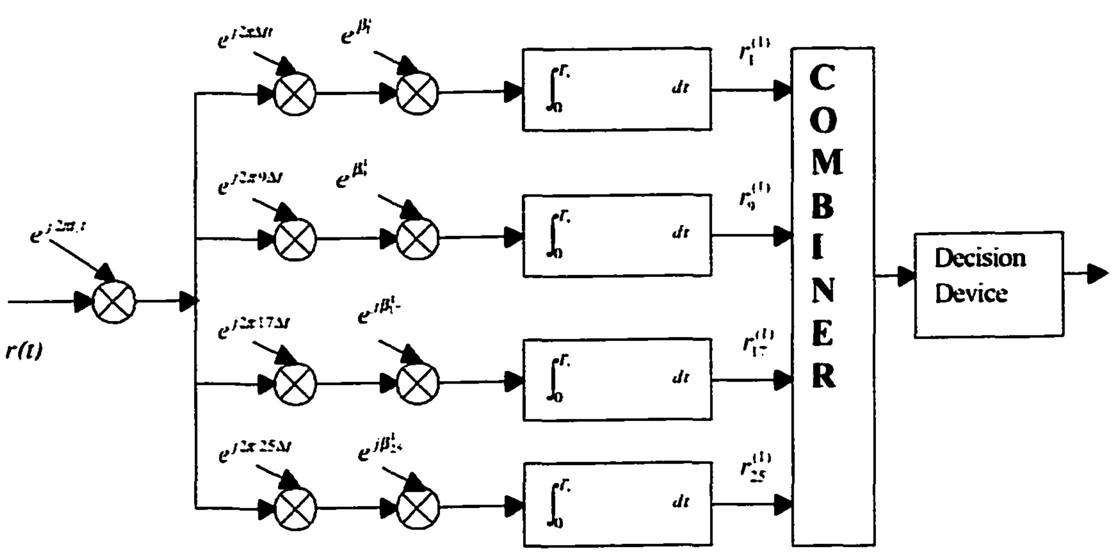

Figure 10.3 FD-MC-CDMA Receiver

The i^{th} carrier generates the decision variable

$$r_i^{(1)} = \alpha_i b_1 + \alpha_i \sum_{\substack{k \in U_1 \\ k \neq 1}} b_k \operatorname{Re}[e^{j(\beta_i^{(k)} - \beta_i^{(1)})}] + \eta_i \qquad i = 1,9,17,25 \tag{10.4}$$

where U_l is the set of up to four active users in user 1's carrier set.

Next, an optimal combining strategy is used to combine all L=4 carriers in user 1's set to best exploit frequency diversity and minimize MAI. To accomplish this, we employ the maximum likelihood combining scheme (MLC): Given $\bar{r}^{(1)} = (r_1^{(1)}, r_9^{(11)}, r_{17}^{(1)}, r_{25}^{(1)})$, the maximum likelihood criteria requires a decision based on

$$P(\bar{r}^{(1)} \mid b_1 = 1) \gtrless P(\bar{r}^{(1)} \mid b_1 = -1) \tag{10.5}$$

where $\gtrless$ means if the term on the right is greater than the one on the left, output bit 1; otherwise decide -1. Assuming no knowledge of the other users' spreading codes, the MAI on different carriers can be viewed as independent from one another, in which case

$$P(\bar{r}^{(1)} \mid b_1) = \prod_{i \in \{1,9,17,25\}} P(r_i^{(1)} \mid b_1) = \prod_{i \in \{1,9,17,25\}} P(\eta_i' = r_i^{(1)} - \alpha_i b_1) \tag{10.6}$$

where η_i' is a random variable with mean 0 and variance $(K_1 - 1)\alpha_i^2 + N_0/2$, K_l is the number of active users on user 1's carrier set, and $N_0/2$ is the variance of the additive Gaussian noise. Employing a Gaussian approximation for the MAI with variance $(K_1 - 1)\alpha_i^2 + N_0/2$ in equation (11.6), the maximum likelihood decision rule corresponds to:

$$R^{(1)} = \sum_{i \in \{1,9,17,25\}} r_i^{(1)} \cdot \frac{\alpha_i}{(K_1 - 1)\alpha_i^2 + N_0/2} \tag{10.7}$$

After the ML combining, a hard decision device makes the following decision on the output data bit:

$$\hat{b}_l = \begin{cases} +1 & \text{if} \quad R^{(l)} > 0 \\ -1 & \text{otherwise} \end{cases} \tag{10.8}$$

To test the performance of the proposed FD-MC-CDMA system, simulations are performed assuming a system with N=32 carriers. Four-fold diversity is assumed in the channel model, that is:

$$BW = N \cdot \Delta f = 4 \cdot (\Delta f)_c \tag{10.9}$$

where BW is the total bandwidth of the system and $(\Delta f)_c$ is the coherence bandwidth of the channel. As benchmarks, a traditional MC-CDMA system using over all N=32 carriers and an FDMA system are both simulated.

Figure 10.4 presents the performance curves in terms of average bit error rate (BER) versus number of users for fixed SNR=10dB, and Figure 10.5 presents the BER versus SNR when the number of active users in the system is 8. The solid line (marked with hollow circles) represents the traditional MC-CDMA system. The dotted line (marked with solid circles) represents FDMA, and the dashed line (marked with stars) the novel FD-MC-CDMA system (with 8 sets of 4 carriers each as in Figure 10.1).

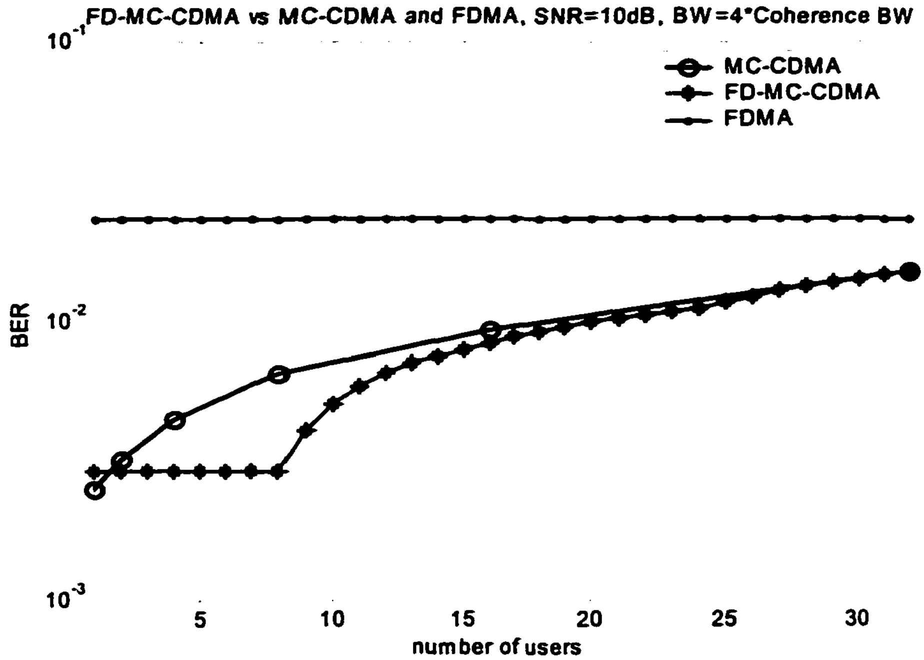

Figure 10.4 Simulation Result 1 for FD-MC-CDMA

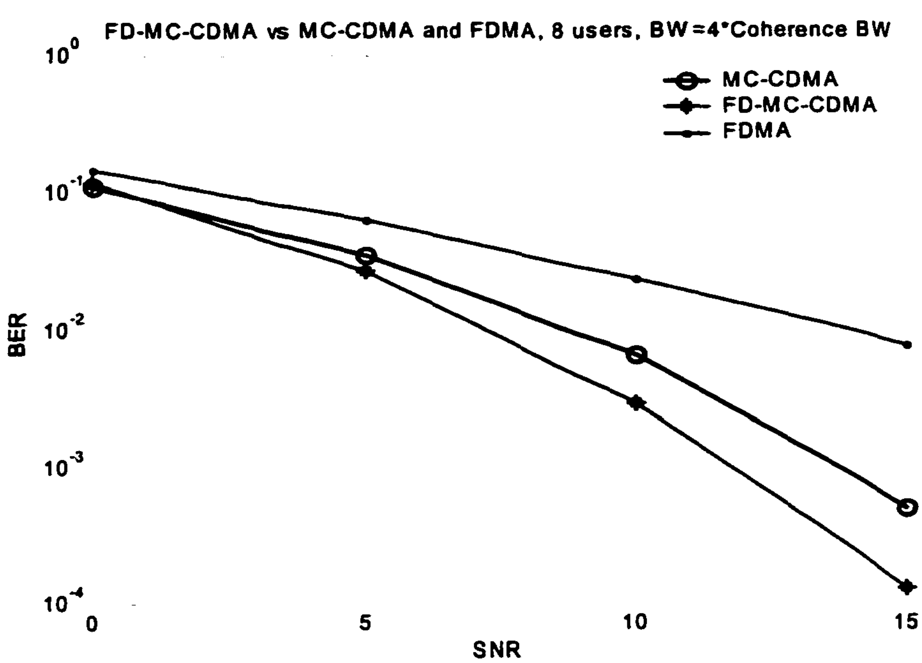

Figure 10.5 Simulation Result 2 for FD-MC-CDMA

These results confirm that this novel scheme outperforms both FDMA and MC-CDMA. At lower loads, the performance gains are even more prominent.

It is also important to notice that the FD-MC-CDMA system can be easily updated to support users with different QOS requirements; this is handled by assigning users to different subcarrier groups based on their QOS requirements.

10.2 FD-MC-CDMA with Multi User Detection

In the last section, we proposed a novel frequency domain multiple access architecture: FD-MC-CDMA. Simulation results show that FD-MC-CDMA outperforms both MC-CDMA and FDMA. However, when the system is fully loaded, the performance gain is very small. In this section, we significantly improve the performance benefits of the proposed FD-MC-CDMA system by the introduction of a MUD (multi user detection) [52]. One very elegant feature of FD-MC-CDMA systems is that truly optimal ML (maximum likelihood) MUDs are available at low complexity. This results because, even with N users on the system (where N is large), each user experience only up to $L-1$ interferers (where L is small). As a result, ML MUD complexity is in the order of 2^L (e.g. $2^4 = 16$) and not 2^N (e.g. $2^{32} = 4.3 \cdot 10^9$).

User 1's FD-MC-CDMA receiver implemented as a MUD, is shown in Figure 10.6. Here, the received signal is decomposed into its L information-bearing carriers and despread by user 1's spreading code. The i^{th} carrier for $i \in \{1,9,17,25\}$ generates the decision variable

$$r_i^{(1)} = \alpha_i b_1 + \alpha_i \sum_{\substack{k\in U_1 \\ k\neq 1}} b_k \,\mathrm{Re}[e^{j(\beta_i^{(k)}-\beta_i^{(1)})}] + \eta_i \qquad i = 1,9,17,25 \tag{10.10}$$

where U_1 is the set of K ($K \le L$) users in the first carrier set. The number of interferers in user 1's carrier set is no more than L-1 (e.g., 4-1=3). Hence, the optimal ML multi user detector for user 1 can be constructed with low complexity.

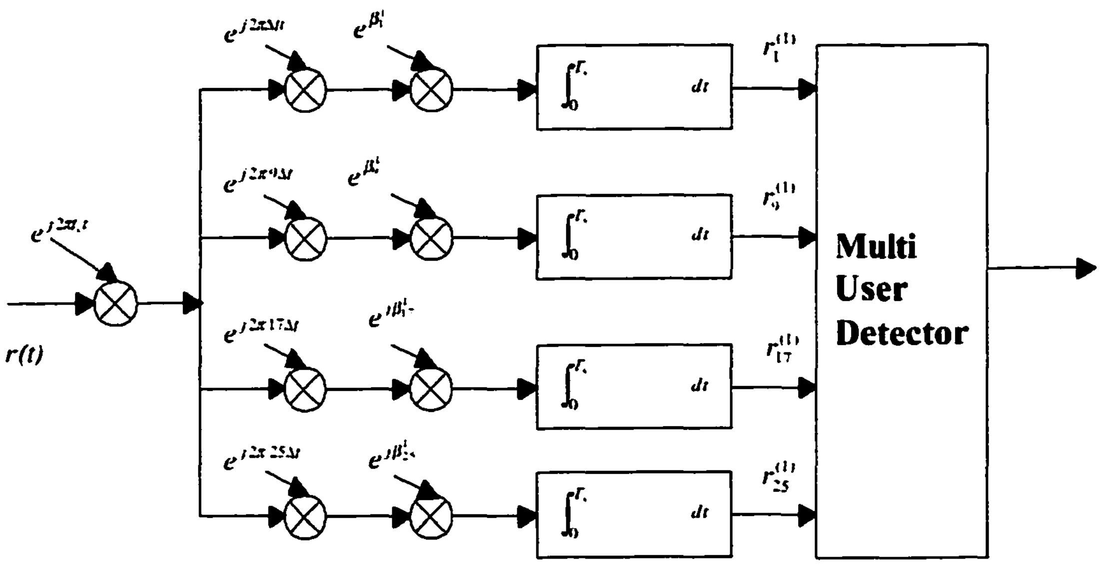

Figure 10.6 MUD Receiver for FD-MC-CDMA

Defining $\bar{r}^{(1)} = (r_1^{(1)}, r_9^{(1)}, r_{17}^{(1)}, r_{25}^{(1)})$, the maximum likelihood criteria leads to:

$$P(\bar{r}^{(1)} | b_1 = -1) \gtrless P(\bar{r}^{(1)} | b_1 = 1) \tag{10.11}$$

where $\gtrless$ refers to: if the term on the right is greater than that on the left, decide the bit 1; otherwise decide -1. The ML MUD defining equation is easily shown to reduce to

$$\sum_{\substack{\hat{b}_k,\\ k\in U_1,\\ k\neq 1}} \sum_{i=1,9,17,25} \left(r_i^{(l)} - (\alpha_i + \alpha_i \sum_{k\in U_1} \hat{b}_k \beta_i^k \beta_i^1) \right)^2 \gtrless \sum_{\substack{\hat{b}_k,\\ k\in U_1,\\ k\neq 1}} \sum_{i=1,9,17,25} \left(r_i^{(l)} - (-\alpha_i + \alpha_i \sum_{k\in U_1} \hat{b}_k \beta_i^k \beta_i^1) \right)^2$$

(10.12)

$$\sum_{\substack{\hat{b}_k,\\ k\in U_1,\\ k\neq 1}} f_1(\hat{b}_k) \gtrless \sum_{\substack{\hat{b}_k,\\ k\in U_1,\\ k\neq 1}} f_2(\hat{b}_k) \qquad (10.13)$$

where $f_1(\hat{b}_k)$ refers to the inner sum on the left hand side of equation (10.12) and $f_2(\hat{b}_k)$ refers to the corresponding sum on the right hand side.

Equation (10.12) is solved by computing each term in each sum and then determining which sum is larger: for example, with $K=L=4$ users on the system, i.e., $U_1 = \{1,9,17,25\}$, a total of 16 terms are computed. Furthermore, if the MUD receiver is intended to detect only user 1's bit, it is assumed that the codes for other users are not known: this may increase the number of terms evaluated in the calculation of $f(.)$ (since each term is averaged over possible spreading codes): the total number of terms computed in this case is $2^K \cdot \binom{L-1}{K-1} = 2^K \cdot C_{L-1}^{K-1} = 2^K \cdot \frac{(L-1)!}{(K-1)!(L-K)!}$. It is important to note that the optimal receiver only requires the following information: (1) the number of active users; (2) estimates of gains (α_i's) and (3) estimates of phase offsets (ϕ_i's), consistent with the requirement of most traditional MC-CDMA receivers.

To test the performance of the proposed FD-MC-CDMA system with an ML MUD receiver, simulations are performed assuming a system with N=32 carriers. Four-fold diversity is assumed over the transmit bandwidth, that is:

$$BW = N \cdot \Delta f = 4 \cdot (\Delta f)_c \tag{10.14}$$

where BW is the total bandwidth of the system and $(\Delta f)_c$ is the coherence bandwidth of the channel.

As a result, the FD-MC-CDMA system emulated employs N/L=8 sets of L=4 users each. As benchmarks, a traditional MC-CDMA system where each user employs all N=32 carriers is simulated, as is an FDMA system with N=32 carriers and one user per carrier.

Figure 10.7 presents the performance curves in terms of average bit error rate (BER) versus number of users for fixed SNR=10dB, and Figure 10.8 presents the BER versus SNR when the number of active users in the system is 16. In both curves, the solid line (marked with hollow circles) represents the traditional MC-CDMA system. The dotted line (marked with solid circles) represents FD-MC-CDMA system without a MUD, the dashed line (marked with stars) the FD-MC-CDMA system with an optimal MUD receiver. Finally, the dotted line is the performance of FDMA.

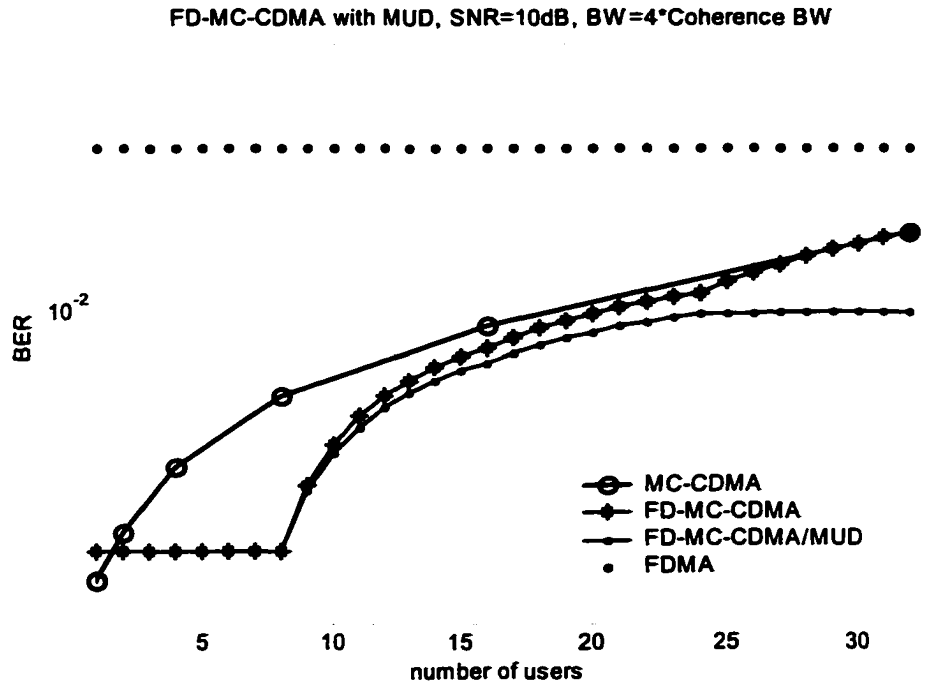

Figure 10.7 Simulation Results 1 for FD-MC-CDMA with MUD

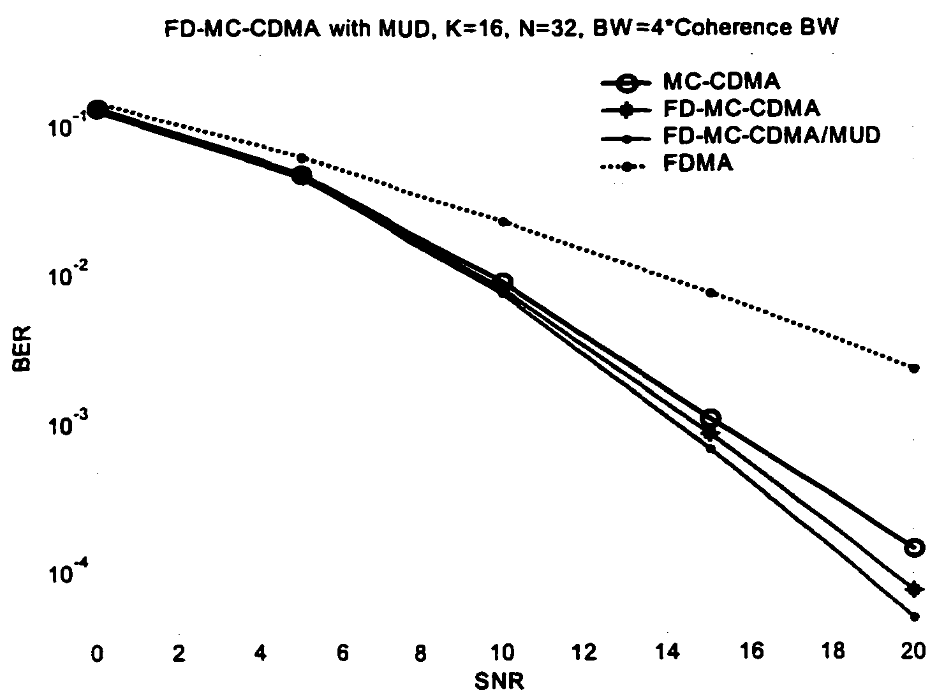

Figure 10.8 Simulation Results 2 for FD-MC-CDMA with MUD

It is apparent from these results that the FD-MC-CDMA with a MUD significantly outperforms traditional MC-CDMA. Specifically, as the number of users grows, the performance benefits relative to MC-CDMA increase. At N=32, performance of FD-MC-CDMA with MUDs is comparable to that of MC-CDMA with only 16 users. That is, FD-MC-CDMA supports twice as many users as MC-CDMA at the same performance level. Considering that the optimal multi user detection receiver for MC-CDMA is too complex to build, FD-MC-CDMA provides a suitable method to achieve the frequency diversity benefits, minimize the MAI, and benefit from the performance gain of a MUD, all the while maintaining low complexity.

10.3 Conclusions

A novel multiple access architecture (FD-MC-CDMA) is proposed in this chapter to simultaneously exploit frequency diversity and minimize MAI. By dividing the whole transmission bandwidth into smaller sets of subcarriers, and by choosing these subcarriers to be non-contiguous, the same amount of frequency diversity is exploited with notably less MAI. Simulation results confirm that FD-MC-CDMA outperforms MC-CDMA (and FDMA) in frequency selective fading channels.

Moreover, a optimal ML MUD is designed to fully exploit the frequency diversity and improve the performance. In traditional MC-CDMA, the optimal ML multi-user detection receiver is too complicated to build; hence, sub-optimal receivers are used. In FD-MC-CDMA, by allowing users to share smaller sets of subcarriers, truly optimal ML MUDs are constructed at low complexity. Simulation results confirm that FD-MC-CDMA with MUDs significantly outperforms MC-CDMA (and FDMA) in frequency selective fading channels while maintaining comparable complexity.

Chapter 11 Ultra Wideband MC-CDMA and CI/MC-CDMA

As discussed in Chapter 6, future-generation wireless communication systems, designed to support very-high-rate data services, will require ultra-wide frequency bands. However, the frequency spectrum is a very scarce resource and has (for the most part) already been allocated to different entities in small blocks. No one entity owns a contiguous ultra-wide bandwidth. Hence, any ultra wideband communication will need to construct a system that operates over non-contiguous frequency bands.

In this chapter, we extend the MC-CDMA and CI/MC-CDMA architectures such that they operate over non-adjacent frequency bands [50]. In this way, the MC-CDMA and CI/MC-CDMA systems support ultra-wideband communications by operating over a large set of non-contiguous frequency bands, where each band may be either unlicensed or appropriately licensed.

We ensure that these proposed systems (1) exploit the full diversity benefits available over non-adjacent bands, maximizing performance, and (2) exploit the total bandwidth to maximize network capacity, as measured by number of users (per cell).

11.1 Overview of Ultra Wideband MC-CDMA and CI/MC-CDMA

As presented in Chapter 8, MC-CDMA is a strong candidate for next generation wireless communication systems. In MC-CDMA, each user's information bearing signal is sent simultaneously over N carriers, and each carrier is encoded with a +1 or −1 in accordance with a pre-assigned spreading sequence. Specifically, in MC-CDMA, assuming downlink communication for ease in presentation, the total transmitted signal corresponds to

$$S(t) = \mathrm{Re}\{\sum_{k=0}^{K-1} b_k c_k(t) e^{j2\pi f_c t}\} \tag{11.1}$$

where b_k is user k's information bit, K is the total number of active users, and $c_k(t)$ is user k's spreading code, corresponding to

$$c_k(t) = \sum_{i=0}^{N-1} e^{j\beta_i^{(k)}} e^{j2\pi i\Delta f t} \cdot g(t) \tag{11.2}$$

Here, i is the carrier index, N is the number of carriers in each user's code, $e^{j\beta_i^{(k)}}$ is the i^{th} component of user k's spreading sequence, and $g(t)$ is a unit amplitude rectangular waveform of symbol duration T_s.

Using equation (11.2), MC-CDMA signals correspond to

$$S(t)=\sum_{k=0}^{K-1} b_k \operatorname{Re}\left\{\sum_{i=0}^{N-1} e^{j\beta_i^{(i)}} e^{j2\pi f_c t} e^{j2\pi i\Delta f t}\right\}\cdot g(t) \tag{11.3}$$

Traditionally, to support N orthogonal users, Hadamard-Walsh codes are employed as spreading sequences. That is, $\beta_i^{(k)}$ is 0 or π in accordance with well-known principles.

In Chapter 8, Carrier Interferometry (CI) spreading codes were applied to MC-CDMA systems, leading to CI/MC-CDMA. With CI codes, N orthogonal users are supported by: for user k, apply $\beta_i^{(k)}=i\cdot k\frac{2\pi}{N}$. These CI codes, when applied to MC-CDMA, result in less MAI (multiple access interference) at the receiver when compared to MC-CDMA with Hadamard-Walsh codes (Chapter 8).

Additionally, in CI/MC-CDMA, up to $2N$ users can be supported on N carriers, i.e., an additional group of N users can be supported above and beyond the original N orthogonal users. This is achieved by applying:

$$\beta_i^{(k)}=i\cdot k\frac{2\pi}{N} \quad k=0,\ldots,N-1 \tag{11.4}$$

to generate the spreading codes for the first N users, and

$$\beta_i^{(k)}=i\cdot k\frac{2\pi}{N}+i\cdot\frac{\pi}{N} \quad k=N,\ldots,2N-1 \tag{11.5}$$

to generate the spreading codes for the second N users.

Now let's define

$$f_i = f_c + i\Delta f \tag{11.6}$$

Using this notation, the MC-CDMA (and CI/MC-CDMA) signal of equation (11.3) can be rewritten as

$$S(t) = \sum_{k=0}^{K-1} b_k \operatorname{Re}\left\{\sum_{i=0}^{N-1} e^{j\beta_i^{(i)}} e^{j2\pi f_i t}\right\} \cdot g(t) \tag{11.7}$$

Carrier frequencies f_p and f_q in equation (11.7) are required to be orthogonal to each other for all $p \neq q$. Mathematically, this corresponds to

$$\int_0^{T_s} \operatorname{Re}[e^{j(2\pi f_p t + \phi_p)} e^{j(2\pi f_q t + \phi_q)}]dt = 0 \qquad p \neq q \tag{11.8}$$

Traditionally, MC-CDMA subcarrier frequencies are chosen according to $f_i = f_c + i\Delta f$ where $\Delta f = 1/T_s$, the minimal frequency separation necessary to satisfy the orthogonality condition in (11.8). In this way, MC-CDMA operates over N continuous subcarriers (Figure 8.2).

However, many other solutions to equation (11.8) exist. For example, consider the case of four equal bandwidth, non-adjacent frequency bands, beginning at f_0, f_1, f_2, and f_3 respectively. Assume each band is capable of supporting $N'=16$ carriers separated by $\Delta f = 1/T_s$. Together these frequency bands could form a system with $N=64$ carriers. To satisfy equation (11.8), carrier frequencies are chosen as follows:

$$
f_i = \begin{cases} i\Delta f + f_0 & i = 0,1,2,\cdots\cdots 15 \\ (i-16)\Delta f + f_1 & i = 16,17,18,\cdots\cdots 31 \\ (i-32)\Delta f + f_2 & i = 32,33,34,\cdots\cdots 47 \\ (i-48)\Delta f + f_3 & i = 48,49,50,\cdots\cdots 63 \end{cases} \tag{11.9}
$$

where $\Delta f = 1/T_s$. In this way, an MC-CDMA system operates over 4 non-adjacent frequency bands. This system supports N=64 users when employing Hadamard-Walsh codes. When employing CI codes, the system support N=64 orthogonal users, followed by an additional N=64 pseudo-orthogonal users. Figure 11.1 illustrates the non-contiguous frequency bands.

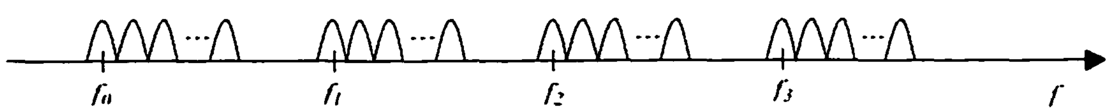

Figure 11.1 Non-adjacent Frequency Bands
to Support Ultra Wideband Communications

In general, analogous systems can be constructed to operate over L non-adjacent bands, with l_n carriers separated by $\Delta f = 1/T_s$ in the n^{th} frequency band. In this way, an MC-CDMA or CI/MC-CDMA system can support ultra-wideband communications over non-contiguous bands.

11.2 Transmitter and Receiver Structure for Ultra Wideband MC-CDMA

The transmitter structure for MC-CDMA and CI/MC-CDMA systems supporting ultra wideband communications is shown in Figure 11.2.

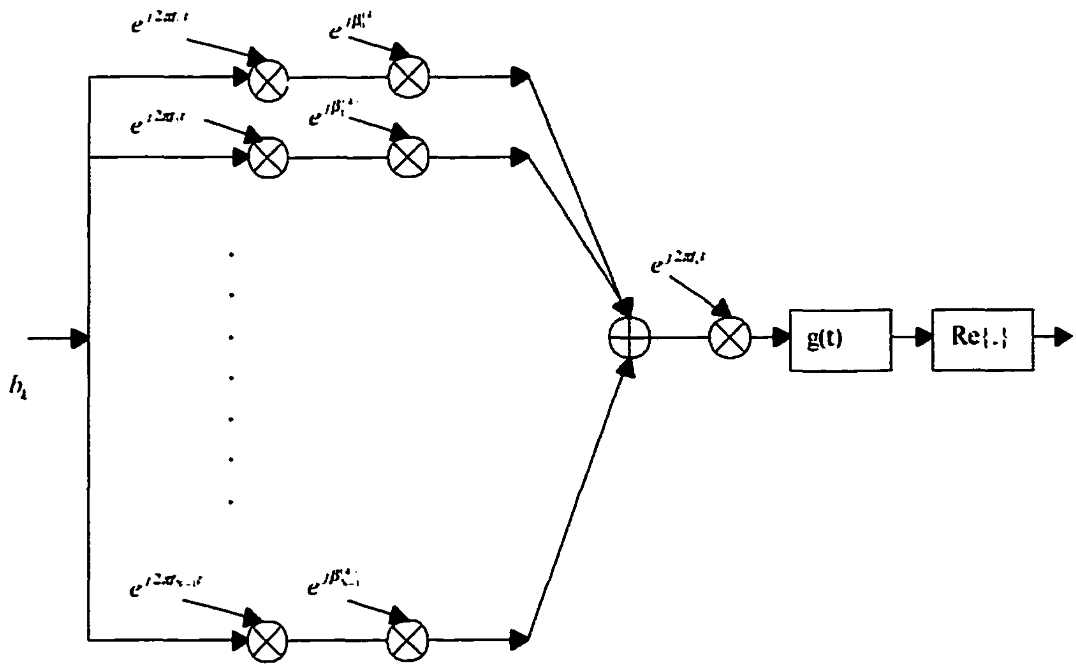

Figure 11.2 UWB MC-CDMA Transmitter Over Non-contiguous Frequency Bands

After transmission through a frequency selective fading channel, the received signal in ultra wideband MC-CDMA corresponds to (assuming the transmit signal in (11.7))

$$r(t) = \sum_{k=0}^{K-1} b_k \operatorname{Re}[\sum_{i=0}^{N-1} \alpha_i e^{j\beta_i^{(k)}} e^{j(2\pi f_i t + \phi_i)}] g(t) + \eta(t) \tag{11.10}$$

where α_i is the gain and φ_i the phase offset in the i^{th} subcarrier due to the channel fade, and $\eta(t)$ represents additive white Gaussian noise. Typically, the α_i's are correlated for carriers within each contiguous band, but uncorrelated from one band to the next. To simplify the analysis, exact phase synchronization is assumed.

User l's receiver for an ultra wideband MC-CDMA system operating over non-contiguous frequency bands is shown in Figure 11.3.

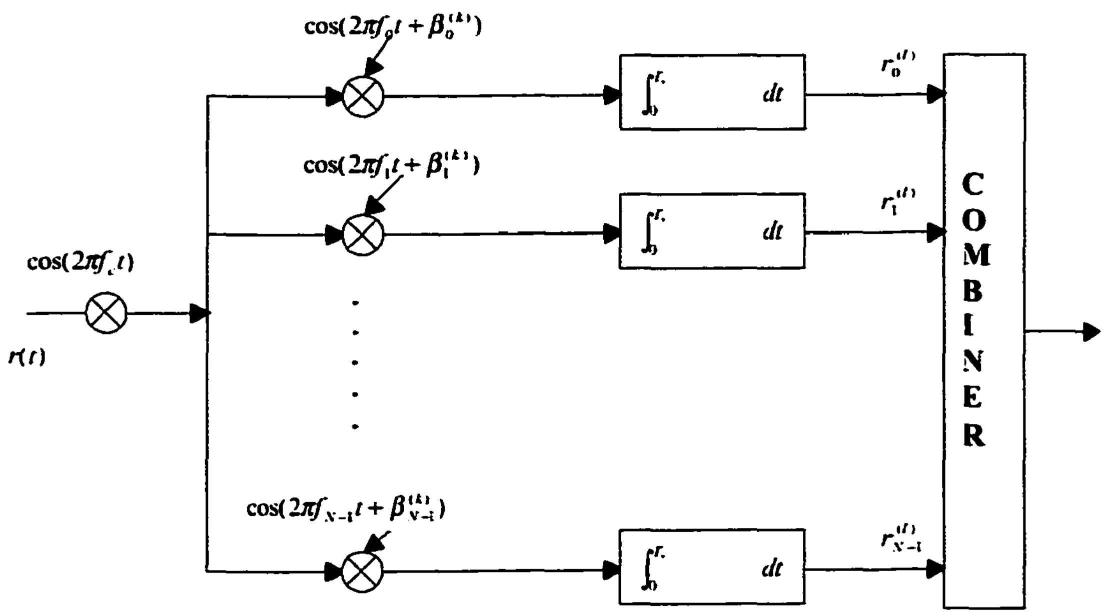

Figure 11.3 UWB MC-CDMA receiver over non-contiguous frequency bands

Here, the received signal is decomposed into its N carriers and despread by the l^{th} user's spreading code. The i^{th} carrier generates the decision variable

$$r_i^{(l)} = \alpha_i b_l + \alpha_i \sum_{\substack{k=0 \\ k \neq l}}^{K-1} b_k \operatorname{Re}[e^{j(\beta_i^{(k)} - \beta_i^{(l)})}] + \eta_i \tag{11.11}$$

Much like MC-CDMA and CI/MC-CDMA systems operating over contiguous frequency bands, ML (maximum likelihood) combining is used here (across the frequency components) to create a final decision variable for user l (Chapter 9):

$$R^{(l)} = \sum_{i=0}^{N-1} r_i^{(l)} \frac{\alpha_i}{(K-1)\alpha_i^2 P_i + N_0/2} \tag{11.12}$$

where, for MC-CDMA,

$$P_i = E[(\mathrm{Re}[e^{j(\beta_i^{(k)}-\beta_i^{(l)})}])^2] = 1 \tag{11.13}$$

and, for CI/MC-CDMA,

$$P_i = E[(\mathrm{Re}[e^{j(\beta_i^{(k)}-\beta_i^{(l)})}])^2] = \begin{cases} 1 & i = 0, N/2 \\ (N/2-1)/(N-1) & else \end{cases} \tag{11.14}$$

In this way, the receiver benefits from the frequency diversity available over all bands.

11.3 Simulation Results

To test the performance of proposed ultra wideband MC-CDMA and CI/MC-CDMA systems built over non-contiguous frequency bands, simulations are performed using four non-adjacent frequency bands. Assuming a very high-data-rate ($R=1/T_s$), each band contains 8 carriers separated by $\Delta f = 1/T_s$. The TU (Typical Urban) channel model [57], first presented in section 3.4, is assumed to accurately represent each non-adjacent band.

As benchmarks, traditional MC-CDMA and CI/MC-CDMA systems operating over N=32 contiguous subcarriers are also simulated. Figure 11.4 shows the BER versus SNR for fully loaded systems (K=32 users) and Figure 11.5 shows the BER versus system load (number of users) with SNR=10dB.

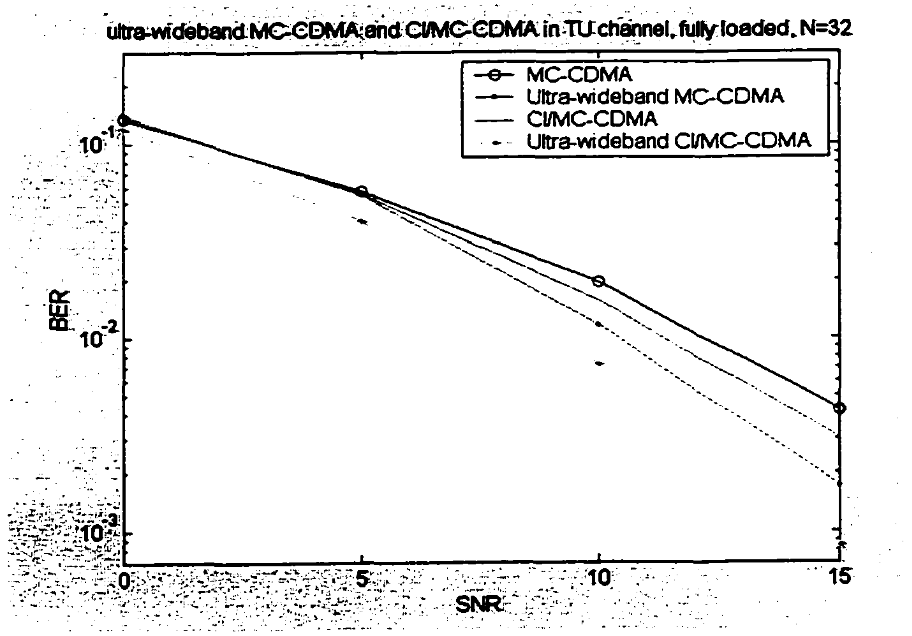

Figure 11.4 Simulation Results 1 for UWB MC-CDMA and CI/MC-CDMA

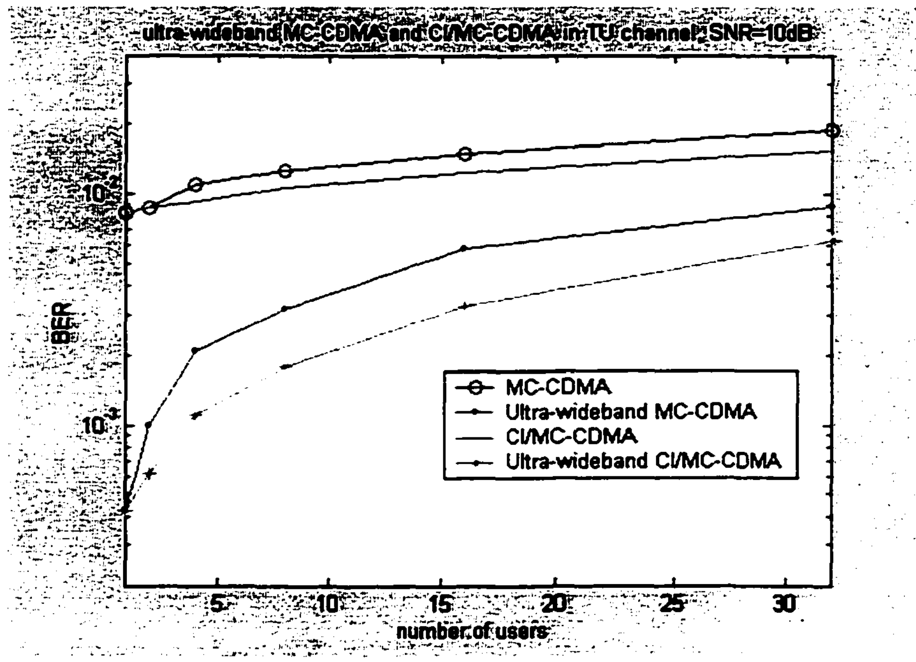

Figure 11.5 Simulation Results 2 for UWB MC-CDMA and CI/MC-CDMA

These simulation results demonstrate that MC-CDMA (and CI/MC-CDMA) can (1) operate over non-adjacent frequency bands, (2) support the same number of users as an MC-CDMA (CI/MC-CDMA) system with equal number of contiguous carriers, and (3) provide higher performance, afforded by the larger diversity gain.

11.4 Conclusions

Future high-data-rate communication services will require ultra wide frequency bands. Such frequency bands are currently unavailable in today's environment, as spectra has, for the most part, been auctioned in small blocks. For high-rate communication over ultra wide bands, systems will be required to operate over multiple narrow/midsize frequency bands simultaneously. In this chapter, we demonstrate how MC-CDMA and CI/MC-CDMA systems can be adapted to operate over a large set of non-contiguous bands, while exploiting very large diversity benefits and achieving high network capacities. This makes these systems ideally suited for future generation ultra wideband wireless.

Part IV

Conclusions and Future Work

Chapter 12 Conclusions

In this dissertation, we significantly improve upon the performances and network capacities of current DS-CDMA and MC-CDMA systems.

We begin by introducing novel CI *chip shaping* into current DS-CDMA systems, creating the innovative CI/DS-CDMA system (Chapter 3). It is shown that this CI/DS-CDMA system has significantly improved performance and offers a doubling in network capacity. Specifically, by applying multi-carrier based chip shapes, CI/DS-CDMA receivers exploit frequency diversity instead of path diversity in multipath fading channels. That is, at receiver side, the CI/DS-CDMA signal is decomposed onto its carriers and optimally recombined to best exploit diversity and minimize interference and noise. In this way, the poor performance (e.g., error floor) observed in traditional DS-CDMA systems is overcome. Simulation results show dramatically improved BER performance when this new architecture is applied (when compared to a traditional DS-CDMA system).

Moreover, by introducing pseudo-orthogonal chips (with minimum cross correlation to the original chips) into the CI/DS-CDMA system, we demonstrate increases in the network capacity by 100% while still outperforming traditional DS-CDMA.

We also propose and apply novel CI *spreading codes* into current DS-CDMA systems (Chapter 4). In a multipath fading channel, these complex CI codes introduce a multipath interference with reduced power (when compared to Hadamard-Walsh codes), and as a direct result, achieve better BER performance (relative to that of HW codes). Simulation results confirm that the novel CI codes can notably outperform Hadamard-Walsh codes (and other spreading codes) in multipath fading channels.

Furthermore, two orthogonal CI spreading codes sets (with minimum cross correlation between sets) are introduced into the DS-CDMA system. In this way, $2N$ users are supported in a system with a processing gain of N. These CI codes demonstrate much lower intra-path interference, and improved signal-to-interference ratio, relative to other proposed pseudo-orthogonal codes, and as a direct result, achieve better BER performance. Simulations indicate that the novel CI codes strongly outperform traditional pseudo-orthogonal coding methods while doubling network capacity. Moreover, CI codes can be designed for any processing gain N (unlike HW codes which requires $N=2^m$).

We also demonstrate how our novel CI *chip shaping* scheme enables DS-CDMA to operate over non-adjacent frequency bands in a way that is identical to its operation if all these bands are made contiguous. That is, we now add the ability to operate over non-adjacent bands to the benefits of CI chip shaping – in addition to its very high performance (by exploiting frequency diversity instead of path diversity) and its ability to double network capacity. With the exception of the chip shape and a receiver design which operates over non-contiguous bands, this new system retains all the features of a traditional DS-CDMA system.

As it will be months if not years before CI codes and CI chip shapes are embraced by academic and industrial communities, we also derive an optimal combining scheme for today's DS-CDMA RAKE receivers based on the maximum likelihood criteria (Chapter 6). This improves performance of current DS-CDMA systems. Simulation indicates that the novel combining scheme can strongly outperform other combining schemes. Moreover, (1) the proposed combining scheme does not require any additional information relative to traditional MRC and (2) the added computation load is very small.

By applying CI chip shapes to today's real world systems, we demonstrate how the IEEE 802.11 Wireless LAN physical layer can be dramatically improved. It is shown that our proposed IEEE 802.11 system with CI chip shapes supports four times the throughput of the traditional DSSS system, while simultaneously achieving a 2dB performance gain at a probability of error of 10^{-3}.

In the next part of the thesis, we propose improvements to current *MC-CDMA* systems.

We derived the maximum likelihood combining (MLC) scheme for MC-CDMA and CI/MC-CDMA. This scheme is optimal from the standpoint of minimizing the probability of error performance. It is shown that MLC is very close to MMSEC in a fully loaded system, justifying the selection of MMSEC over other combining schemes.

We propose FD-MC-CDMA (Chapter 10), a novel multiple access architecture based on achieving the best of MC-CDMA and FDMA. This system exploits frequency diversity benefits with minimizing MAI degradation. Specifically, in FD-MC-CDMA, instead of sending all users' information bits over all carriers, smaller sets of carriers are employed to support smaller numbers of users (with the same capacity and throughput for the overall system). Simulation results show that FD-MC-CDMA outperforms MC-CDMA and FDMA in frequency selective fading channel. Furthermore, a truly optimal multi user detection receiver (based on the maximum likelihood (ML) criteria) is employed (Chapter 10) in FD-MC-CDMA to optimize system performance. Of practical interest is the fact that the complexity of an ML MUD in FD-MC-CDMA is low, a direct consequence of FD-MC-CDMA's division of users into small subsets. Simulation results show FD-MC-CDMA with an optimal ML MUD significantly outperforming traditional MC-CDMA and FDMA in frequency selective fading channels, while offering a comparable system complexity.

Finally, we demonstrate how MC-CDMA systems can be adapted to operate over a large set of non-contiguous bands, while exploiting very large diversity benefits and achieving high network capacities (Chapter 11). This makes the MC-CDMA systems ideally suited for future generation ultra wideband wireless communications.

In summary, DS-CDMA and MC-CDMA represent key multicarrier technologies. There is little doubt that these technologies will continue to find widespread application.

There is also little doubt that more and more users will demand access to the wireless network, and that these users will demand higher data rate and higher quality of services. To meet these demands, DS-CDMA and MC-CDMA systems must extend beyond their limited performance and network capacities.

This thesis provides a number of innovative, powerful techniques to enable DS-CDMA and MC-CDMA systems to move beyond these limitations and meet the need of future generation wireless networks.

Chapter 13 Future Work

In this thesis, we significantly improve the performance and network capacity of existing DS-CDMA and MC-CDMA systems via the CI approach. Some directions for further research are highlighted in this final chapter.

13. 1 Zero-bandwidth Expansion Channel Coding via Pseudo-orthogonal CI Codes

In Chapter 4 and 8 of this thesis, we suggested the use of $2N$ codes in CDMA systems with a processing gain of N: Specifically, we suggest the simultaneous use of N CI codes and N Offset CI codes. In this part of the future work, we use the N Offset CI codes to transmit redundancy bits generated via a rate ½ channel coder. By doing this, the BER performance of CDMA systems can be dramatically improved via channel coding, while still maintaining high throughputs.

Figure 13.1 illustrates this proposed research.

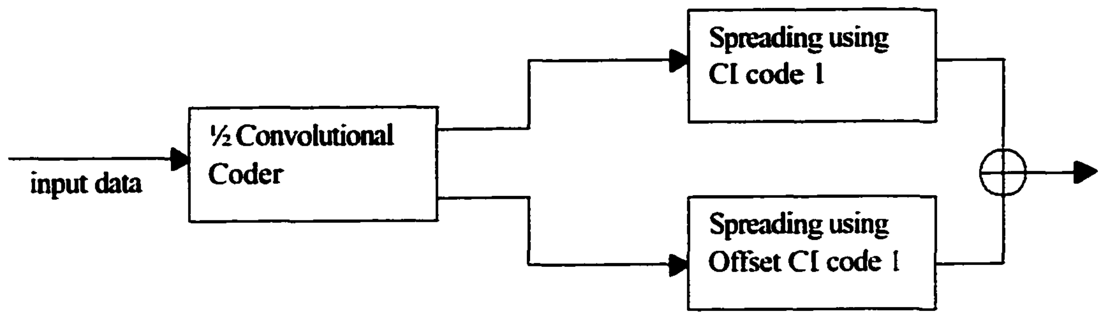

(a) Transmitter

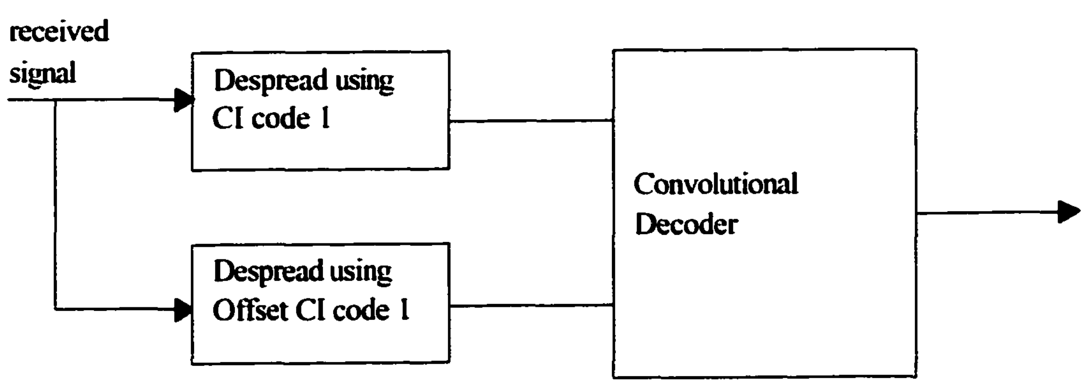

(b)Receiver

Figure 13.1 Diagram of Zero-bandwidth expansion CI/MC-CDMA

13.2 Zero-bandwidth Expansion Channel Coding via Pseudo-orthogonal CI Chips

In Chapter 3, we introduced pseudo-orthogonal chips, and demonstrated that these are tolerated by the CI/DS-CDMA system (in multipath fading channels). We now propose the use of these pseudo-orthogonal chips to transmit redundancy bits generated by a rate ½. This enables large the BER performance benefits in the CI/DS-CDMA system, while still maintaining large throughput.

Figure 13.2 illustrates the proposed future work in a block diagram form.

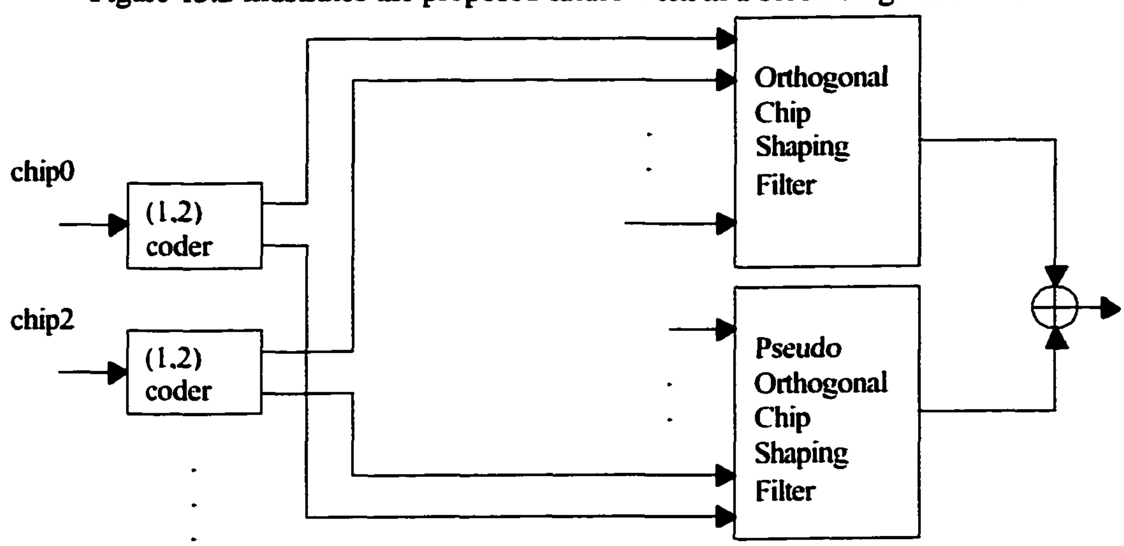

(a) Transmitter

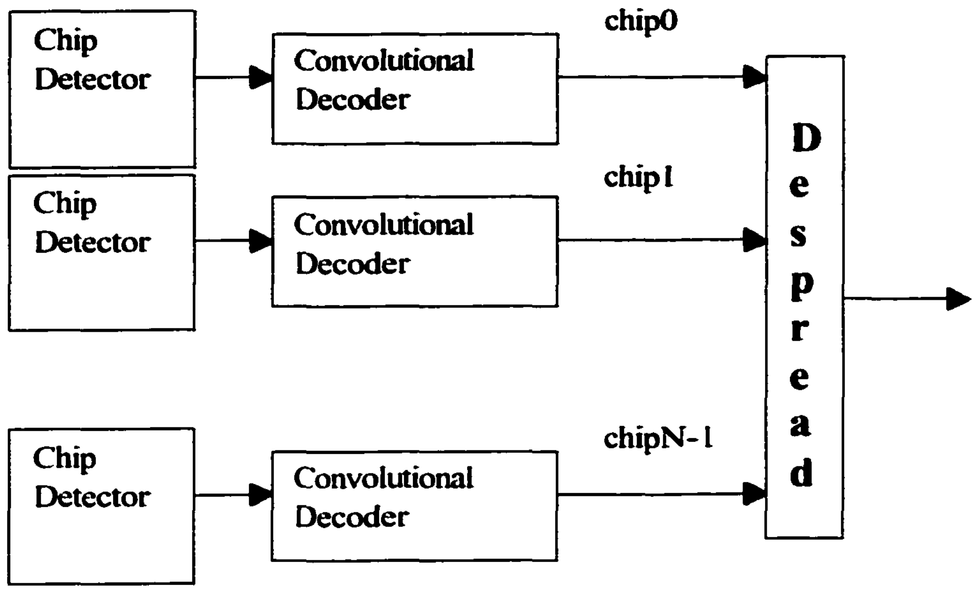

(b) Receiver

Figure 13.2 Diagram for Zero-bandwidth expansion CI/DS-CDMA

13.3 FD-CI-MC-CDMA

In Chapter 10, we proposed the FD-MC-CDMA system which exploits frequency diversity while minimizing MAI. However, we only used traditional Hardamard-Walsh codes in this part of the research. Since CI/MC-CDMA systems outperform MC-CDMA systems using traditional H-W codes, it seems natural to extend FD-MC-CDMA systems to create FD-CI-MC-CDMA.

These three subsections illustrate some of the many directions that will be considered in the future. There is no doubt that research on DS-CDMA and MC-CDMA systems will continue to be important for years to come.

Reference:

[1] J. G. Proakis, *Digital Communications*, Mc-Graw Hill, 2nd ed., 1991.

[2] T.S. Rappaport, *Wireless Communications-Principles and Practice*. New Jersey: Prentice Hall, 1996

[3] A.J. Viterbi, *CDMA: Principles of Spread Spectrum Communication*, Addison-WeSley Publishing Company, 1995

[4] R. Prasad. *CDMA for Wireless Personal Communications*. Artech House Publisers, 1996.

[5] P.W. Dent, *CDMA Subtractive Demodulation*, U.S. Patent #5218619

[6] W.C.Y. Lee, "Overview of Cellular CDMA", *IEEE Trans. on Vehicular Technology*, Vol. 40, No. 2, May, 1991

[7] D. J. Goodman, "Second Generation Wireless Information Networks", *IEEE Trans. on Vehicular Technology*, Vol. 40, No. 2, May, 1991

[8] G. L. Stuber, C. Kchao, "Analysis of Multiple-Cell DS-CDMA Cellular Mobile Radio System", *IEEE J. Selected Areas in Communication*, Vol. 10, No. 4, May 1992

[9] K.S. Gilhousen, I.M. Jocobs, A.J. Viterbi, "On the Capacity of a Cellular CDMA system", *IEEE Trans. on Vehicular Technology* 40(2), 1991, pp 303-312

[10] U. S. Goni and A. M. D. Turkmani, "BER Performance of a Direct-Sequence CDMA system in Multipath Fading Mobile Radio Channels with Rake Reception", *IEEE 44th Vehicular Technology Conference*, 1994, pp. 747-751

[11] A.F. Naguib, A. Paulraj, T. Kailath, "Capacity Improvement with Base-Station Antenna Arrays in Cellular CDMA", *IEEE Trans. On Vehicular Technology* 43(3), 1994, pp. 691-698

[12] M.B. Pursley, "Performance Evaluation for Phase-Coded Spread-Spectrum Multiple Access Communication-Part I: System Analysis", *IEEE Trans. Comm.*, 1977, COM-25, pp. 795-799

[13] M.K. Simon, J.K. Omura, R.A.Scholtz, and B.K. Levitt, *Spread Spectrum Communications*, Vol. I, II, III, Computer Science Press, Rockville, Maryland, 1985

[14] G.L. Turin, "Introduction to Spread Spectrum Antimultipath Techniques and Their Application to Urban Digital Radio", *Proc. IEEE*, 1980, 68, pp. 328-354

[15] A.J. Viterbi, "Overview of Mobile and Personal Communication", *Modern Radio Science*, Oxford University Press, Oxford, U.K., 1993

[16] A.J. Viterbi, R. Padovani, "Implications of Mobile Cellular CDMA", *IEEE Communications Magazine*, 1992, December, pp. 38-41

[17] A.J. Viterbi, A.M. Viterbi, K.S. Gilhousen, and E. Zehavi, "Soft Handoff Extends CDMA cell Coverage and Increases Reverse Link Capacity", *IEEE J. Selected Areas in Communications*, 1994, 12(8), pp. 1281-1288

[18] A.M. Viterbi, A.J. Viterbi, "Erlang Capacity of a Power Controlled CDMA system", *IEEE J. Selected Areas in Communication*, 1993, 11(6), pp. 892-900

[19] S. Kandala, E.S. Sousa, S. Pasupathy, "Multi-User Multi-Sensor Detectors for CDMA Networks", *IEEE Trans. on Communications*, Vol. 43, 1995, pp. 946-957

[20] Allen Salmasi, "An Overview of CDMA Applied to the Design of Personal Communication Networks", *Third Generation Wireless Information Networks,* Edited by Nanda Goodman, 1992

[21] Qualcomm Inc., "An Overview of the Application of CDMA to Digital Cellular Systems and Personal Cellular Networks", Qualcomm Inc. Document No. Ex 60-10010, May 1992

[22] L. B. Milstein et al, "Performance Evaluation for Cellular CDMA", *IEEE J. Selected Areas in Communication*, Vol. 10, No. 4, May 1992

[23] Jhong Sam Lee and Leonard E. Miller, *CDMA Systems Engineering Handbook*, Artech House Publishers, 1998

[24] Sergio Verdu, *Multiuser Detection*, Cambridge University Press, 1998

[25] N. Yee, J-P. Linnartz and G. Fettweis, "Mulitcarrier CDMA in Indoor Wireless Radio Networks", *Proc. Of IEEE PIMRC '93*, Yokohama, Japan, Sept. 1993. pp. 109-13.

[26] K. Fazel, S. Kaiser and M. Schnell, "A Flexible and High Performance Mobile Communications System Based on Orthogonal multi-carrier SSMA", *Wireless Personal Communications 2*, pp. 121-144, 1995

[27] T. Mueeler, K. Brueninghauss and H. Rohling, "Performance of Coherent OFDM-CDMA for Broadband Mobile Communications", *Wireless Personal Communications2*, pp. 295-305, 1996

[28] N. Yee and J. P. Linnartz, "Controlled Equalization of Multi-carrier CDMA in an Indoor Rician Fading Channel", *Proc. of VTC'94*, pp. 1665-1669, Stockholm 1994

[29] K. Fazel, "Performance of CDMA/OFDM for Mobile Communication Systems", *ICUPC'93*, pp. 975-979, 1993

[30] D. N. Kalofonis and J. G. Proakis, "Performance of the Multi-Stage Detector for a MC-CDMA System in a Rayleigh Fading Channel", *Globecom'96*, pp. 1784-1788, 18-22 November 1996, London, UK

[31] S. Zhou, G. B. Giannakis and A. Swami, "Comparison of Digital Multi-carrier with Direct Sequence Spread Spectrum in the Presence of Multipath", *Proc. of ICASSP'01*, Vol. IV, pp. 2225-2228, May 7-11, 2001, Salt Lake City, Utah

[32] A. Chouly, A. Brajal and S. Jourdan. Orthogonal Multicarrier Techniques Applied to Direct Sequence Spread Spectrum CDMA Systems. *Proc. Of IEEE GLOBECOM '93*, Houston, Nov, 1993. pp. 1723-28.

[33] L. Vandendorpe. Mulitone Direct Sequence CDMA System in an Indoor Wireless Environment. *Proc. Of IEEE First Symposium of Communications and Vehicular Technology* in the Benelux, Delft, The Netherlands, Oct. 1993. pp. 4.1.1-4.1.8.

[34] S. Hara *et al.* Transmission Performance Analysis of Multicarrier Modulation in Frequency Selective Fast Rayleigh Fading Channel. *Wireless Personal Communications*, vol. 2, no. 4, 1995/1006. pp. 335-56.

[35] E. Sourour and M. Nakagawa. Performance of Orthogonal Mulitcarrier CDMA in a multipath Fading Channel. *IEEE Trans. Communications*. vol 44, no. 3, Mar. 1996. pp. 356-67.

[36] S. Hara and R. Prasad. DS-CDMA, MC-CDMA and MT-CDMA for Mobile Multi-Media Communications. *Proc. Of IEEE VTC '96*, Atlanta, Apr. 1996. pp. 1106-10.

[37] R. Prasad and S. Hara. An Overview of Multicarrier CDMA. *Proc. Of IEEE ISSTA '96*, Mainz, Germany, Sept. 1996. pp. 107-14.

[38] B. M. Popovic, "Spreading Sequences for Multicarrier CDMA Systems", *IEEE Trans. on Comm.*, Vol. 47, No. 6, June 1999

[39] Z. Wu and C. R. Nassar, "High-Performance High-Capacity DS-CDMA via Carrier Interformetry", submitted to *IEEE Transactions on Communications*

[40] Z. Wu, C.R. Nassar, "High-performance DS-CDMA via Carrier Interferometry Chip Shaping", *Proceedings of The Thirteenth Conference on Wireless Communications, Wireless'2001*, Calgary, Canada, 2001

[41] C. R. Nassar, Z. Wu, "High Performance Broadband DS-CDMA via Carrier Interferometry Chip Shaping", *Third International Symposium on Advanced Wireless Communication Technology*, September 4-6, Boulder, 2000

[42] Z. Wu, C.R. Nassar, "High-capacity DS-CDMA for Next Generation Wireless Communication Systems via Carrier Interferometry Chip Shaping", *Proceedings of IEEE 2001 International Conference on Third Generation Wireless and Beyond, 3Gwireless'2001*, San Francisco, CA, 2001

[43] Z. Wu, C. R. Nassar, "Ultra Wideband DS-CDMA Via Innovations in Chip Shaping", *IEEE Vehicular Technology Conference Proceedings, IEEE VTC'2001 Fall*, Atlantic City, NJ, October, 2001

[44] Z. Wu, C. R. Nassar, "Novel Orthogonal Codes for DS-CDMA with Improved Crosscorrelation Characteristics in Multipath Fading Channels", submitted to *IEEE Vehicular Technology Conference, VTC Spring 2002*, Birmingham, Alabama

[45] Z. Wu, C. R. Nassar, "High Capacity High Performance DS-CDMA with Carrier Interferometry Codes", submitted to *2002 International Conference on Third Generation Wireless and Beyond*, May 2002, San Francisco, California

[46] D. Wiegandt, Z. Wu and C. R. Nassar, "High-Performance, High-Throughput IEEE 802.11 DSSS WLAN via Carrier Interferometry", *Proceedings of IEEE Emerging Technologies Symposium on Broadband Communications*, September 10-11, Richardson, TX, 2001

[47] Z. Wu, D. Wiegandt, C.R.Nassar, "High-Performance IEEE 802.11 DSSS WLAN via Carrier Interferometry Chip Shaping with Quadruple Throughput", *submitted to IEEE Wireless Communications and Networking Conference, WCNC'2002*

[48] Z. Wu, C. R. Nassar, "Maximum Likelihood Combining for MC-CDMA", submitted to *IEEE Vehicular Technology Conference, VTC Spring 2002*, Birmingham, Alabama

[49] Z. Wu, C. R. Nassar, "Novel Orthogonal Codes for MC-CDMA with Low Crosscorrelation in Frequency Selective Fading Channels", submitted to *IEEE International Conference on Communications*, *ICC2002*, New York City, May 2002

[50] Z. Wu, C. R. Nassar, "Ultra Wideband MC-CDMA and CI/MC-CDMA Systems", submitted to IEEE International Conference on Communications, submitted to *IEEE International Conference on Communications, ICC2002*, New York City, May 2002

[51] Z. Wu, C.R. Nassar and B. Natarajan, "FD-MC-CDMA: A Frequency-based Multiple Access Architecture for High Performance Wireless Communication", *proceedings of IEEE Radio and Wireless Conference, RAWCON'2001*, August 19-22, Waltham, MA, 2001

[52] Z. Wu, C. R. Nassar, "FD-MC-CDMA with Multi User Detection: Exploiting Frequency Diversity for High Performance Wireless Communication", submitted to *2002 International Conference on Third Generation Wireless and Beyond*, May 2002, San Francisco, California

[53] Holma, H., and A. Toskala, eds, *WCDMA for UMTS: Radio Access For Third Generation Mobile Communications*, New York: Wiley, 2000

[54] Juha Korhonen, *Introduction to 3G Mobile Communications*, Boston: Artech House, 2001

[55] C. R. Nassar, B. Natarajan, Z. Wu, D. Wiegandt, S. A. Zekavat and S. Shattil, Multi-carrier Technologies for Wireless Communication, Kluwer Academic Publishers, 2001

[56] Z. Wu, C. R. Nassar, "MMSE Combining for CI/DS-CDMA", *Proceedings of IEEE Radio and Wireless Conference, RAWCON 2000*, Denver, September 10-13, 2000

[57] COST-207: "Digital land mobile radio communications", Final report of the COST-Project 207, Commission of the European Community, Brussels, 1989

[58] William C. Jakes, *Microwave Mobile Communications*, IEEE Press, 1974

[59] B. Natarajan, C.R. Nassar and V. Chandrasekhar, "Generation of Correlated Rayleigh Fading envelops for spread spectrum applications", *IEEE Communication Letters*, Vol. 4. No.1. Jan, 2000, pp9-11

[60] Donald C. Cox, "Delay Doppler Characteristics of Multipath Propagation at 910 MHz in a Suburban Mobile Radio Environment", *IEEE Transactions on Antennas and Propagation*, Vol. AP-20, No. 5, Sep. 1972

[61] Donald C. Cox, "900 MHz Urban Mobile Radio Propagation: Multipath Characteristics in New York City", *IEEE Transactions on Communications*, Vol. Com-21, Nov. 1973

[62] Donald C. Cox, Robert P. Leck, "Distributions of Multipath Delay Spread and Average Excess Delay for 910-MHz Urban Mobile Radio Paths", *IEEE Transactions on Antennas and Propagations*, Vol. Ap-23, No. 2, Mar. 1975

[63] Donald C. Cox, Robert P. Leck, "Correlation Bandwidth and Delay Spread Multipath Propagation Statistics for 910-MHz Urban Mobile Radio Channels", *IEEE Transactions on Communications*, Vol. Com-23, No. 11, Nov 1975

[64] Daniel M. J. Devasirvatham, "Time Delay Spread and Signal Level Measurements of 850 MHz Radio Waves in Building Environments", *IEEE Transactions on Antennas and Propagation*, Vol. AP-34, No. 11, Nov. 1986

[65] Theodore S. Rappaport, Scott Y. Seidel and Rajendra Singh, "900-MHz Multipath Propagation Measurements for U.S. Digital Cellular Radiotelephone", *IEEE Transactions on Vehicular Technology*, Vol. 39, No. 2, May 1990

[66] Pete Spice, RF Coordinator, DIA Spectrum Management Group. Interview by Arnold Alagar. Denver, CO. May 1999.

[67] Regis Lindsay, Ramp Controller, United Airlines. Interview by Arnold Alagar. Denver, CO. May 1999.

[68] B. Vojcic, R. Whinnery, C. Kocinski, A. Hashizume, "Radio Network Design and Multiple Access for Airport Surface Traffic Automation," *IEEE Vehicle Navigation and Information Systems Conference,* Ottawa, Ontario, Canada, 1993.

[69] Z. Wu, C. R. Nassar, "High Capacity High Performance DS-CDMA via Advances in Chip Shaping", submitted to *IEEE International Conference on Communications, ICC2002*, New York City, May 2002

[70] J. G. Wade, *Signal Coding and Processing*, Ellis Horwood Limited, 1987

[71] H. Sari, F. Vanhaverbeke and M. Moeneclaey, "Multiple Access Using Two Sets of Orthogonal Signal Waveforms", IEEE Communication Letters, Jan. 2000, Vol. 4, No. 1, pp. 4-6

[72] D. Lee and L. B. Milstein, "Comparison of Multicarrier DS-CDMA Broadcast Systems in a Multipath Fading Channel", IEEE Trans. on Comm., Vol. 47, No. 12, December 1999

[73] S. Kondo and L. B. Milstein, "On the Use of Multicarrier Direct Sequence Spread Spectrum Systems", Proc. IEEE MILCOM, Boston, MA, Oct. 1993

[74] S. Kondo and L. B. Milstein, "On the Performance of Multicarrier DS CDMA Systems", IEEE Trans. on Comm., Vol. 44, Feb. 1996

[75] D. N. Rowitch and L. B. Milstein, "Convolutional Coding for Direct Sequence Multicarrier CDMA", Proc. IEEE MILCOM, San Diego, CA, Nov. 1995

[76] D. Lee, H. Lee and J. Kim, "Performance of a Modified Multicarrier Direct Sequence CDMA System", ETRI J., Vol. 19, Apr. 1997

[77] W. Xu and L. B. Milstein, "Performance of Multicarrier DS CDMA Systems in the Presence of Correlated Fading", Proc. VTC, Phoenix, AZ, May 1997

[78] S. Kondo and L. B. Milstein, "Multicarrier CDMA System with Cochannel Interference Cancellation", Proc. VTC, Stockholm, Sweden, June 1994

[79] Z. Wu, C.R. Nassar, S. Lu, "A Novel ML Combining RAKE Receiver for DS-CDMA", *proceedings of IEEE Pacific-Rim Conference on Communications, Computers and Signal Processing, PACRIM'2001*, August 26-28, Victoria, Canada, 2001

[80] ISO/IEC 8802.11:1999 (ANSI/IEEE Std 802.11, 1999 Edition), *Information Technology—Telecommunications and Information Exchange Between Systems—Local and Metropolitan Area Networks—Specific Requirements, Part 11: Wireless LAN Medium Access Control (MAC) and Physical Layer (PHY) Specifications*, August 1999.

[81] H. Hashemi, "The indoor propagation channel," *Proc. IEEE*, vol.81, no. 7, July 1993, pp. 943-68.

[82] TR 101 112 V3.1.0, UMTS 30.03 Version 3.1.0, November 1997

[83] B. Natarajan, C.R. Nassar, S. Shattil, M. Michelini and Z. Wu, "High-Performance MC-CDMA via Carrier Interferometry Codes", *IEEE Transactions on Vehicular Technology*, vol. 50, no. 6, November 2001.

[84] C. R. Nassar, B. Natarajan and S. Shattil, "Introduction of Carrier Interference to Spread Spectrum Multiple Access", *IEEE Emerging Technologies Symposium*, Dallas, Texas, April 1999

[85] Z. Wu, B. Natarajan, C.R.Nassar, "High-Performance, High-Capacity MC-CDMA via Carrier Interferometry", *Proceedings of IEEE Symposium on Personal, Indoor and Mobile Radio Communications, PIMRC'01*, September 30-October 3, San Diego, CA, 2001

[86] B. Natarajan and C. R. Nassar, "Crest Factor Considerations in MC-CDMA with Carrier Interferometry Codes", *Proc. IEEE PACIM*, Vol. 2, August 2001

[87] Balasubramaniam Natarajan, Carl R. Nassar, "Introducing Novel FDD and FDM in MC-CDMA to Enhance Performance", *Proc. of IEEE RAWCON* '00, pp. 29-32

[88] Steve Shattil, Zhiqiang Wu, Arnold Alagar, Carl R. Nassar, "Wireless Communication System Design for Airport Surface Management Part 1: Airport Ramp Measurements at 5.8 GHz", *IEEE international Conference on Communications 2000*, New Orleans, June 18-22, 2000

[89] Zhiqiang Wu, Carl R. Nassar, "Wireless Communication System Architecture and Physical Layer Design for Airport Surface Management", *IEEE VTC2000*, Boston, September 22-28, 2000

[90] Z. Wu, C. R. Nassar, "Optimum Combining for Multicarrier DS-CDMA Systems", submitted to *IEEE Wireless Communications and Networking Conference, WCNC'2002*